NAVAL POSTGRADUATE SCHOOL
MONTEREY, CALIFORNIA

19970123 043

DISSERTATION

SMART COMPOSITE PLATE SHAPE CONTROL USING PIEZOELECTRIC MATERIALS

by

M. Adnan Elshafei

September, 1996

Dissertation Supervisor : Brij N. Agrawal

Approved for public release; distribution is unlimited.

DTIC QUALITY INSPECTED 1

REPORT DOCUMENTATION PAGE

Form Approved OMB No. 0704-0188

Public reporting burden for this collection of information is estimated to average 1 hour per response, including the time for reviewing instruction, searching existing data sources, gathering and maintaining the data needed, and completing and reviewing the collection of information. Send comments regarding this burden estimate or any other aspect of this collection of information, including suggestions for reducing this burden, to Washington Headquarters Services, Directorate for Information Operations and Reports, 1215 Jefferson Davis Highway, Suite 1204, Arlington, VA 22202-4302, and to the Office of Management and Budget, Paperwork Reduction Project (0704-0188) Washington DC 20503.

1. AGENCY USE ONLY *(Leave blank)*	2. REPORT DATE September 1996	3. REPORT TYPE AND DATES COVERED Ph. D desertation

4. TITLE AND SUBTITLE

SMART COMPOSITE PLATE SHAPE CONTROL USING PIEZOELECTRIC MATERIALS

5. FUNDING NUMBERS

6. AUTHOR(S)

M. ADNAN ELSHAFEI

7. PERFORMING ORGANIZATION NAME(S) AND ADDRESS(ES)

Naval Postgraduate School
Monterey CA 93943-5000

8. PERFORMING ORGANIZATION REPORT NUMBER

9. SPONSORING/MONITORING AGENCY NAME(S) AND ADDRESS(ES)

10. SPONSORING/MONITORING AGENCY REPORT NUMBER

11. SUPPLEMENTARY NOTES

The views expressed in this thesis are those of the author and do not reflect the official policy or position of the Department of Defense or the U.S. Government.

12a. DISTRIBUTION/AVAILABILITY STATEMENT

Approved for public release; distribution is unlimited

12b. DISTRIBUTION CODE

13. ABSTRACT

In the present work, the shape control of fiber reinforced composite plate with embedded piezoelectric actuators is investigated. A finite element formulation is developed for modeling a laminated composite plate that has distributed piezoelectric actuators and sensors subjected to both mechanical and electrical loads. A simple, higher order, shear deformation theory with H a mil ton's principle is used to formulate the equations of motion. The model represents the parabolic distribution of transverse shear stresses and the non linearity of in-plane displacements across the thickness. The model is valid for both segmented and continuous piezoelectric elements, which can be either surface bonded or embedded in the laminated plate. A four-node, bilinear, isoparametric, rectangular element with seven degrees of freedom at each node is developed. The electric potential is treated as a generalized electric coordinate like the generalized displacement coordinates at the mid-plane of the actuator layers.

For shape control, an optimization algorithm, based on a finite element technique, is presented for an optimal applied voltage to each actuator to minimize the error between the desired shape and the actual shape. The error (objective) function is the mean squareof the error between the point in the actual surface and the corresponding point in the desired surface. Based on these techniques, two computer programs have been developed, an finite element modeling of a composite plate with piezoelectric actuators and an optimization model of the actuator voltages for shape control. The present work demonstrate the feasibility of the application of the piezoelectric actuators for the shape control of composite plates used in aerospace structures.

14. SUBJECT TERMS

Composite Materials-Piezoelectric Materials-Finite Element-Shape Control-Optimization

15. NUMBER OF PAGES 135

16. PRICE CODE

17. SECURITY CLASSIFICATION OF REPORT	18. SECURITY CLASSIFICATION OF THIS PAGE	19. SECURITY CLASSIFICATION OF ABSTRACT	20. LIMITATION OF ABSTRACT
Unclassified	Unclassified	Unclassified	UL

NSN 7540-01-280-5500 Standard Form 298 (Rev. 2-89)
Prescribed by ANSI Std. 239-18 298-102

Approved for public release; distribution is unlimited

SMART COMPOSITE PLATE SHAPE CONTROL USING PIEZOELECTRIC MATERIALS

Mostafa Adnan Elshafei
Lt. Col. Egyptian Airforce
B.Sc., Military Technical College, Cairo-Egypt,1981
M. Sc., Faculty Of Engineering, Cairo University-Egypt,1990

Submitted in partial fulfillment of the
requirements for the degree of

DOCTOR OF PHILOSOPHY IN AERONAUTICAL AND ASTRONAUTICAL ENGINEERING

from the
NAVAL POSTGRADUATE SCHOOL
September, 1996

Author: Elshafei
M. Adnan Elshafei

Approved by:

B. N. Agrawal
Brij N. Agrawal,
Professor of Aeronautics & Astronautics
Dissertation Supervisor

Gerald H. Lindsey,
Professor of Aeronautics & Astronautics

Sandra L. Scrivener
Sandra L. Scrivener,
Assistant Professor of Aeronautics
& Astronautics

Joshua H. Gordis,
Assistant Professor of Mechanical Engineering

Sherif Michael,
Associate Professor of Electrical Engineering

Approved by: Daniel J. Collins
Daniel J. Collins, Chairman, Department of Aeronautics & Astronautics

Approved by:
Maurice Weir, Associate Provost For Instruction

ABSTRACT

For the spacecraft and aircraft designers, the ability to change and control the shape of the structures has been a challenging problem. For a spacecraft, it is highly desirable to change the reflector shape in orbit to compensate for the surface errors and also to perform antenna beam shaping. In the case of aircraft, the shape control of propellers, helicopter rotor blades, and aircraft wings can increase efficiency and maneuverability and reduce vibration and noise of the vehicles. In the present work, the shape control of fiber reinforced composite plates with embedded piezoelectric actuators is investigated.

In the present study, a finite element formulation is developed for modeling a laminated composite plate that has distributed piezoelectric actuators and sensors subjected to both mechanical and electrical loads. A simple, higher order, shear deformation theory with Hamilton's principle is used to formulate the equations of motion. The model represents the parabolic distribution of transverse shear stresses and the non-linearity of in-plane displacements across the thickness. The model is valid for both segmented and continuous piezoelectric elements, which can be either surface bonded or embedded in the laminated plate. A four-node, bilinear, isoparametric, rectangular element with seven degrees of freedom at each node is developed. The electric potential is treated as a generalized electric coordinate like the generalized displacement coordinates at the mid-plane of the actuator layers.

For shape control, an optimization algorithm, based on a finite element techniques, is presented for an optimal applied voltage to each actuator to minimize the error between the desired shape and the actual shape. The error (objective) function is the mean square of the error between the point in the actual surface and the corresponding point in the desired surface. Based on these techniques, two computer programs have been developed, a finite element modeling of a composite plate with piezoelectric actuators and an optimization model of the actuator voltages for shape control. The present work demonstrates the feasibility of the application of the piezoelectric actuators for the shape control of composite plates used in aerospace structures.

TABLE OF CONTENTS

I. INTRODUCTION 1

II. FINITE ELEMENT ANALYSIS OF A COMPOSITE PLATE 11

A. INTRODUCTION 11
B. GENERAL THEORY 12
C. STRAIN-DISPLACEMENT RELATIONS 15
D. STRESS-STRAIN RELATION 16
E. STRESS RESULTANT-STRAIN RELATION 21
F. VARIATIONAL PRINCIPLE 23
G. FINITE ELEMENT FORMULATION 24
H. EQUATION OF MOTION 30
I. NUMERICAL INTEGRATION 33
J. FREE VIBRATION ANALYSIS 34
K. STRESS ANALYSIS 34
L. VALIDATION 35

III. FINITE ELEMENT ANALYSIS OF A SMART COMPOSITE PLATE.....47

A. INTRODUCTION..... 47
B. VARIATIONAL PRINCIPLE 51
C. FINITE ELEMENT FORMULATION 57
D. EQUATION OF MOTION 60
1. PLATE WITH ACTUATORS ONLY 60
2. PLATE WITH ACTUATORS AND SENSORS 65
E. NUMERICAL INTEGRATION ..... .68
F. VALIDATION 69

IV. SHAPE CONTROL AND OPTIMIZATION 77

A. INTRODUCTION 77
B. PROBLEM STATEMENT 77
C. ERROR FUNCTION Λ 79
D. FINITE ELEMENT FORMULATION 83
E. NUMERICAL INTEGRATION 88
F. OPTIMIZATION ALGORITHM 88
G. SOLUTION PROCEDURE 90
H. VALIDATION 90

V. CONCLUSIONS 101

APPENDIX A: NUMERICAL INTEGRATION 103
APPENDIX B: COMPUTER PROGRAMS 107
LIST OF REFERENCES 111
INITIAL DISTRIBUTION LIST 119

LIST OF FIGURES

Figure 2.1 : Deformation of the normal to the mid-plane..... 12

Figure 2.2 : An off-axis unidirectional lamina 20

Figure 2.3 : Actual and master element 25

Figure 2.4 : Local discrete least squares smoothing 34

Figure 2.5 : Distribution of the in-plane normal stress σ_{xx} for a simply 40
supported laminated square plate $(0^0/90^0/0^0)$ subjected to
double sinusoidal load.

Figure 2.6: Distribution of the in-plane normal stress σ_{yy} for a simply 41
supported laminated square plate $(0^0/90^0/0^0)$ subjected to
double sinusoidal load

Figure 2.7: Distribution of the in-plane normal stress σ_{xz} for a simply 42
supported laminated square plate $(0^0/90^0/0^0)$ subjected to
double sinusoidal load

Figure 2.8 : Effects of the fiber angles & span to thickness ratio on 45
the dimensionless fundamental frequency for a laminate
$(\theta^0/-\theta^0/\theta^0/-\theta^0)$.

Figure 3.1 : Composite plate with piezoelectric sensors and actuators 49
complete covered the surface.

Figure 3.2 : Composite plate with distributed segmented piezoelectric 50
sensors and actuators

Figure 3.3: Bending deflection vs. length to thickness ratio for the 72
a smart plate subjected to double sinusoidal mechanical load.

Figure 3.4: Bending deflection vs. length to thickness ratio for 73
a smart plate subjected to double sinusoidal electrical
and mechanical loads.

Figure 3.5: Normalized central deflection vs. applied voltages for 74
a smart plate subjected to uniformly electrical load.

Figure 3.6: Grid point deflection for simply supported smart plate 73
subjected to a double sinusoidal electrical and mechanical
loads.

Figure 4.1 : z_0 coordinate shows a point location on element of the 78
finite element grid.

Figure 4.2: Original surface, actual surface, and desired surface 79
in x-z plane.

Figure 4.3: Difference between the actual surface and the desired 81
surface in the x-z plane.

Figure 4.4: Flow chart of solution procedure 91

Figure 4.5: Element numbers for different actuator positions for 92
a simply supported square composite plate (a=b)

Figures 4.6: Actual and desired transverse deflection at the grid point 94
for actuator at the fifth element

Figures 4.7: Actual and desired transverse deflection at the grid point 95
for actuators at elements number two and eight.

LIST OF TABLES

Table 2.1: Boundary conditions for various different conditions 36
(x = constant).

Table 2.2: Three-Layers cross ply ($0^0/90^0/0^0$) square plate subjected 37
to sinusoidal loading ($t_1=t_3 = t/4$, $t_2=t/2$)

Table 2.3: Dimensionless fundamental frequency for four layers 44
layers ($0^0/90^0/0^0/90^0$) with span to thickness ration equal five.

Table 3.1: Analogy between mechanical and electrical quantities. 54

Table 4.1: Error function values at different actuator positions for 95
applied voltage equal 100 volt.

Table 4.2: Optimal applied voltage and error function at different 98
actuator positions

Table 4.3: Optimal applied voltages and error functions for the case 98
of four actuators used at a time.

Table 4.4: Optimal applied voltages and error functions for the case 99
of pair of actuator used at a time

Table A.1: Weights and Gauss points for the Gauss Legendre 105
quadrature

NOTATION

x, y, z	Cartesian coordinates.
a, b	Plate dimensions.
t	Plate thickness
U_0, V_0, W_0	Displacement along x, y, & z directions on mid-plane
U, V, W	Displacement along x, y, & z directions
ϕ_x, ϕ_y	Rotation of normal to the mid-plane about y and x directions.
σ_{ij}	Normal stresses
τ_{ij}	Shear stresses.
ε_{ij}	Strains.
C_{ij}	Stiffness coefficients for a composite plate.
Q_{ij}	Transformed reduced stiffness coefficients.
E_1, E_2	Modulus of elasticity along longitudinal and transverse direction
ν_{ij}	Poisson's ratios
G_{12}, G_{13}	Rigidity modulus.
θ	Fiber orientation angle with respect to x axis.
$\{N\}$	Stress resultants.
$[\overline{D}]$	Rigidity matrix
$[A]$	Extensional stiffness matrix
$[B]$	Coupling stiffness matrix
$[D]$	Bending stiffness matrix
$[E]$,$[F]$, &$[H]$	Higher order matrices
δ	Variational
$\mathfrak{I}$	Lagrangian
W	Work done by external forces.
λ	Kinetic energy

$\hbar$	Potential energy
$\dot{q}$	Velocity (time derivative of the generalized displacement q);
v	Volume
N_i, f, g_i, h_i	Interpolation functions
$[N]$	Matrix of interpolation function for mass matrix
ξ, η	Local coordinates of a point
$[B]$	Strain-nodal DOF relations.
$\|J\|$	Determinant of the Jacobian matrix
$[K_e], [M_e]$	Element stiffness and mass matrix
$[K], [M]$	Global stiffness and mass matrix.
$[\overline{m}]$	Matrix of the normal and rotation inertia.
$\{P_{Me}\}$	Load vector
q_0	Load intensity
$\{D\}$	Electric displacement vector
$[e]$	Dielectric permittivity matrix
$[\varepsilon^s]$	Dielectric matrix at constant mechanical strain (permittivity component)
$[E]$	Electric field vector
$\{c\}$	Elasticity matrix for a constant electric field
s_1 and s_2	Surface areas at which the mechanical and electrical loads are applied
μ	Surface charge density
$\Phi^L(x,y,z)$	Electric potential function
Φ_0^L	Generalized electric coordinate at the mid plane of the actuator and sensor layers.
Φ_{0i}^e	Generalized electric coordinate at the ith node.

$\{\Phi_0^e\}$	Nodal generalized electric coordinate vector.
$\{\overline{\Phi}\}$	Global generalized electric coordinate
$[N_\Phi]$	Interpolation function for the electric field
$[B_\Phi]$	Differentiation of N_Φ
$\{g\}$	Electric excitation
$\{G\}$	Global electric excitation vector
$\{\overline{\Phi}\}_s$	Voltage from sensor layer.
$\{F\}$	Global mechanical load vector
$\{F_f\}$	Feedback force.
Z_0	Coordinate of a point of an element of the finite element grid
Λ	Error function
Ω_e	Element domain
Δ	Difference between the z-coordinate of points on the surface
Δ	Difference between the z-coordinate of points on the surface of the desired shape and the actual shape.
$\overline{\Lambda}$	Structure objective function.

I. INTRODUCTION

Advanced structures with integrated self-monitoring and control capabilities are becoming increasingly important due to the rapid development of 'intelligent' space structures. Those smart structures that have actuators distributed throughout are defined as adaptive, or actuated, structures. Examples of such adaptive structures are conventional aircraft wings with articulated leading-and trailing-edge control surfaces, robotic systems with articulated manipulators and end effectors and spacecraft antenna reflectors. Structures that have sensors distributed throughout are a subset referred to as sensory. These structures have sensors which can detect displacements, strains or other mechanical states or properties like electromagnetic states or properties, temperature, heat flow, or damage. Applications of this technology might include damage detection in long life structures, or embedded or conformal RF antennas within a structure. The overlap structures, which contain both actuators and sensors implicitly linked by closed-loop control, are referred to as controlled structures. A subset of controlled structures are active structures, distinguished from controlled structures by extensively distributed actuators, which have structural functionality and are part of the load bearing system.

Intelligent structures are a subset of active structures that have highly distributed actuator and sensor systems with structural functionality and, in addition, distributed control functions and computing architecture [Ref. 1].

Smart structures have applications due to their ability to change shape. Some of these are for spacecraft antennas, to compensate for surface error and thermal distortion to improve antenna performance, and to change the antenna beam shape in orbit. They may be used for and submarine and helicopter shape control as well. An aeroelastic application to aircraft structures is quasi-static control of camber, dynamic control, and flutter suppression. Smart structures can be used in acoustic control by developing an adaptive structure in which the structural response can be modified with varying input disturbances.

The piezoelectric material is one of the smart materials that can be used as an actuator and sensor. Piezoelectricity refers to the phenomenon of generating an electric charge in a material when subjecting it to mechanical stress, which is known as a direct piezoelectric effect. The converse piezoelectric effect is described as an induced strain in response to an applied electric field.

Piezoelectric properties occur naturally in some crystalline materials and can be induced in other polycrystalline materials. The distortion of the crystal domain produces the piezoelectric effect. The domain may be aligned/poled by the application of a large electric field, usually at high temperature. Subsequent application of the electric field will produce additive strains in the local domain, which translate into a global strain in the material.

The piezoelectric effect was discovered in 1880 by Pierre and Jacques Curie. The direct piezoelectric effect has been used for a long time in sensors such as accelerometers. Use of the converse effect, however, has until recently been restricted to ultrasonic transducers. Barium titanate, discovered in 1940, was the first widely used piezoceramic. Lead zirconate titanate (PZT) [Ref. 2], discovered in1954, has now largely superseded barium titanate because of its stronger piezoelectric effect.

A β-phase polymeric piezoelectric, polyvinylidene fluoride (PVDF), was initially discovered by Kawai in 1969 [Ref. 3]. Raw polymeric PVDF (α-phase) is an electrical insulator, and it does not have any intrinsic piezoelectric properties. If the raw material is polarized during the manufacturing process, PVDF transforms to a β-phase , a tough and flexible semi-crystalline material, and can be made to strain either in one or two directions in the film plane. Since β-phase PVDF possesses a strong direct piezoelectric effect, it has been used in many transducer applications; e.g., sonar, medical ultrasonic equipment, robot tractile sensors, acoustic pick-ups, force and strains gages, etc. Due to its distinct characteristics, such as flexibility, durability, manufacturability, etc., PVDF is commonly used in such structural systems.

As a first step in the following work, a finite element analysis of a graphite/epoxy, fiber reinforced, composite, laminated plate is developed, using a simple higher-order shear deformation theory [Ref. 4]. Multi-layered composites have found wide use in many weight-sensitive structures, such as aircraft, spacecraft antennas, and missile structural components, where high strength-to-weight and stiffness-to-weight ratios are required. A laminate is a multi-layered composite made up of several individual layers (laminae) in which the fibers are oriented in a predetermined direction to provide efficiently the required strength and stiffness parameters in each laminae.

For analysis and design of structural laminates, a classical plate theory (CPT) [Refs. 5,6,7, & 8] has been used in which it is assumed that normals to the mid-plane before deformation remain straight and normal to the mid-plane after deformation (classical Kirchhoff hypotheses). This theory under-predicts deflections and over-predicts natural frequencies and buckling loads. These results are due to the neglect of transverse shear strains in the classical theory. These errors are even higher for a plate made of advanced composites like graphite epoxy and boron-epoxy, whose elastic modulus to shear modulus ratio are very large (i.e., of the order of 25 to 40 instead of 2.6 for a typical isotropic materials). These high ratios render classical theories inadequate for the analysis of composite plates. An adequate theory must account for transverse shear strains.

Many plate theories have been proposed to incorporate the influence of the transverse shear strains. In one of these, the Reissner-Mindlin plate theory [Ref. 9], transverse shear and rotary inertia effects are included, and it contains a displacement field which accounts for linear, or higher-order, variations of mid-plane displacements through the thickness, but on the other side the deviation increases with increasing mode numbers. A theory for laminated isotropic plates by Stavsky [Ref. 10]. has been generalized to laminated anisotropic plates by Yang, Norris et. al. [Ref. 11]. Whitney [Ref. 12] has presented an approximate method to incorporate the influence of shear deformation on plate deflection, in a flexural vibration and buckling analysis. Elasticity solutions by Pagano and his

associates [Refs. 13, 14, 15, & 16] indicated the inadequacy of the classical laminate theory. These shear deformation theories do not satisfy the conditions of zero transverse shear stresses on the top and bottom surfaces of the plate, and they require a shear correction to the transverse shear stiffness. Three-dimensional theories of laminates, in which each layer is treated as a homogeneous anisotropic medium [Refs. 17, 18, & 19] are intractable as the number of layers becomes moderately large.

Different higher-order laminated plate theories have been proposed, which account for the transverse shear strains. Examples of such theories are, Whitney and Pagano [Ref. 20], Whitney et. al [Refs. 21,22], Lo et al. [Ref. 23] and Nelson et. al. [Ref. 24] In these higher-order theories, an additional dependent unknown is introduced into the theory with each additional power of the thickness coordinate.

A simple two-dimensional theory of plates that accurately describes the global behavior of laminated plates seems to be a compromise between accuracy and ease of analysis. A simple, higher-order theory described by Reddy [Ref. 25], is such a theory, as it is accounts not only for transverse shear strain but also for a parabolic variation of the transverse shear strains through the thickness. Consequently, there is no need to use shear correction coefficients in computing the shear stresses. This theory is used as a prime base in this finite element analysis.

The finite element analysis of laminated composite plates has been presented by several authors, Reddy et. al. [Refs. 26,36], and Noor [Refs.37,38], for bending and vibration analyse. Mawenya [Ref. 40], developed a general quadratic isoparametric multilayer curved plate element, and Panda[Ref.41], presented a superparametric, quadratic plate element for the plate bending analysis. Fortier and Rossettos [Ref. 42], Sinha and Rath [Ref. 43], analyzed free vibration and buckling of thick plates of unsymmetric cross-ply construction. Dong [Ref. 44] has given the solution for the dynamic response of a simply-supported rectangular plate.

In the first part of the present work, a finite element model for a laminated composite plate is developed using a simple, higher-order, shear deformation theory with

Hamilton's principle for the formulation of the equations of motion [Refs. 45,46]. A standard, four node, rectangular element with seven degrees of freedom at each node is developed for the analysis of a flexible laminated plate having a constant thickness for any individual layer. The displacement model is so chosen because it can represent adequately the parabolic distribution of transverse shear stresses and the non-linearity of in-plane displacements across the thickness. A bending, free vibration and stress analysis problem is examined for different loadings, boundary conditions, and fiber orientation angles. The results are compared with existing analytical and numerical solutions. Hence the present element formulation demonstrates its applicability for a wide variety of laminate composite plates.

Given the result of continuous competing requirements for improving the weight, interdisciplinary performance, temperature stability, versatility, and reliability of propulsion and aerospace components, the development of a new generation of composite materials, called ' intelligent/smart composite materials ' is receiving growing attention, which is the concern of this dissertation.

The reader is referred to books, Cady [Ref. 47], Ikeda [Ref. 48], and Nye [Ref. 49], for piezoelectricity and for the development of the constitutive relations for piezoelectric materials. Tiersten [Ref.50], and Rogacheva [Ref. 51], contain methods for solving the differential equations of the theory for piezoelectrical plates and shells, respectively .

Several researchers have studied the interaction between the mechanical properties and the electric field. Crawley et. al. [Ref. 52], developed piezoelectric elements for laminated beams, and with his co-workers[Ref. 53], has expanded the work and considered the piezoelectric actuators to be plies of laminated plate and used the Rayleigh Ritz method to study the deformations of a smart plate. They also modeled the induced strain actuation for a beam [Ref. 54], and for a truss element[Ref. 55]. Lee [Refs. 56, 57], derived a theory for laminated piezoelectric plates based upon classical plate theory. His experimental [Ref. 58], results showed that PVDF or $PVDF_2$ actuators can generate

plate bending and twisting independently or simultaneously, and they are suitable for active damping control of a flexible structure.

Tiersten [Ref. 50] modeled single-layer piezoelectric plates, including the charge equations, but did not study laminates. Wang and Rogers [Ref. 59], applied the classical laminated plate theory to model laminated plates with spatially distributed actuators. Tzou et. al. [Ref. 60], derived governing equations for piezoelectric shells using first order theory. Mitchell and Reddy [Ref. 61], presented a hybrid theory for enhancing laminated plates based on modeling the electric potential through the laminate thickness with a 1-D finite element. Hagood et. al. [Ref. 62], modeled the effects of the dynamic coupling between a structure and an electrical network through the piezoelectric effect for a cantilever beam. State space models were developed for three important cases: direct voltage driven electrodes, direct charge driven electrodes, and an indirect drive case, where the piezoelectric electrodes were connected to an arbitrary electrical circuit with embedded voltage and current sources. Ray et. al. [Ref. 63], presented the exact solutions for a two dimensional analysis of a plate composed of piezoelectric material. This study led to exact solutions for a composite plate with piezoelectric actuators and sensors [Refs. 64, 65]. Lee [Ref. 67], developed an analytical approach via state space equations. Heyliger [Ref. 68], developed an exact solution for the free vibration analysis.

The previous solutions do not provide the results for large complicated structures with integrated materials. Thus, the necessity for approximate techniques, such as the finite element method arises. A few papers have been developed addressing the analysis of intelligent structures by the finite element method. Allik and Hughes [Ref. 69], presented a tetrahedral finite element for three-dimensional electroelasticity. Based on this model, Tzou [Ref. 70], proposed a method for isotropic plates using isoparametric hexahedron solid elements. Kagawa et. al [Ref. 71], developed a method for a transversely vibrating bar with electrostrictive transducers. McDearmon [Ref. 72] and Tzou [Ref. 73], developed a method for simple cases of deformation. Ha et. al.[Ref. 74] analyzed a composite plate by using a three dimensional brick element. Both elements used in these

methods made the problem complex, costly and required some special techniques to overcome inaccuracies and disadvantages of modeling a plate with 3-D elements. These elements display excessive shear stiffness as the element thickness decreases. The two dimensional quadrilateral plate element developed by Hwang et. al. [Ref. 75], is more efficient than solid elements, but it appears to have restricted modeling capabilities. Hwang et. al. [Ref.76], proposed a model based on classical laminated plate theory, which neglects the effects of transverse shear stresses, and hence is inadequate for the analysis of moderately thick composite structures. Chandrashekhara, et. al. [Ref. 77], developed a model based on the first order shear deformation theory, which needed a shear correction coefficient. Static analysis or an intelligent plate was presented by Ray [Ref. 78], using a higher order shear deformation theory, which added additional dependent unknowns and made the problem costly to solve.

In the second part of the present work, a finite element formulation is developed for modeling the static and dynamic response of laminated composite plates with distributed piezoelectric actuators and sensors subjected to both mechanical and electrical loading. A simple higher-order shear deformation theory with Hamilton's principle is used to formulate the equation of motion of the system in which the piezoelectric layer is treated as a normal lamina. The displacement model represents the parabolic distribution of transverse shear stresses and the non-linearity of in-plane displacements across the thickness. The model is valid for both segmented and continuous piezoelectric elements, which can be either surface bonded or embedded in the laminated plate. The piezoelectric layer can be isotropic or orthotropic, and the structure core can be anisotropic (graphite/epoxy, etc.) or isotropic (aluminum). A new, four-noded, bilinear, isoparametric, rectangular element with seven mechanical degrees of freedom and one electrical degree of freedom at each node is developed. The electric potential is treated as a generalized electric coordinate like the generalized displacement coordinates at the mid-plane of the actuator layers. The structural deformations due to electrical and mechanical loads are computed and compared to the available analytical and finite element results.

The third part of this dissertation is directed toward shape control and optimization of the actuator voltages. Several works have been completed in vibration control. For example Baz et. al. [Ref. 79], Challopadhyay [Ref. 80], Chandrashekhara [Ref. 77], Park el. at. [Ref. 76], Tzou [Ref. 81, 82], Anderson and Hagood [Ref. 83], and Hagood et. al. [Ref. 84]. Wang and Fuller [Ref. 85, 86, 87, & 88], have done several papers for active structural acoustic control using piezoelectric actuators. A few studies have been done in the shape control and optimization. Ghosh [Ref. 89] showed a model for plate shape control by using PZT, Agrawal et. al. [Ref. 90], developed a mathematical model for deflection using a finite difference technique and estimated the optimal actuation voltages. Kirby [Ref. 91], and Koconis et. al. [Ref. 92], presented an analytical method to determine the voltages needed to achieve a specified desired shape with minimum error between the actual shape and the desired shape. Based on Koconis method, Varadarajan et. al. [Ref. 93], showed a model for shape control of a laminated plate.

In the third part of the present work, an optimization algorithm based on the finite element technique is developed to determine the optimal voltages applied to the actuator to minimize the error between the desired shape and the actual shape. The error function is defined as the mean square of the error between the points in the actual surface and the points in the desired surface for each element of the finite element grid. The original shape and the desired shape of the plate are specified. Thus the objective is to find the optimal actuator voltage to get minimum error between the desired shape and the actual shape. The analysis is based on small deformation theory, therefore, the specified desired shape must be within the region of small deformation from the original shape.

Two Matlab codes were developed. The first code, 'COMPZ' is an interactive finite element code. It is able to solve a laminated composite plate, with or without piezoelectric layers, subjected to mechanical and electric loads for different boundary conditions. The code is able to analyze either a complete or a quarter plate analysis to save computational time, and it will perform a bending, free vibration analysis, and

a stress analysis for the individual layers. It is valid for different types of material for both piezoelectric or laminated layers (anisotropic, isotropic, etc.).

The second Matlab code, 'OPTSHP', is able to analyze the structure and compute the change in shape due to mechanical and electrical loads. This code includes a loop containing an optimization algorithm coupled with a Matlab Optimization Toolbox to compute the voltage applied to each actuator to minimize the objective function. The numerical results are presented for each part of the analysis.

II. FINITE ELEMENT ANALYSIS OF A COMPOSITE PLATE

A. INTRODUCTION

The partial differential equation governing composite laminates of arbitrary geometry and boundary conditions can not be solved in closed form [Ref. 95]. Analytical solutions of plate theories are available in the literature (i.e., Navier solutions, Levy solutions). The Rayleigh-Ritz and Galerkin methods can also be used to determine approximate analytical solutions, but they too are limited to simple geometries because of the difficulty in constructing approximation functions for complicated geometries. The use of numerical methods facilitates the solution of these complicated problems. Among numerical methods, the finite element method is the most effective.

There are several types of finite element models that have been developed for plate theories. These can be grouped into three major categories: displacement models, mixed and hybrid models, and equilibrium models.

The displacement finite element models of plate theories are based on the principles of virtual displacements, where all governing equations are expressed in terms of the displacements. The mixed and hybrid finite element models are based on modified or mixed variations of the plate theories, in which both displacements and stresses are independently approximated. The equilibrium models are based on the principle of virtual forces. Among the three types of models, the displacement finite element models are the most commonly used in commercial finite element programs.

The objective of this chapter is to develop a finite element model for a laminated composite plate, using a simple, higher-order, shear deformation theory. The model is then validated for different boundary conditions and loading cases. Bending, free vibration and stress analyses are performed using the proposed theory.

B. GENERAL THEROY

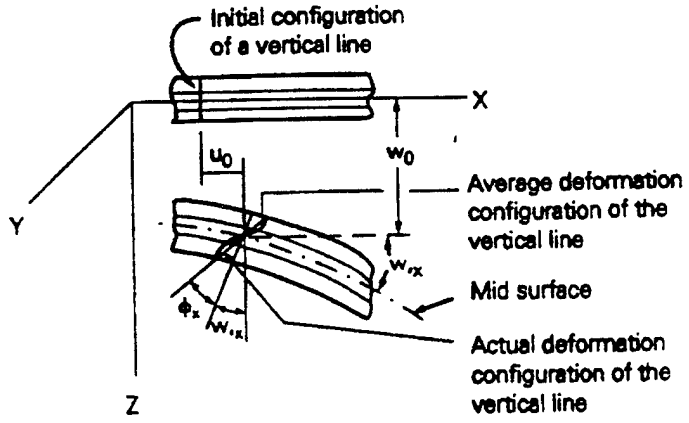

Figure 2.1: Deformation of the normal to the mid-plane "From Ref. [45]."

A typical rectangular laminated plate has a length a, width b, and thickness t. The laminate is composed of a number of perfectly bonded orthotropic layers (laminae), which are placed sequentially one after another. A coordinate system is adopted such that the x-y plane coincides with the mid-plane of the plate, and the z axis is perpendicular to the plane. The present theory is formulated based on the following displacement fields [Ref. 45];

$$U(x,y,z) = U(x,y,0) + z\phi_x(x,y,0) + z^2\zeta_x(x,y,0) + z^3\varsigma_x(x,y,0) \qquad (2.1)$$
$$= U_0 + z\phi_{x0} + z^2\zeta_{x0} + z^3\varsigma_{x0}$$

$$V(x,y,z) = V(x,y,0) + z\phi_y(x,y,0) + z^2\zeta_x(x,y,0) + z^3\varsigma_y(x,y,0)$$
$$= V_0 + z\phi_{y0} + z^2\zeta_{y0} + z^3\varsigma_{y0}$$

$$W(x,y,z) = W(x,y,0) = W_0$$

where;

U_0, V_0 and W_0 are the displacements of a point on the reference surface with coordinates (x_0, y_0, z_0). ϕ_x and ϕ_y are the average rotations about the Y and X axes respectively of the normal to the mid-surface of the undeformed plate, and z is the distance of a point from the mid-plane along the Z axis as shown in Figure (2.1). The remaining terms correspond to higher order rotations. Applying the conditions that the top and the bottom surface are free from transverse shear stresses;

$$\tau_{xz}(x,y,\pm t/2) = 0 \qquad \text{and} \quad \tau_{yz}(x,y,\pm t/2) = 0 \qquad (2.2)$$

where t is the plate thickness. For an orthotropic plate, this means that the shear strains are zeros, i.e.

$$\varepsilon_{xz}(x,y,\pm t/2) = 0 \qquad \text{and} \quad \varepsilon_{yz}(x,y,\pm t/2) = 0; \qquad (2.3)$$

Differentiating equation (2.1) and substituting in equation (2.3)

$$\varepsilon_{xz} = \partial U / \partial z + \partial W / \partial x \tag{2.4}$$

$$\varepsilon_{xz}\Big|_{z=\pm t/2} = \phi_{x0} + 2z\zeta_{x0} + 3z^2\varsigma_{x0} + \partial W / \partial x\Big|_{z=\pm t/2} = 0$$

$$\varepsilon_{xz}\Big|_{z=\pm t/2} = \phi_{x0} \pm t\zeta_{x0} + (3/4)t^2\varsigma_{x0} + \partial w / \partial x = 0$$

$$\varepsilon_{yz} = \partial V / \partial z + \partial W / \partial y \tag{2.5}$$

$$\varepsilon_{yz}\Big|_{z=\pm t/2} = \phi_{y0} + 2z\zeta_{y0} + 3z^2\varsigma_{y0} + \partial W / \partial y\Big|_{z=\pm t/2} = 0$$

$$\varepsilon_{yz}\Big|_{z=\pm t/2} = \phi_{y0} \pm t\zeta_{y0} + (3/4)t^2\varsigma_{y0} + \partial w / \partial y = 0$$

By solving equations (2.4) and (2.5), we get

$$\zeta_{x0} = 0; \qquad \zeta_{y0} = 0; \tag{2.6}$$

$$\varsigma_{x0} = -\frac{4}{3t^2}\left(\phi_{x0} + \partial w / \partial x\right) \qquad \text{and} \qquad \varsigma_{y0} = -\frac{4}{3t^2}\left(\phi_{y0} + \partial w / \partial y\right)$$

Substituting equation (2.6) into equation (2.1), we get

$$U(x,y,z) = U_0 + z\left[\phi_{x0} - \frac{4}{3}\left(\frac{z}{t}\right)^2\left(\phi_{x0} + \partial w / \partial x\right)\right] \tag{2.7}$$

$$V(x,y,z) = V_0 + z\left[\phi_{y0} - \frac{4}{3}\left(\frac{z}{t}\right)^2\left(\phi_{y0} + \partial w / \partial y\right)\right]$$

$$W(x,y,z) = W_0$$

The displacements at any point in the plate are given in terms of the seven unknown quantities $U_0, V_0, W_0, \phi_{x0}, \phi_{y0}, \partial w/\partial x$, and $\partial w/\partial y$.

C. STRAIN-DISPLACEMENT RELATIONS

The linear strain-displacement relation in the Cartesian coordinate system is

$$\{\varepsilon\} = \begin{Bmatrix} \varepsilon_x \\ \varepsilon_y \\ \varepsilon_{xy} \\ \varepsilon_{xz} \\ \varepsilon_{yz} \end{Bmatrix} = \begin{Bmatrix} \partial U/\partial x \\ \partial U/\partial y \\ (\partial U/\partial y + \partial V/\partial x) \\ (\partial U/\partial z + \partial W/\partial x) \\ (\partial V/\partial z + \partial W/\partial y) \end{Bmatrix} \tag{2.8}$$

By substituting equation (2.7) into equation (2.8), we get

$$\{\varepsilon\} = \begin{Bmatrix} \varepsilon_x \\ \varepsilon_y \\ \varepsilon_{xy} \\ \varepsilon_{xz} \\ \varepsilon_{yz} \end{Bmatrix} = \begin{Bmatrix} U_{0,x} + z(\phi_{x0,x} - 4(\partial^2 w/\partial x^2 + \phi_{x0,x})z^2/3t^2 \\ V_{o,y} + z(\phi_{y0,y} - 4(\partial^2 w/\partial y^2 + \phi_{y0,y})z^2/3t^2 \\ U_{0,y} + V_{0,x} + z(\phi_{x0,y} + \phi_{y0,x} - 4(2\partial^2 w/\partial x\partial y + \phi_{x0,y} + \phi_{y0,x})z^2/3t^2) \\ \phi_{xo} - 4(z/t)^2(\partial w/\partial x + \phi_{x0}) + \partial W_0/\partial x \\ \phi_{y0} - 4(z/t)^2(\partial w/\partial y + \phi_{y0}) + \partial W_0/\partial y \end{Bmatrix}$$

or

$$\{\varepsilon\} = \begin{Bmatrix} \varepsilon_x^0 \\ \varepsilon_y^0 \\ \varepsilon_{xy}^0 \\ \varepsilon_{xz}^0 \\ \varepsilon_{yz}^0 \end{Bmatrix} + z\begin{Bmatrix} K_x^1 \\ K_y^1 \\ K_{xy}^1 \\ 0 \\ 0 \end{Bmatrix} + z^2\begin{Bmatrix} 0 \\ 0 \\ 0 \\ K_{xz}^2 \\ K_{yz}^2 \end{Bmatrix} + z^3\begin{Bmatrix} K_x^3 \\ K_y^3 \\ K_{xy}^3 \\ 0 \\ 0 \end{Bmatrix} \tag{2.9}$$

where;

$$\varepsilon_x^0 = U_{0,x};$$

$$\varepsilon_y^0 = V_{0,y};$$

$$\varepsilon_{xy}^0 = U_{0,y} + V_{0,x};$$

$$\varepsilon_{xz}^0 = \phi_{x0} + W_{0,x};$$

$$\varepsilon_{yz}^0 = \phi_{y0} + W_{0,y};$$

$$K_x^1 = \phi_{x0,x};$$

$$K_y^1 = \phi_{y0,y};$$

$$K_{xy}^1 = \phi_{x0,y} + \phi_{y0,x};$$

$$K_{xz}^2 = -4(\partial w/\partial x + \phi_{x0})/t^2;$$

$$K_{yz}^2 = -4(\partial w/\partial y + \phi_{y0})/t^2;$$

$$K_x^3 = -4(\partial^2 w/\partial x^2 + \phi_{xo,x})/(3t^2);$$

$$K_y^3 = -4(\partial^2 w/\partial y^2 + \phi_{y0,y})/(3t^2);$$

and

$$K_{xy}^3 = -4(2\partial^2 w/\partial x\partial y + \phi_{x0,y} + \phi_{y0,x})/3t^2); \qquad (2.10)$$

which includes linear strains, curvatures, twists and other higher order curvatures.

D. SRESS-STRAIN RELATIONS

For anisotropic lamina, there are no planes of symmetry for the material properties. If there is one plane of material property symmetry, where the plane of symmetry is z=0 a material is termed monoclinic, and has 13 independent elastic constants . For a monoclinic

material, the stress-strain relationship is:

$$\begin{Bmatrix} \sigma_x \\ \sigma_y \\ \sigma_z \\ \sigma_{xy} \\ \sigma_{xz} \\ \sigma_{yz} \end{Bmatrix} = \begin{bmatrix} C_{11} & C_{12} & C_{13} & C_{14} & 0 & 0 \\ C_{21} & C_{22} & C_{23} & C_{24} & 0 & 0 \\ C_{31} & C_{32} & C_{33} & C_{34} & 0 & 0 \\ C_{41} & C_{42} & C_{43} & C_{44} & 0 & 0 \\ 0 & 0 & 0 & 0 & C_{55} & C_{56} \\ 0 & 0 & 0 & 0 & C_{65} & C_{66} \end{bmatrix} \begin{Bmatrix} \varepsilon_x \\ \varepsilon_y \\ \varepsilon_z \\ \varepsilon_{xy} \\ \varepsilon_{xz} \\ \varepsilon_{yz} \end{Bmatrix} \tag{2.11}$$

Since the normal stress σ_z is small, it can be neglected. The corresponding ε_z can be eliminated by putting σ_z equal to zero in equation (2.11). This gives the reduced stress-strain relationship as

$$\begin{Bmatrix} \sigma_x \\ \sigma_y \\ \sigma_{xy} \\ \sigma_{xz} \\ \sigma_{yz} \end{Bmatrix} = \begin{bmatrix} C'_{11} & C'_{12} & C'_{14} & 0 & 0 \\ C'_{21} & C'_{22} & C'_{24} & 0 & 0 \\ C'_{41} & C'_{42} & C'_{44} & 0 & 0 \\ 0 & 0 & 0 & C'_{55} & C'_{56} \\ 0 & 0 & 0 & C'_{65} & C'_{66} \end{bmatrix} \begin{Bmatrix} \varepsilon_x \\ \varepsilon_y \\ \varepsilon_{xy} \\ \varepsilon_{xz} \\ \varepsilon_{yz} \end{Bmatrix} \tag{2.12}$$

where;

$$C'_{11} = C_{11} - \frac{C_{13}C_{13}}{C_{33}};$$

$$C'_{12} = C_{12} - \frac{C_{13}C_{23}}{C_{33}};$$

$$C'_{14} = C_{14} - \frac{C_{13}C_{43}}{C_{33}};$$

$$C'_{21} = C_{21} - \frac{C_{23}C_{13}}{C_{33}};$$

$$C'_{22} = C_{22} - \frac{C_{23}C_{23}}{C_{33}};$$

$$C_{24}^{'} = C_{24} - \frac{C_{23}C_{43}}{C_{33}};$$

$$C_{41}^{'} = C_{41} - \frac{C_{43}C_{13}}{C_{33}};$$

$$C_{42}^{'} = C_{42} - \frac{C_{43}C_{23}}{C_{33}};$$

$$C_{44}^{'} = C_{44} - \frac{C_{43}C_{43}}{C_{33}};$$

$$C_{55}^{'} = C_{55}; \qquad C_{56}^{'} = C_{56};$$

$$C_{65}^{'} = C_{65}; \quad \text{and} \quad C_{66}^{'} = C_{66} \tag{2.13}$$

or in short form; $C_{ij}^{'} = C_{ij} - C_{i3}C_{j3} / C_{33}$ for i, j = 1,2,4

$C_{ij}^{'} = C_{ij}$ for i, j = 5,6

and the C_{ij} coefficients [Refs. 96, 97];

$$C_{11} = \frac{1 - \upsilon_{23}\upsilon_{32}}{E_2E_3\Delta}; \tag{2.14}$$

$$C_{12} = \frac{\upsilon_{21} + \upsilon_{31}\upsilon_{23}}{E_2E_3\Delta} = \frac{\upsilon_{12} + \upsilon_{32}\upsilon_{13}}{E_1E_3\Delta};$$

$$C_{13} = \frac{\upsilon_{31} + \upsilon_{21}\upsilon_{32}}{E_2E_3\Delta} = \frac{\upsilon_{13} + \upsilon_{12}\upsilon_{23}}{E_1E_2\Delta};$$

$$C_{22} = \frac{1 - \upsilon_{13}\upsilon_{31}}{E_1E_3\Delta};$$

$$C_{23} = \frac{\upsilon_{32} + \upsilon_{12}\upsilon_{31}}{E_1E_3\Delta} = \frac{\upsilon_{23} + \upsilon_{21}\upsilon_{13}}{E_1E_2\Delta};$$

$$C_{33} = \frac{1 - \upsilon_{12}\upsilon_{21}}{E_1E_2\Delta};$$

$C_{44} = G_{12}$;

$C_{55} = G_{13}$;

$C_{66} = G_{23}$;

and;

$$\Delta = \frac{1 - \upsilon_{12}\upsilon_{21} - \upsilon_{23}\upsilon_{32} - \upsilon_{31}\upsilon_{13} - 2\upsilon_{21}\upsilon_{32}\upsilon_{13}}{E_1 E_2 E_3}$$

where E_1, E_2, E_3 are the Young's moduli in the 1, 2, and 3 directions, respectively; υ_{ij} is the Poisson's ratio for transverse strain in the j-direction when stressed in the i-direction.

For orthotropic lamina there are two orthogonal planes of material property symmetry for the material, and symmetry will exist relative to the third mutually orthogonal plane. The stress-strain relations equation (2.11), in coordinates aligned with principal material directions have no interaction between normal stresses and shearing strains; i.e., $C_{14} = C_{24} = C_{34} = C_{45} = 0$; Thus the stress-strain relation of an orthotropic lamina is;

$$\begin{Bmatrix} \sigma_x \\ \sigma_y \\ \sigma_{xy} \\ \sigma_{xz} \\ \sigma_{yz} \end{Bmatrix} = \begin{bmatrix} C_{11}' & C_{12}' & 0 & 0 & 0 \\ C_{21}' & C_{22}' & 0 & 0 & 0 \\ 0 & 0 & C_{44}' & 0 & 0 \\ 0 & 0 & 0 & C_{55}' & 0 \\ 0 & 0 & 0 & 0 & C_{66}' \end{bmatrix} \begin{Bmatrix} \varepsilon_x \\ \varepsilon_y \\ \varepsilon_{xy} \\ \varepsilon_{xz} \\ \varepsilon_{yz} \end{Bmatrix} \tag{2.15}$$

If the fibers are oriented at an angle θ with the x-axis as shown in Figure 2.2, the transformed stress-strain relation for a lamina will be

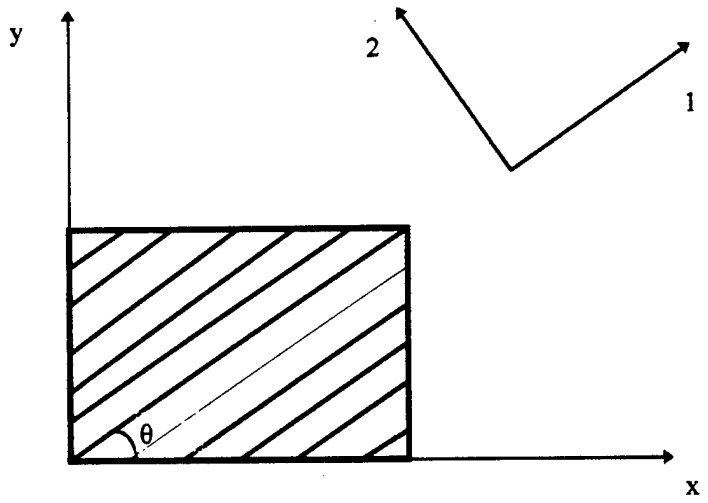

Figure 2.2: An off-axis unidirectional lamina.

$$\begin{Bmatrix} \sigma_x \\ \sigma_y \\ \sigma_{xy} \\ \sigma_{xz} \\ \sigma_{yz} \end{Bmatrix} = \begin{bmatrix} Q_{11} & Q_{12} & Q_{14} & 0 & 0 \\ Q_{21} & Q_{22} & Q_{24} & 0 & 0 \\ Q_{41} & Q_{42} & Q_{44} & 0 & 0 \\ 0 & 0 & 0 & Q_{55} & Q_{56} \\ 0 & 0 & 0 & Q_{65} & Q_{66} \end{bmatrix} \begin{Bmatrix} \varepsilon_x \\ \varepsilon_y \\ \varepsilon_{xy} \\ \varepsilon_{xz} \\ \varepsilon_{yz} \end{Bmatrix} \tag{2.16}$$

in short form;

$$[\sigma] = [Q]\{\varepsilon\} \tag{2.17}$$

where;

$$Q_{11} = C_{11}^{'}\cos^4\theta + 2(C_{12}^{'} + 2C_{44}^{'})\cos^2\theta\sin^2\theta + C_{22}^{'}\sin^4\theta \tag{2.18}$$

$$Q_{12} = (C_{11}^{'} + C_{22}^{'} - 4C_{44}^{'})\cos^2\theta\ \sin^2\theta + C_{12}^{'}(\cos^4\theta + \sin^4\theta)$$

$$Q_{14} = (C_{11}^{'} - 2C_{44}^{'} - C_{12}^{'})\cos^3\theta\sin\theta + (C_{12}^{'} - C_{22}^{'} + 2C_{44}^{'})\cos\theta\sin^3\theta$$

$$Q_{22} = C_{11}^{'}\sin^4\theta + 2(C_{12}^{'} + 2C_{44}^{'})\cos^2\theta\sin^2\theta + C_{22}^{'}\cos^4\theta$$

$$Q_{24} = (C_{11}^{'} - 2C_{44}^{'} - C_{12}^{'})\cos\theta\sin^3\theta + (C_{12}^{'} - C_{22}^{'} + 2C_{44}^{'})\cos^3\theta\sin\theta$$

$$Q_{44} = (C_{11}^{'} + C_{22}^{'} - 2C_{44}^{'})\cos^2\theta\sin^2\theta + C_{44}^{'}(\cos^4 + \sin^4\theta)$$

$$Q_{55} = C_{55}^{'}\cos^2\theta + C_{66}^{'}\sin^2\theta$$

$$Q_{56} = (C_{55}^{'} - C_{66}^{'})\cos\theta\sin\theta$$

$$Q_{66} = C_{55}^{'}\sin^2\theta + C_{66}^{'}\cos^2\theta$$

E. STRESS RESULTANT-STRAIN RELATIONS

Combining equation (2.9) with equation (2.16) and integrating layer-by-layer over the thickness, the following relations of the stress resultant are obtained [Ref. 96];

$$(N_x, M_x, P_x) = \int_{-t/2}^{t/2} \sigma_x(1, z, z^3)dz; \qquad (2.19)$$

$$(N_y, M_y, P_y) = \int_{-t/2}^{t/2} \sigma_y(1, z, z^3)dz;$$

$$(N_{xy}, M_{xy}, P_{xy}) = \int_{-t/2}^{t/2} \sigma_{xy}(1, z, z^3)dz;$$

$$(Q_{xz}, R_{xz}) = \int_{-t/2}^{t/2} \sigma_{xz}(1, z^2)dz$$

and

$$(Q_{yz}, R_{yz}) = \int_{-t/2}^{t/2} \sigma_{yz}(1, z^2)dz.$$

The above equations can be set in the matrix form as;

$$\begin{Bmatrix} N_x \\ N_y \\ N_{xy} \\ Q_{xz} \\ Q_{yz} \\ M_x \\ M_y \\ M_{xy} \\ R_{xz} \\ R_{yz} \\ P_x \\ P_y \\ P_{xy} \end{Bmatrix} = \begin{bmatrix} A_{11} & A_{12} & A_{14} & 0 & 0 & B_{11} & B_{12} & B_{14} & 0 & 0 & E_{11} & E_{12} & E_{14} \\ & A_{22} & A_{24} & 0 & 0 & B_{21} & B_{22} & B_{24} & 0 & 0 & E_{21} & E_{22} & E_{24} \\ & & A_{44} & 0 & 0 & B_{41} & B_{42} & B_{44} & 0 & 0 & E_{41} & E_{42} & E_{44} \\ & & & A_{55} & A_{56} & 0 & 0 & 0 & D_{55} & D_{56} & 0 & 0 & 0 \\ & & & & A_{66} & 0 & 0 & 0 & D_{65} & D_{66} & 0 & 0 & 0 \\ & & & & & D_{11} & D_{12} & D_{14} & 0 & 0 & F_{11} & F_{12} & F_{14} \\ & & & & & & D_{22} & D_{24} & 0 & 0 & F_{21} & F_{22} & F_{24} \\ & & & & & & & D_{44} & 0 & 0 & F_{41} & F_{42} & F_{44} \\ & & & & & & & & F_{55} & F_{56} & 0 & 0 & 0 \\ & & & & & & & & & F_{66} & 0 & 0 & 0 \\ & & Sym. & & & & & & & & H_{11} & H_{12} & H_{14} \\ & & & & & & & & & & & H_{22} & H_{24} \\ & & & & & & & & & & & & H_{44} \end{bmatrix} \begin{Bmatrix} \varepsilon_x^0 \\ \varepsilon_y^0 \\ \varepsilon_{xy}^0 \\ \varepsilon_{xz}^0 \\ \varepsilon_{yz}^0 \\ K_x^1 \\ K_y^1 \\ K_{xy}^1 \\ K_{xz}^2 \\ K_{yz}^2 \\ K_x^3 \\ K_y^3 \\ K_{xy}^3 \end{Bmatrix}$$

or in compact form

$$\{N\} = [\overline{D}]\{\varepsilon^0\} \tag{2.20}$$

where ;

$[\overline{D}]$=Rigidity matrix

$[A]$ = Extensional stiffness matrix

$[B]$ = Coupling stiffness matrix

$[D]$ = Bending stiffness matrix

$[E]$,$[F]$, and$[\mathrm{H}]$ = Higher order matrices

which are given for n layer by:

$$(A_{ij}, B_{ij}, D_{ij}, E_{ij}, F_{ij} H_{ij}) = \sum_{k=1}^{n} \int_{z_k}^{z_{k+1}} Q_{ij}(1, z, z^2, z^3, z^4, z^6) dz \qquad \text{(for j,i=1,...,6)} \tag{2.21}$$

F. VARIATIONAL PRINCIPLE

The generalizd form of Hamilton's principle, which states that the variation of the Lagrangian during any time interval must be zero, has the form:

$$\int_{t1}^{2} \delta(\Im + W)dt = 0, \tag{2.22}$$

where t_1 and t_2 are the time interval.

The Lagrangian $\Im$ of a body is defined by the summation of all kinetic energy λ and potential energy $\hbar$.

$$\Im = \int_V (\lambda - \hbar)dV \tag{2.23}$$

where;

$$\lambda = \int_V \frac{1}{2}\rho\{\dot{q}\}^T\{\dot{q}\}dV \tag{2.24}$$

$$\hbar = \int_V \frac{1}{2}\{\varepsilon\}^T\{\sigma\}dV \tag{2.25}$$

Thus the Lagrangian is

$$\Im = \int_V \left[\frac{1}{2}\rho\{\dot{q}\}^T\{\dot{q}\} - \frac{1}{2}\{\varepsilon\}^T\{\sigma\}\right]dV \tag{2.26}$$

where;

$\dot{q}$ is the velocity (time derivative of the displacement q);

$\Im$ is the Lagrangian;

V is the volume.

The virtual work δW done by the external applied force is

$$\delta W = \int_s \{\delta q\}^T \{P_s\}ds \tag{2.27}$$

where;

s is the surface areas at which the mechanical load is applied

P_s is a surface load vector (N/m^2).

Substituting equations (2.26) and (2.27) into the Hamilton's equation (2.22), yields the variational equation as:

$$\int_{t_1}^{t_2} [\int_V \delta(\frac{1}{2}\rho\{\dot{q}\}^T\{\dot{q}\} - \frac{1}{2}\{\varepsilon\}^T\{\sigma\})dV + \int_s \{\delta q\}^T\{P_s\}ds]\ dt = 0 \tag{2.28}$$

Since all the variations must vanish at $t = t_1$ and $t = t_2$, by substituting equation (2.17), and taking the variation, the variational equation takes the form:

$$\int_V \rho\{\delta q\}^T\{\ddot{q}\}\,dV + \int_V \{\delta\varepsilon\}^T[Q]\{\varepsilon\}\,dV - \int_s \{\delta q\}^T\{P_s\}ds = 0 \tag{2.29}$$

G. FINITE ELEMENT FORMULATION

The objective is to define the degrees of freedom $U_0, V_0, \phi_{x0}, \phi_{y0}, W_0, w_x$, and w_y in the plate in terms of nodal displacements and rotations by using a bilinear, isoparametric, rectangular element with four node. Each node of the element has seven degrees of freedom. Similar interpolation functions for the element coordinates x and y; the in-plane displacements U_0 and V_0 and the two rotations ϕ_{x0} and ϕ_{y0} were used. They were defined by;

$$p = \sum_{i=1}^{4} N_i p_i \tag{2.30}$$

where;

p is the value of the variable at any point in the element

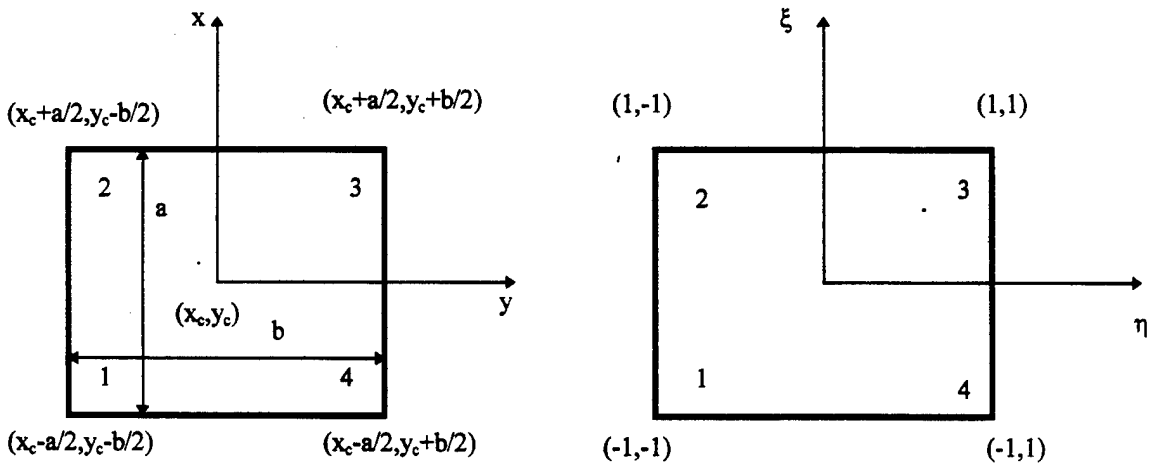

Actual element

Master element

$$\xi = 2(x - x_c)/a, \quad \eta = 2(y - y_c)/b$$

Figure 2.3: Actual and master element.

p_i is its value at node point

N_i is the interpolation function, which in the natural coordinate system (ξ,η) is;

$$N_i = 1/4(1 + \xi\xi_i)(1 + \eta\eta_i) \tag{2.31}$$

where;

ξ and η are the local coordinates of the point, and $\xi_i = -1,1,1,-1$ and

$\eta_i = -1,-1,1,1$ for $i = 1,..,4$, as shown in Figure (2.3)

The transverse displacement is interpolated using a non-conforming shape function [Ref. 98], which can be given by;

$$w(x,y) = \begin{bmatrix} f_1 & g_1 & h_1 & f_2 & g_2 & h_2 & f_3 & g_3 & h_3 & f_4 & g_4 & h_4 \end{bmatrix} \begin{bmatrix} W_{01} \\ w_{,x1} \\ w_{,y1} \\ W_{02} \\ \cdot \\ \cdot \\ \cdot \\ w_{,x4} \\ w_{,y4} \end{bmatrix} \tag{2.32}$$

where for $i = 1 \rightarrow 4$

$$f_i = (1/8)(1+\xi\xi_i)(1+\eta\eta_i)(2+\xi\xi_i+\eta\eta_i-\eta^2-\xi^2) \tag{2.33}$$

$$g_i = (a/16)\xi_i(1+\xi\xi_i)^2(1+\eta\eta_i)(\xi\xi_i-1)$$

$$h_i = (b/16)\eta_i(1+\eta\eta_i)^2(1+\xi\xi_i)(\eta\eta_i-1)$$

where;

$$\xi = 2(x-x_c)/a, \quad \eta = 2(y-y_c)/b, \tag{2.34}$$

(x_c, y_c) are the centroid coordinates of the plate , and the non-dimensional coordinates of the nodes are (-1,-1), (1,-1), (1,1), and (-1,1), respectively.

The nodal displacement vector $\{q_1\}$ at the first node point on the reference surface is;

$$\{q_1\} = \begin{bmatrix} U_{01} & V_{01} & \phi_{x01} & \phi_{y01} & W_{01} & w_{,x1} & w_{,y1} \end{bmatrix}^T \tag{2.35}$$

and the element displacement vector $\{q_e\}$ is;

$$\{q_e\} = \begin{bmatrix} q_1 & q_2 & q_3 & q_4 \end{bmatrix}^T \tag{2.36}$$

The generalized displacement vector at a point is

$$\{q\} = \begin{bmatrix} U_0 & V_0 & \phi_{x0} & \phi_{y0} & W_0 & w_{,x} & w_{,y} \end{bmatrix}^T \tag{2.37}$$

Substituting equations (2.30) and (2.37) in to equation (2.10), we obtain the strain vector at the mid-plane in a matrix form

$$
\begin{Bmatrix} \varepsilon_x^0 \\ \varepsilon_y^0 \\ \varepsilon_{xy}^0 \\ \varepsilon_{xz}^0 \\ \varepsilon_{yz}^0 \\ K_x^1 \\ K_y^1 \\ K_{xy}^1 \\ \overline{K}_{xz}^2 \\ \overline{K}_{yz}^2 \\ \overline{K}_x^3 \\ \overline{K}_y^3 \\ \overline{K}_{xy}^3 \end{Bmatrix} =
\begin{bmatrix}
N_{1,x} & & & & & & & \cdots \\
 & N_{1,y} & & & & & & \cdots \\
N_{1,y} & N_{1,x} & & & & & & \cdots \\
 & & N_1 & & f_{1,x} & g_{1,x} & h_{1,x} & \cdots \\
 & & & N_1 & f_{1,y} & g_{1,y} & h_{1,y} & \cdots \\
 & & N_{1,x} & & & & & \cdots \\
 & & & N_{1,y} & & & & \cdots \\
 & & N_{1,y} & N_{1,x} & & & & \cdots \\
 & & N_1 & & f_{1,x} & g_{1,x} & h_{1,x} & \cdots \\
 & & & N_1 & f_{1,y} & g_{1,y} & h_{1,y} & \cdots \\
 & & N_{1,x} & & f_{1,xx} & g_{1,xx} & h_{1,xx} & \cdots \\
 & & & N_{1,y} & f_{1,yy} & g_{1,yy} & h_{1,yy} & \cdots \\
 & & N_{1,y} & N_{1,x} & 2f_{1,xy} & 2g_{1,xy} & 2h_{1,xy} & \cdots
\end{bmatrix}
\begin{Bmatrix} U_{01} \\ V_{01} \\ \phi_{x01} \\ \cdot \\ \cdot \\ \cdot \\ U_{02} \\ V_{02} \\ \cdot \\ \cdot \\ \cdot \\ U_{04} \\ V_{04} \\ \phi_{x04} \\ \phi_{y04} \\ W_{04} \\ w_{4,x} \\ w_{4,y} \end{Bmatrix}
$$

where;

$\overline{K}_{xz}^2 = K_{xz}^2 / \ell_1$; $\quad \overline{K}_{yz}^2 = K_{yz}^{2;} / \ell_1$

$\overline{K}_x^3 = K_x^3 / \ell_2$; $\quad \overline{K}_y^3 = K_y^3 / \ell_2$;

$\overline{K}_{xy}^3 = K_{xy}^3 / \ell_2$;

$\ell_1 = -4/t^2$; $\quad \ell_2 = -4/3t^2$.

In a short form $$\{\varepsilon^0\} = [B]\{q_e\}. \tag{2.38}$$

where the nodal strain-displacement matrix B is given by

$$[B] = \begin{bmatrix} [B_1] & [B_2] & [B_3] & [B_4] \end{bmatrix} \tag{2.39}$$

The first, second, and higher order derivatives of the interpolation functions which are expressed in equations (2.38) and (2.39) can be evaluated with respect to the global coordinates. An additional computations were involved which can be expressed as. Let Ψ represent one of the interpolation functions which has been used (i.e. N_i, f_i, g_i, and/or h_i).

The first order derivatives with respect to the global coordinates are related to those with respect to the local (or element) coordinates according to:

$$\begin{Bmatrix} \frac{\partial \Psi_i}{\partial x} \\ \frac{\partial \Psi_i}{\partial y} \end{Bmatrix} = \begin{bmatrix} \frac{\partial x}{\partial \xi} & \frac{\partial y}{\partial \xi} \\ \frac{\partial x}{\partial \eta} & \frac{\partial y}{\partial \eta} \end{bmatrix}^{-1} \begin{Bmatrix} \frac{\partial \Psi_i}{\partial \xi} \\ \frac{\partial \Psi_i}{\partial \eta} \end{Bmatrix} \equiv [J]^{-1} \begin{Bmatrix} \frac{\partial \Psi_i}{\partial \xi} \\ \frac{\partial \Psi_i}{\partial \eta} \end{Bmatrix} \tag{2.40}$$

where the Jacobian matrix $[J]$ is evaluated using the approximation of the geometry which may take the form:

$$\begin{aligned} x &= x_c + \xi a/2; \\ y &= y_c + \eta b/2 \end{aligned} \tag{2.41}$$

or

$$\begin{aligned} x &= \frac{x_1 + x_4}{2} + \xi a/2; \\ y &= \frac{y_1 + y_4}{2} + \eta b/2 \end{aligned}$$

The second order derivatives of Ψ_i with respect to the global coordinates (x, y) are given by:

$$\begin{Bmatrix} \frac{\partial^2\Psi_i}{\partial x^2} \\ \frac{\partial^2\Psi_i}{\partial y^2} \\ \frac{\partial^2\Psi_i}{\partial x\partial y} \end{Bmatrix} = [J_1]^{-1}\left(\begin{Bmatrix} \frac{\partial^2\Psi_i}{\partial \xi^2} \\ \frac{\partial^2\Psi_i}{\partial \eta^2} \\ \frac{\partial^2\Psi_i}{\partial \xi\partial \eta} \end{Bmatrix} - [J_2]\begin{Bmatrix} \frac{\partial\Psi_i}{\partial x} \\ \frac{\partial\Psi_i}{\partial y} \end{Bmatrix} \right) \tag{2.42}$$

where;

$$[J_1] = \begin{bmatrix} \left(\frac{\partial x}{\partial \xi}\right)^2 & \left(\frac{\partial y}{\partial \xi}\right)^2 & 2\frac{\partial y}{\partial \xi}\frac{\partial x}{\partial \xi} \\ \left(\frac{\partial x}{\partial \eta}\right)^2 & \left(\frac{\partial y}{\partial \eta}\right)^2 & 2\frac{\partial x}{\partial \eta}\frac{\partial y}{\partial \eta} \\ \frac{\partial x}{\partial \eta}\frac{\partial x}{\partial \xi} & \frac{\partial y}{\partial \eta}\frac{\partial y}{\partial \xi} & \frac{\partial x}{\partial \eta}\frac{\partial y}{\partial \xi} + \frac{\partial y}{\partial \eta}\frac{\partial x}{\partial \xi} \end{bmatrix} \tag{2.43}$$

$$[J_2] = \begin{bmatrix} \frac{\partial^2 x}{\partial \xi^2} & \frac{\partial^2 y}{\partial \xi^2} \\ \frac{\partial^2 x}{\partial \eta^2} & \frac{\partial^2 y}{\partial \eta^2} \\ \frac{\partial^2 x}{\partial \eta\partial \xi} & \frac{\partial^2 y}{\partial \xi\partial \eta} \end{bmatrix} \tag{2.44}$$

The elements of the matrices $[J_1]$ and $[J_2]$ are computed using equation (2.41).

The generalized strain at a point is related to the reference surface strain as:

$$\varepsilon = [B_1]\{\varepsilon_0\} \tag{2.45}$$

where;

$$[B_1]=\begin{bmatrix} 1 & 0 & 0 & 0 & 0 & z & 0 & 0 & 0 & 0 & z^3 & 0 & 0 \\ 0 & 1 & 0 & 0 & 0 & 0 & z & 0 & 0 & 0 & 0 & z^3 & 0 \\ 0 & 0 & 1 & 0 & 0 & 0 & 0 & z & 0 & 0 & 0 & 0 & z^3 \\ 0 & 0 & 0 & 1 & 0 & 0 & 0 & 0 & z^2 & 0 & 0 & 0 & 0 \\ 0 & 0 & 0 & 0 & 1 & 0 & 0 & 0 & 0 & z^2 & 0 & 0 & 0 \end{bmatrix} \tag{2.46}$$

The reference surface (mid plane) strain can be expressed as;

$$\varepsilon_0 = [B]\{q_e\} \tag{2.47}$$

Thus;

$$\varepsilon = [B_1][B]\{q_e\} \tag{2.48}$$

By using the transformed stress-strain relation,

$$[\sigma] = [Q]\{\varepsilon\} \tag{2.17}$$

in equation (2.49) ,

$$[\sigma] = [Q][B_1][B]\{q_e\} \tag{2.49}$$

H. EQUATION OF MOTION

By substituting equations (2.48) and (2.49) in the Hamliton's equation (2.29) gives the system equations of motion:

$$\int_V \{\delta q_e\}^T \rho [N]^T [N] dV \{\ddot{q}_e\} + \int_V \{\delta q_e\}^T [B]^T [B_1]^T [Q][B_1][B] dV \{q_e\} - \int_S \{\delta q_e\}^T [N]^T \{P_s\} ds = 0 \tag{2.50}$$

In matrix form, the equations of motion can be expressed as:

$$[M_e]\{\ddot{q}_e\} + [K_e]\{q_e\} = \{P_{Me}\} \tag{2.51}$$

where the element mass matrix is;

$$[M_e] = \int_V \rho [N]^T [N] dV \tag{2.52}$$

$$= \int_A [N]^T [\overline{m}][N] d(area)$$

The shape function matrix $[N]$ is given by [Ref. 47];

$$[N] = \sum_{i=1}^{4} \begin{bmatrix} N_i & 0 & 0 & 0 & 0 & 0 & 0 \\ 0 & N_I & 0 & 0 & 0 & 0 & 0 \\ 0 & 0 & N_I & 0 & 0 & 0 & 0 \\ 0 & 0 & 0 & N_I & 0 & 0 & 0 \\ 0 & 0 & 0 & 0 & f_i & g_i & h_i \\ 0 & 0 & 0 & 0 & f_{i,x} & g_{i,x} & h_{i,x} \\ 0 & 0 & 0 & 0 & f_{i,y} & g_{i,y} & h_{i,y} \end{bmatrix} \tag{2.53}$$

$\sum$ denotes the matrix assemblage for the element four nodes, and

$$[\overline{m}] = \begin{bmatrix} I_1 & 0 & 0 & 0 & 0 & 0 & 0 \\ 0 & I_1 & 0 & 0 & 0 & 0 & 0 \\ 0 & 0 & I_2 & 0 & 0 & 0 & 0 \\ 0 & 0 & 0 & I_2 & 0 & 0 & 0 \\ 0 & 0 & 0 & 0 & I_1 & 0 & 0 \\ 0 & 0 & 0 & 0 & 0 & I_2 & 0 \\ 0 & 0 & 0 & 0 & 0 & 0 & I_2 \end{bmatrix} \tag{2.54}$$

in which I_1 and I_2 are the normal and rotational inertia, respectively;

$$(I_1, I_2) = \sum_{i=1}^{n} \int_{z_i}^{z_{i+1}} \rho^i [1, z^2] dz \tag{2.55}$$

where ρ^i is the mass density of the i^{th} layer. The element stiffness matrix has the form;

$$\begin{aligned} [K_e] &= \int_V [B]^T [B_1]^T [Q][B_1][B] dV \\ &= \int_A [B]^T [\overline{D}][B] dA \end{aligned} \tag{2.56}$$

where the rigidity matrix $[\overline{D}]$ for n number of layers is given by;

$$[\overline{D}_{ij}] = \sum_{k=1}^{n} \int_{z_k}^{z_{k+1}} Q_{ij}(1, z, z^2, z^3, z^4, z^6) dz \qquad \text{(for j, i =1,...6)} \tag{2.57}$$

The rigidity matrix $\overline{D}$ is given in equation (2.20), and the mechanical excitation force is given by;

$$[\mathrm{P}_{Me}] = \iint [N_F]^T \{P_s\} ds \tag{2.58}$$

Thus the consistent load vector at node i is

$$\{\mathrm{P}_{Me_i}\} = \int q_0 \begin{bmatrix} 0 \\ 0 \\ 0 \\ 0 \\ f_i \\ g_i \\ h_i \end{bmatrix} ds \tag{2.59}$$

where; q_0 is the intensity of the load per unit area.

Assembling all elemental equations gives the global dynamic system equation:

$$[M]\{\ddot{q}\}+[K]\{q\}=\{P_M\} \tag{2.60}$$

I. NUMERICAL INTEGRATION

The elements of the equation of motion (2.51), which are given individually in equations (2.52), (2.56) and (2.59) can be integrated numerically using Gauss Legendre quadrature (see App. A). A full integration technique of 3×3 Gauss points is used to perform the integrations, and it gives satisfactory results (comparing to the exact and available finite element solutions) for all plates.

$$\begin{aligned}[M_e] &= \int_{A_e}[N]^T[\overline{m}][N]dA_e \\ &= \int_{-1}^{+1}\int_{-1}^{+1}[N]^T[\overline{m}][N]|J|d\xi d\eta\end{aligned} \tag{2.61}$$

$$\begin{aligned}[K_e] &= \int_{-1}^{+1}\int_{-1}^{+1}[B]^T[\overline{D}][B]dA_e \\ &= \int_{-1}^{+1}\int_{-1}^{+1}[B]^T[\overline{D}][B]|J|d\xi d\eta\end{aligned} \tag{2.62}$$

$$\{P_{Me}\}=\sum_{i=1}^{4}\int_{-1}^{+1}\int_{-1}^{+1}q_0\begin{bmatrix}0\\0\\0\\0\\f_i\\g_i\\h_i\end{bmatrix}|J|d\xi d\eta \tag{2.63}$$

J. FREE VIBRATION ANALYSIS

A free vibration analysis can be performed using the equation of motion (2.60), where the right hand side equals zero (the work done by external forces is equal to zero for the free vibration analysis). The effects of the degree of orthotropy, of different stacking sequences, aspect ratio (span-to-thickness ratio) of the structure, numbers of layers and orientation angles of the fibers, on the natural frequencies and mode shapes are demonstrated in the validation part.

K. STRESS ANALYSIS

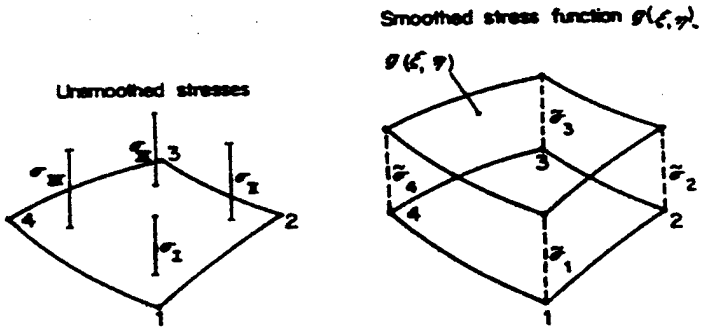

Figure 2.4: Local discrete least squares smoothing "From Ref. [99]."

By solving equation (2.60) for a static deflection, the element displacement vector is computed , which can be substituted into the generalized strain at a point equation (2.48), then into equation (2.17) to get the stress vector at any point in the structure. Stresses are obtained at 2×2 Gauss sampling points, as shown in Figure (2.4) [Ref. 99].

In local discrete smoothing [Ref. 99], it is assumed that $g(\xi,\eta)$ is an exact least squares fit to selected values of $\sigma(\xi,\eta)$ at the Gaussian integration points shown in Figure (2.4). (exact least squares fit is one which passes through all the sampling points and is therefore interpolatory in nature). Thus, the smoothed corner nodal stresses $\tilde{\sigma}_1,\tilde{\sigma}_2,\tilde{\sigma}_3$, and $\tilde{\sigma}_4$ may be obtained from the expression.

$$\begin{Bmatrix}\tilde{\sigma}_1\\ \tilde{\sigma}_2\\ \tilde{\sigma}_3\\ \tilde{\sigma}_4\end{Bmatrix} = \begin{bmatrix} 1+\frac{\sqrt{3}}{2} & -\frac{1}{2} & 1-\frac{\sqrt{3}}{2} & -\frac{1}{2} \\ -\frac{1}{2} & 1+\frac{\sqrt{3}}{2} & -\frac{1}{2} & 1-\frac{\sqrt{3}}{2} \\ 1-\frac{\sqrt{3}}{2} & -\frac{1}{2} & 1+\frac{\sqrt{3}}{2} & -\frac{1}{2} \\ -\frac{1}{2} & 1-\frac{\sqrt{3}}{2} & -\frac{1}{2} & 1+\frac{\sqrt{3}}{2} \end{bmatrix} \begin{Bmatrix}\sigma_I\\ \sigma_{II}\\ \sigma_{III}\\ \sigma_{IV}\end{Bmatrix} \qquad (2.64)$$

where $\sigma_I,\sigma_{II},\sigma_{III}$ and σ_{IV} are the unsmoothed stresses at the Gauss points ($\sigma_I = \sigma(\xi_I,\eta_I)$) as shown in Figure (2.4). The smoothed stress values are then modified by finding the average of the nodal stresses of all elements meeting at a common node.

L. VALIDATION:

To test the validity of the finite element analysis technique and to establish its range of applicability, numerical examples are investigated.

Example 1.

A three- layer (0^0-90^0-0^0), simply supported, square plate of three different span to thickness ratios (λ=10,20,100) is tested . The total thickness of the 0^0 and 90^0 layers is the same. Layers at the same orientation have equal thicknesses (i.e. $t_1=t_3$ and $t_1+t_3=t_2$). The material constants are as follows:

Table 2.1: Boundary Conditions for various different conditions (x = constant).

Simply supported	Clamped	Free
$U \neq 0;\quad V = 0;$	$U = 0;\quad V = 0;$	$U \neq 0;\quad V \neq 0;$
$\phi_{x0} \neq 0;\quad \phi_{y0} = 0;$	$\phi_{x0} = 0;\quad \phi_{y0} = 0;$	$\phi_{x0} \neq 0;\quad \phi_{y0} = 0;$
$w = 0;\quad w_{,x} \neq 0;$	$w = 0;\quad w_{,x} = 0;$	$w \neq 0;\quad w_{,x} \neq 0;$
$w_{,y} = 0$	$w_{,y} = 0$	$w_{,y} \neq 0$

E_{11} = 172.4 GPa (25×10^6 psi);

E_{22} = 6.9 GPa (10^6 psi);

$G_{12} = G_{13}$=3.45 GPa (0.5×10^6 psi);

G_{23} = 1.38 GPa (0.2×10^6 psi);

$\nu_{12} = \nu_{13}$=0.25

Aspect Ratio(length to thickness ratio)=10, 20 and 100;

The plate is subjected to a double sinusoidal load

$$q=q_0\sin(\pi x/a)\sin(\pi y/b)$$

where a = b= L; the plate length. Table 2.1 gives the boundary conditions on the edge x = constant. Similar statements can be made for the edge where y is a constant by interchanging the subscripts for x and y. A 4×4 mesh quarter plate system with 3×3 sampling points, is used in all examples. The results are given in Table 2.2 in normalized quantities. The results are normalized as follows:

$$(\bar{\sigma}_x, \bar{\sigma}, \bar{\sigma}_{xy}) = (1/q_0\lambda^2)(\sigma_x, \sigma_y, \sigma_{xy});$$

$$(\bar{\sigma}_{xz}, \bar{\sigma}_{yz}) = (1/q_0\lambda)(\sigma_{xz}, \sigma_{yz});$$

$$\bar{w} = \pi^4 Qw / 12\lambda^4 t q_0;$$

Table 2.2: Three-Layers cross ply ($0^0/90^0/0^0$) square plate [Ref. 45] subjected to sinusoidal loading ($t_1=t_3 = t/4$, $t_2= t/2$).

λ	S.	w_{max}	E_w	σ_1	E_{σ_1}	σ_2	E_{σ_2}	σ_3	E_{σ_3}
10	A	1.468	-14.0	0.577	+3.29	0.318	-21.07	0.0247	-10.5
	B	1.448	-15.27	0.532	-4.43	0.307	-23.82	0.0250	-9.42
	C	1.534	-10.24	0.484	-13.42	0.350	-13.15	-	-
	D	2.034	19.02	0.542	-3.04	-	-	0.0292	+5.80
	E	1.727	1.04	0.493	-11.81	0.407	0.99	-	-
	F	1.714	0.31	0.554	-0.88	0.397	-1.42	0.0273	-1.12
	G	1.709	-	0.559	-	0.403	-	0.0276	-
20	A	1.119	-5.90	0.556	2.76	0.284	-8.22	0.0224	-2.6
	B	1.114	-6.31	0.557	2.58	0.307	-.65	0.0231	0.4
	C	1.136	-4.48	0.511	-5.89	0.287	-7.12	-	-
	D	1.273	7.07	0.546	0.55	-	-	0.0239	3.9
	E	1.191	0.14	0.533	-1.84	0.312	0.97	-	-
	F	1.191	+0.16	0.538	-0.96	0.308	-1.61	0.0229	-1.3
	G	1.189	-	0.543	-	0.309	-	0.0230	-
100	A	1.004	-0.4	0.543	0.7	0.267	-1.48	0.0215	0.33
	B	1.003	-0.496	0.566	5.01	0.284	4.80	0.0223	4.2
	C	1.005	-0.298	0.523	-2.97	0.263	-2.95	-	-
	D	1.015	0.694	0.551	2.23	-	-	0.0219	2.3
	E	0.999	-0.899	0.537	-0.37	0.265	-2.20	-	-
	F	0.997	-1.11	0.523	-2.89	0.263	-2.81	0.0208	-2.35
	G	1.008	-	0.539	-	0.271	-	0.0214	-
CPT		1.000		0.539		0.269		0.0213	

where;

S is the reference source

A Present finite element.

B FE2/Panda and Natarajan [Ref. 41].

C FE1/Reddy [Ref. 27]

D FE3/Mawenya and Davies [Ref. 40].

E ISPQ/Moser et. al. [Ref. 104].

F FE4/Phan and Reddy [Ref.33].

G Exact/Pagano and Hatfield [Ref. 16].

CPT Classical plate theory.

and

$\lambda = a/t$, where t is the structure thickness.

$Q = 4G_{12} + \left[E_{11} + E_{22}(1+2\upsilon_{12})\right]/(1-\upsilon_{12}\upsilon_{21})$;

$w_{max} = \overline{w}(a/2, a/2, 0)$;

$\sigma_1 = \overline{\sigma}_x(a/2, a/2, \pm 1/2)$

$\sigma_2 = \overline{\sigma}_y(a/2, a/2, \pm 1/4)$;

$\sigma_3 = \overline{\sigma}_{xy}(0, 0, \pm 1/2)$;

E_w = error in w from exact value

E_{σ_1} = error in σ_1 from exact value.

E_{σ_2} = error in σ_2 from exact value.

E_{σ_3} = error in σ_3 from exact value.

Table 2.2 shows that the numerical values of all quantities are converge to the CPT results by increasing the span to thickness ratio λ. A model developed by Reddy [Ref. 27], based on the penalty/YNS, (YNS is a theory of Yang, Norris and Stavsky) with eight node quadrilateral elements and five degrees of freedom per node is perform better for small span-to-thickness ratios λ. Elements developed by Panda, Mawenya and Moser, either have too many structural degrees of freedom, or have unsatisfactory performance comparison to the present model. The Phan and Reddy element gives very good results

compared to the exact solution for the thick plate (small λ), but the error of this element increases with the increase the span to thickness ratio. Thus the conclusion is that for higher span to thickness ratios one can use the present element , and for lower span to thickness ratios, Phan's element can be used for better accuracy. For length to thickness ratios equal to fifty, Figures (2,5), (2.6), and (2.7) show the different stress distributions for a composite laminate using the present finite element method.

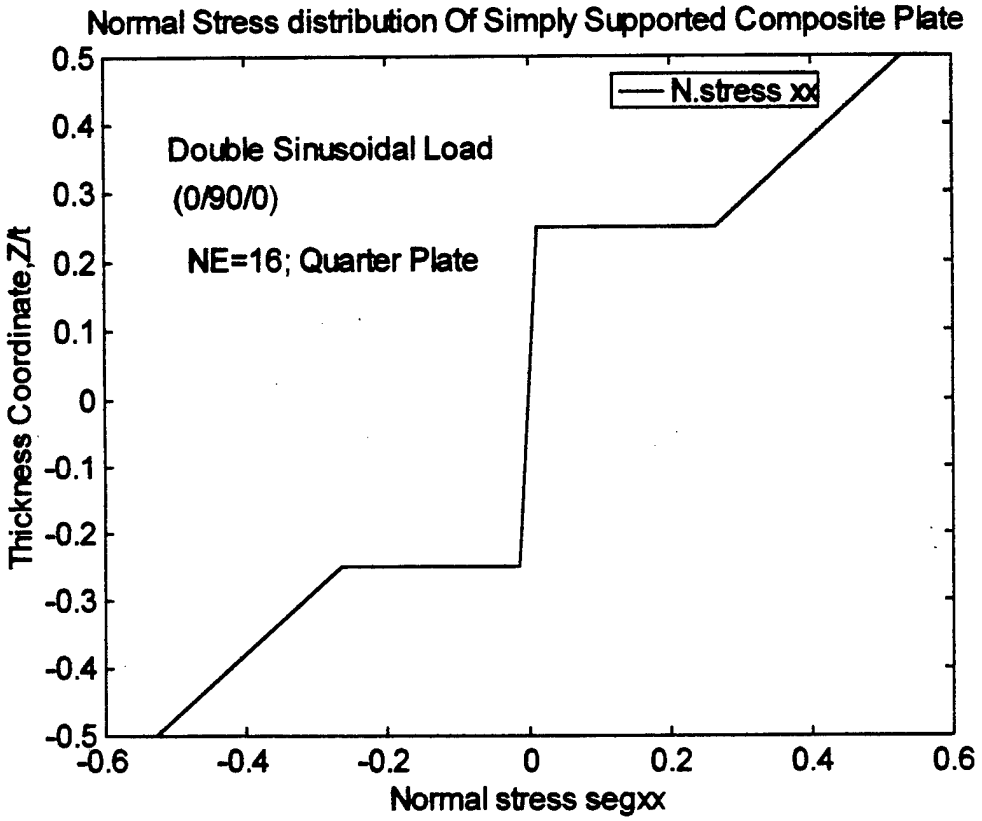

Figure 2.5: Distribution of the in-plane normal stress σ_{xx} for a simply supported laminated square plate ($0^0/90^0/0^0$) subjected to double sinusoidal load.

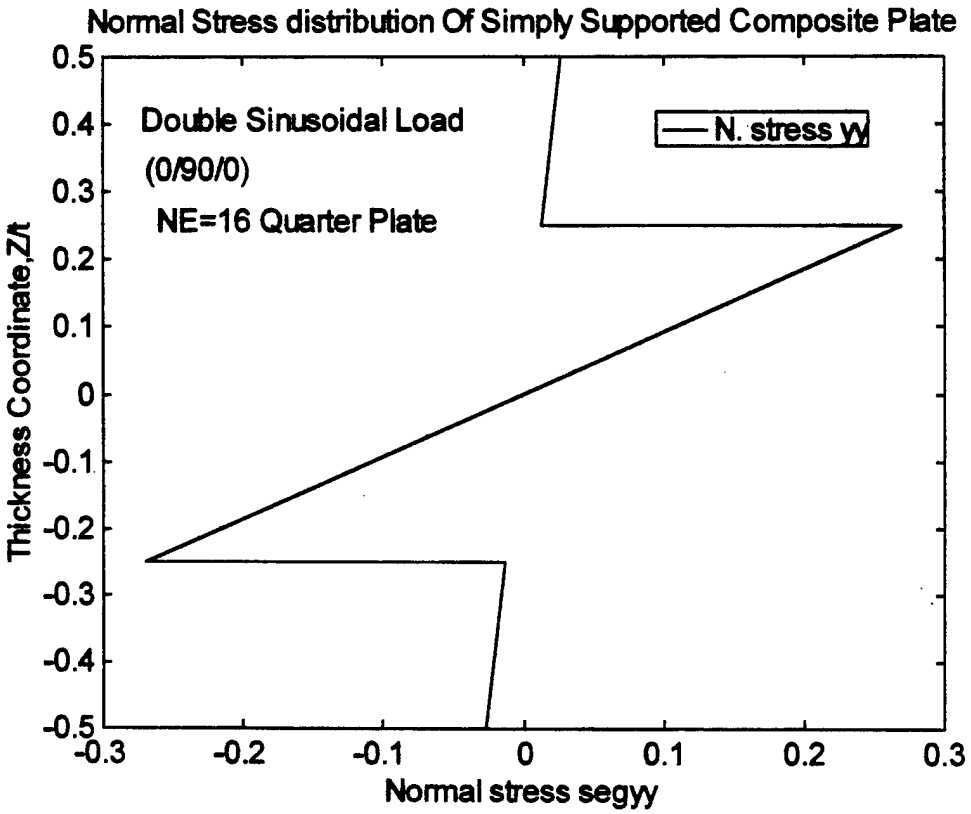

Figure 2.6: Distribution of the in-plane normal stress σ_{yy} for a simply supported laminated square plate ($0^0/90^0/0^0$) subjected to double sinusoidal load

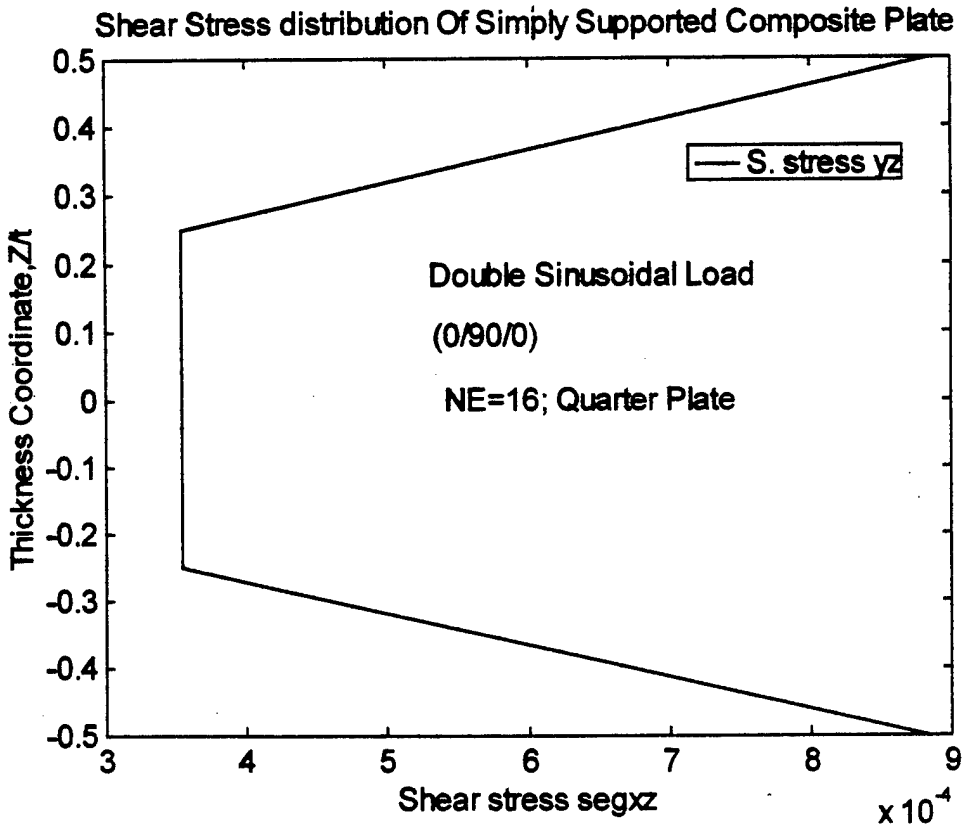

Figure 2.7: Distribution of the transverse shear stress σ_{xz} for a simply supported laminated square plate ($0^0/90^0/0^0$) subjected to double sinusoidal load.

Example 2.

The following material constants are used in the free vibration analysis of a composite plate [Ref. 46];

$E_1/E_2 = 40$; $G_{12} = G_{13} = 0.6E_2$;

$G_{23} = 0.5E_2$, $\nu_{12} = 0.25$

The dimensionless fundamental frequency of the present finite element is compared with different methods of analysis given in Table 2.3, for span to thickness ratio equal to five. The effect of span to thickness ratio and the fiber orientation angles of the dimensionless fundamental frequency are given in Figure 2.8. These results validated the finite element code.

Based on the results, the fundamental frequency can be increased by increasing lamination angle up to 45^0 except the case of two layers in which it decreases. Increasing the number of layers with fixed thickness increases the fundamental frequency due to the decreasing of flexural extensional coupling effect. The dimensionless frequency increases as long as the span to thickness ratio decreases and reaches a maximum value at a fiber angle equal to 45^0.

Table 2.3: Dimensionless fundamental frequency for four layers ($0^0/90^0/0^0/90^0$) with span to thickness ration equal five

Method	*Normalized Natural Frequencies*[*]
Present FE	0.4500
HSDT [a]	0.44694
HSDT [b]	0.44686
HSDT [c]	0.44686
FSDT [b]	0.44083
FSDT [c]	0.45083
Noor [d]	0.42719
CPT [b]	0.66690
CPT [c]	0.66690

Where;

HSDT is the higher order shear deformation theory [Ref. 35].

FSDT is the first order shear deformation theory [Ref. 35].

CPT is the classical laminate plate theory.

[a] Results obtained using the finite element solution [Ref. 35].

[b] Results obtained using the Navier Solution.

[c] Results obtained with the exact solution [Ref. 35].

[d] Results obtained by applying a finite difference scheme to the equations of the three-dimensional elasticity theory.

[*] " From Ref. [35]"

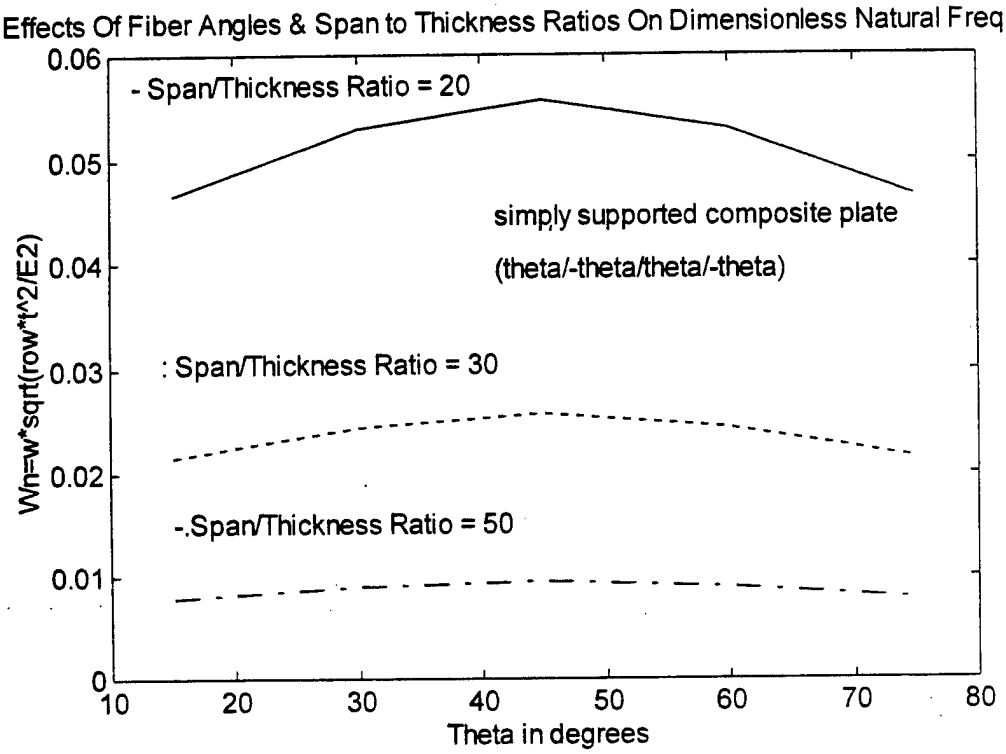

Figure 2.8: Effects of the fiber angles & span to thickness ratio on the dimensionless fundamental natural frequency for a laminate ($\theta^0/-\theta^0/\theta^0/-\theta^0$).

III. FINITE ELEMENT ANALYSIS OF A SMART COMPOSITE PLATE

A. INTRODUCTION

The rapid development of high-speed computers has facilitated the use of computational techniques in a variety of engineering applications. The finite element method is one of the most popular and powerful techniques in modern engineering design and analysis of complicated structures and multifield problems. Most of the research on active piezoelectric structures has focused primarily on experimental and theoretical studies, and there has been little development of general purpose piezoelectric finite element codes [Ref. 99].

In general, experimental models are limited by sizes, cost, and other laboratory unknowns. Theoretical models can be more general, however, analytical solutions are restricted to relatively simple geometries and boundary conditions. In the case of complicated geometries and/or boundary conditions, both theoretical and experimental techniques encounter technical difficulties. Thus, finite element development becomes very important in the modeling and analysis of a elastic/piezoelectric coupled system. A typical elastic/piezoelectric structure is composed of a main elastic continuum, such as aluminum or graphite epoxy, with coupled (surface bounded), or embedded piezoelectric sensors and actuators. The thickness of the main structure can be about two or three times thicker than that of the piezoelectric layer. Thus, it would be very inefficient and time-consuming if the entire structure were modeled by isoparametric hexahedron or tetrahedral solid elements. Thus, the development of a new finite element model applied to piezoelectric composite laminated plates, based on a simple, higher-order, shear deformation theory is essential to investigate the structural response due to the applied field and ways to control the shape of the structure.

In this chapter a finite element model is developed and a simple higher-order shear deformation theory derived with Hamilton's principle used to formulate the equations of motion of the structure. The model is valid for a piezoelectric layer either surface bonded or embedded in the laminated. plate. The piezo-lamina could be patches or completely cover the surface as shown in Figures (3.1) and (3.2). A four noded, bilinear, isoparametric rectangular element with seven mechanical degrees of freedom and one electrical degree of freedom is developed. The electric potential is treated as a generalized electric coordinates, similar to a generalized displacement coordinates at the mid-plane of the actuator layer.

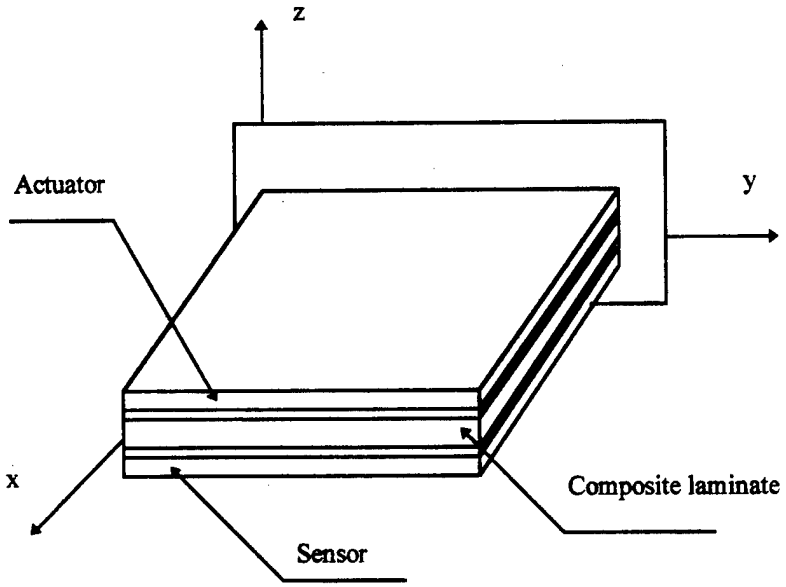

a. Piezoelectric layer complete cover the surface

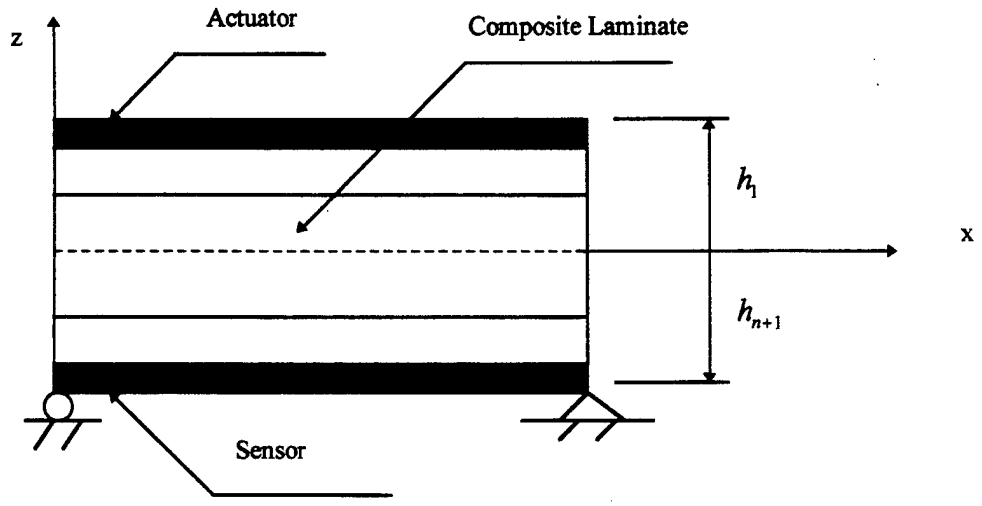

b. Simply supported plate with piezoelectric layer complete cover the surface

Figure 3.1 Composite plate with piezoelectric sensor and actuator completely covering the surface

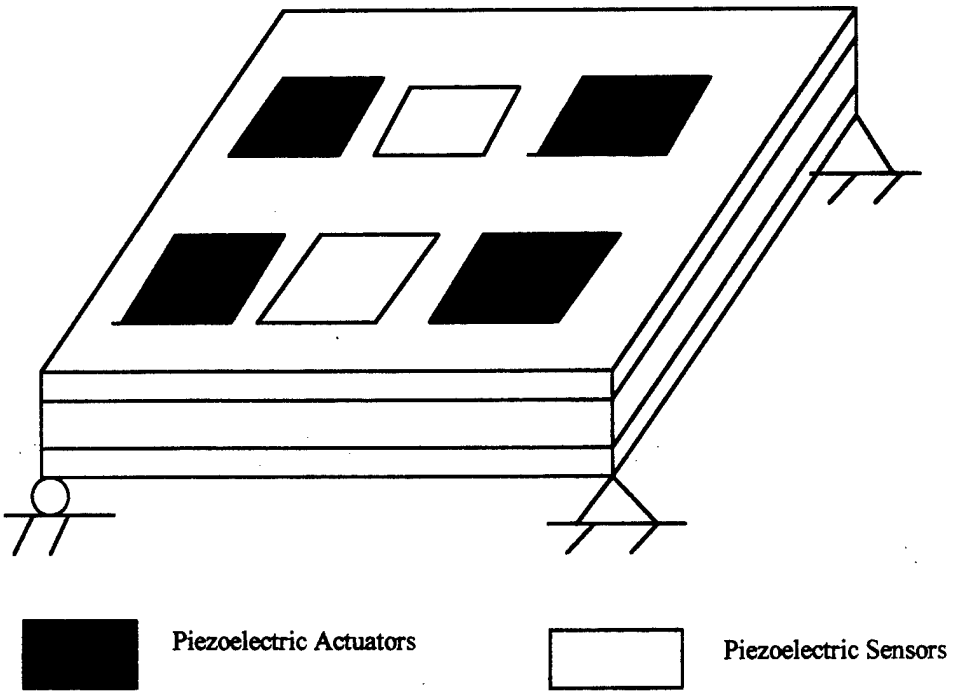

Figure 3.2: Composite plate with distributed segments piezoelectric actuators and sensors

B. VARIATIONAL PRINCIPLE

The linear piezoelectric constitutive equations coupling the elastic field and the electric field can be expressed as [Ref. 47];

$$\begin{Bmatrix} D_x \\ D_y \\ D_z \end{Bmatrix} = \begin{bmatrix} e_{11} & e_{12} & e_{13} & e_{14} & e_{15} & e_{16} \\ e_{21} & e_{22} & e_{23} & e_{24} & e_{25} & e_{26} \\ e_{31} & e_{32} & e_{33} & e_{34} & e_{35} & e_{36} \end{bmatrix} \begin{Bmatrix} \varepsilon_x \\ \varepsilon_y \\ \varepsilon_z \\ \varepsilon_{xy} \\ \varepsilon_{xz} \\ \varepsilon_{yz} \end{Bmatrix} + \begin{bmatrix} \varepsilon_{11}^s & \varepsilon_{12}^s & \varepsilon_{13}^s \\ \varepsilon_{21}^s & \varepsilon_{22}^s & \varepsilon_{23}^s \\ \varepsilon_{31}^s & \varepsilon_{32}^s & \varepsilon_{33}^3 \end{bmatrix} \begin{Bmatrix} E_x \\ E_y \\ E_z \end{Bmatrix} \tag{3.1}$$

$$\begin{Bmatrix} \sigma_x \\ \sigma_y \\ \sigma_z \\ \sigma_{xy} \\ \sigma_{xz} \\ \sigma_{yz} \end{Bmatrix} = \begin{bmatrix} c_{11} & c_{12} & c_{13} & c_{14} & c_{15} & c_{16} \\ c_{12} & c_{22} & c_{23} & c_{24} & c_{35} & c_{36} \\ c_{13} & c_{23} & c_{33} & c_{34} & c_{35} & c_{36} \\ c_{14} & c_{24} & c_{34} & c_{44} & c_{45} & c_{46} \\ c_{15} & c_{25} & c_{35} & c_{45} & c_{55} & c_{56} \\ c_{16} & c_{26} & c_{36} & c_{46} & c_{56} & c_{66} \end{bmatrix} \begin{Bmatrix} \varepsilon_x \\ \varepsilon_y \\ \varepsilon_z \\ \varepsilon_{xy} \\ \varepsilon_{xz} \\ \varepsilon_{yz} \end{Bmatrix} - \begin{bmatrix} e_{11} & e_{12} & e_{13} \\ e_{12} & e_{22} & e_{32} \\ e_{13} & e_{23} & e_{33} \\ e_{14} & e_{24} & e_{34} \\ e_{15} & e_{25} & e_{35} \\ e_{16} & e_{26} & e_{36} \end{bmatrix} \begin{Bmatrix} E_x \\ E_y \\ E_z \end{Bmatrix} \tag{3.2}$$

Equation (3.1) describes the direct piezoelectric effect, which means a charge/voltage generated by an imposed force/pressure to a piezoelectric material. The converse piezoelectric effect is described by equation (3.2) in which induced stress/strain are induced due to an externally applied voltage/charge. The equations can be written simply as:

$$\{D\} = [e]^T \{\varepsilon\} + [\varepsilon^s]\{E\} \tag{3.3}$$

$$\{\sigma\} = [c]\{\varepsilon\} - [e]\{E\} \tag{3.4}$$

where;

$\{D\}$ = Electric displacement vector (Coulomb / meter square)

$[e]$ = Dielectric permittivity matrix (Coulomb / meter square)

$\{\varepsilon\}$ = Strain vector

$[\varepsilon^s]$ = Dielectric matrix at constant mechanical strain (Farad / meter)

(permittivity component)

$[E]$ = Electric field vector (Volt / meter)

$\{\sigma\}$ = Stress vector (Newton/ meter square)

$\{c\}$ = Elasticity matrix for a constant electric field (Newton / meter square)

It is assumed that the principal material coordinates coincide with the coordinates of the problem being analyzed. Thus the constitutive relations for a material having orthohombic mm2 symmetry, including piezoelectric effects, are given by:

$$\begin{Bmatrix} D_x \\ D_y \\ D_z \end{Bmatrix} = \begin{bmatrix} 0 & 0 & 0 & 0 & e_{15} & 0 \\ 0 & 0 & 0 & e_{24} & 0 & 0 \\ e_{31} & e_{32} & e_{33} & 0 & 0 & 0 \end{bmatrix} \begin{Bmatrix} \varepsilon_x \\ \varepsilon_y \\ \varepsilon_z \\ \varepsilon_{xy} \\ \varepsilon_{xz} \\ \varepsilon_{yz} \end{Bmatrix} + \begin{bmatrix} \varepsilon_{11}^s & 0 & 0 \\ 0 & \varepsilon_{22}^s & 0 \\ 0 & 0 & \varepsilon_{33}^s \end{bmatrix} \begin{Bmatrix} E_x \\ E_y \\ E_z \end{Bmatrix} \tag{3.5}$$

$$\begin{Bmatrix} \sigma_x \\ \sigma_y \\ \sigma_z \\ \sigma_{xy} \\ \sigma_{xz} \\ \sigma_{yz} \end{Bmatrix} = \begin{bmatrix} c_{11} & c_{12} & c_{13} & 0 & 0 & 0 \\ c_{21} & c_{22} & c_{23} & 0 & 0 & 0 \\ c_{31} & c_{32} & c_{33} & 0 & 0 & 0 \\ 0 & 0 & 0 & c_{44} & 0 & 0 \\ 0 & 0 & 0 & 0 & c_{55} & 0 \\ 0 & 0 & 0 & 0 & 0 & c_{66} \end{bmatrix} \begin{Bmatrix} \varepsilon_x \\ \varepsilon_y \\ \varepsilon_z \\ \varepsilon_{xy} \\ \varepsilon_{xz} \\ \varepsilon_{yz} \end{Bmatrix} - \begin{bmatrix} 0 & 0 & e_{31} \\ 0 & 0 & e_{32} \\ 0 & 0 & e_{33} \\ 0 & e_{24} & 0 \\ e_{15} & 0 & 0 \\ 0 & 0 & 0 \end{bmatrix} \begin{Bmatrix} E_x \\ E_y \\ E_z \end{Bmatrix} \tag{3.6}$$

In this analysis, the plane stress approximation is made by setting $\sigma_z = 0$, the strain ε_z is eliminated from the constitutive relations, which will takes the following form:

$$\begin{Bmatrix} D_x \\ D_y \\ D_z \end{Bmatrix} = \begin{bmatrix} 0 & 0 & 0 & \bar{e}_{15} & 0 \\ 0 & 0 & \bar{e}_{24} & 0 & 0 \\ \bar{e}_{31} & \bar{e}_{32} & 0 & 0 & 0 \end{bmatrix} \begin{Bmatrix} \varepsilon_x \\ \varepsilon_y \\ \varepsilon_{xy} \\ \varepsilon_{xz} \\ \varepsilon_{yz} \end{Bmatrix} + \begin{bmatrix} \bar{\varepsilon}_{11}^s & 0 & 0 \\ 0 & \bar{\varepsilon}_{22}^s & 0 \\ 0 & 0 & \bar{\varepsilon}_{33}^s \end{bmatrix} \begin{Bmatrix} E_x \\ E_y \\ E_z \end{Bmatrix} \tag{3.7}$$

$$\begin{Bmatrix} \sigma_x \\ \sigma_y \\ \sigma_{xy} \\ \sigma_{xz} \\ \sigma_{yz} \end{Bmatrix} = \begin{bmatrix} \bar{c}_{11} & \bar{c}_{12} & 0 & 0 & 0 \\ \bar{c}_{21} & \bar{c}_{22} & 0 & 0 & 0 \\ 0 & 0 & \bar{c}_{44} & 0 & 0 \\ 0 & 0 & 0 & \bar{c}_{55} & 0 \\ 0 & 0 & 0 & 0 & \bar{c}_{66} \end{bmatrix} \begin{Bmatrix} \varepsilon_x \\ \varepsilon_y \\ \varepsilon_{xy} \\ \varepsilon_{xz} \\ \varepsilon_{yz} \end{Bmatrix} - \begin{bmatrix} 0 & 0 & \bar{e}_{31} \\ 0 & 0 & \bar{e}_{32} \\ 0 & \bar{e}_{24} & 0 \\ \bar{e}_{15} & 0 & 0 \\ 0 & 0 & 0 \end{bmatrix} \begin{Bmatrix} E_x \\ E_y \\ E_z \end{Bmatrix} \tag{3.8}$$

where;

$$\bar{e}_{31} = e_{31} - \frac{c_{13}}{c_{33}} e_{33};$$

$$\bar{e}_{32} = e_{32} - \frac{c_{23}}{c_{33}} e_{33};$$

$$\bar{e}_{24} = e_{24};$$

$$\bar{e}_{15} = e_{15};$$

$$\bar{\varepsilon}_{11}^s = \varepsilon_{11}^s;$$

$$\bar{\varepsilon}_{22}^s = \varepsilon_{22};$$

and

$$\bar{\varepsilon}_{33}^s = \varepsilon_{33} + \frac{e_{33}^2}{c_{33}}$$

Table 3.1 Analogy between mechanical and electrical quantities.

Mechanical	Electrical
Force density P_s (vector)	Charge density μ (scalar)
Displacement q (vector)	Potential Φ (scalar)
Stress σ (second -order tensor)	Flux density D (vector)
Strain ε (second-order tensor)	Electric field E (vector)

The elastic coefficients $\bar{c}_{ij}$ and c_{ij} can be obtained in the same way as C'_{ij} and C_{ij}, which are given in equations (2.13) and (2.14), and the transformation (if necessary) can be computed by the same method described in equation (2.18). The analogy between the mechanical and electrical quantities [Ref. 69] is given in Table 3.1.

The Lagrangian, $\Im$, of a piezoelectric body is defined by the summation of all kinetic energy , λ, and potential energy , $\hbar$, (including strain and electrical energies):

$$\Im = \int_V (\lambda - \hbar) dV \tag{3.9}$$

where;

$$\lambda = \frac{1}{2}\rho\{\dot{q}\}^T\{\dot{q}\} \tag{3.10}$$

and

$$\hbar = \frac{1}{2}\left[\{\varepsilon\}^T\{\sigma\} - \{E\}^T\{D\}\right] \tag{3.11}$$

Thus the Lagrangian is

$$\Im = \int_V \left[\frac{1}{2}\rho\{\dot{q}\}^T\{\dot{q}\} - \frac{1}{2}\left(\{\varepsilon\}^T\{\sigma\} - \{E\}^T\{D\}\right)\right] dV \tag{3.12}$$

where;

$\dot{q}$ is the velocity (time derivative of the displacement q);

$\Im$ is the Lagrangian;

V is the piezoelectric volume.

The virtual work, δW, done by the external surface force and the applied surface charge density , μ, (C/m^2) applied to the piezoelectric body is;

$$\delta W = \int_{s1} \{\delta q\}^T \{P_s\} ds_1 - \int_{s2} \delta \Phi \mu ds_2 \qquad (3.13)$$

where;

s_1 and s_2 are the surface areas at which the mechanical and the electrical loads are applied; respectively

P_s is a surface load vector (N/m^2)

Φ is the electric potential (volt)

The minus sign in equation (3.13) occurs because in the variational principle for the electromechanical medium it turns out that the electric enthalpy $H = U - E_i D_i$; takes the place of the internal energy function U in the Lagrange density; i.e., the effective electrical energy content of H is opposite in sign to that of U.

By using Hamilton's principle

$$\int_{t1}^{2} \delta(\Im + W) dt = 0, \qquad (3.14)$$

where t_1 to t_2 is the time interval, and all variations must vanish at $t = t_1$ and $t = t_2$.

Substituting equations (3.12) and (3.13) into equation (3.14) yields the variational equation as:

$$\int_{t_1}^{t_2}\left[\int_V \delta\left(\frac{1}{2}\rho\{\dot{q}\}^T\{\dot{q}\}-\frac{1}{2}\left(\{\varepsilon\}^T\{\sigma\}-\{E\}^T\{D\}\right)\right)dV+\int_{s_2}\{\delta q\}^T\{P_s\}ds_1-\int_{s_2}\delta\Phi\mu ds_2\right]dt=0 \tag{3.15}$$

By substituting equation (3.3) and (3.4) and taking the variation gives:

$$\int_{t_1}^{t_2}\left[\begin{array}{l}\int_V(\rho\{\delta\ddot{q}\}^T\{\dot{q}\}-\{\delta\varepsilon\}^T[c]\{\varepsilon\}+\{\delta\varepsilon\}^T[e]\{E\}+\{\delta E\}^T[e]^T\{\varepsilon\}+\{\delta E\}^T[\varepsilon^s]\{E\})dV\\+\int_{s_1}\{\delta q\}^T\{P_s\}ds_1-\int_{s_2}\delta\Phi\mu ds_2\end{array}\right]dt=0 \tag{3.16}$$

Since all the variations must vanish at $t=t_1$ and $t=t_2$, the variational equation takes the form:

$$\begin{array}{l}\int_V\left[\rho\{\partial q\}^T\{\ddot{q}\}+\{\delta\varepsilon\}^T[c]\{\varepsilon\}-\{\delta\varepsilon\}^T[e]\{E\}-\{\delta E\}^T[e]^T\{\varepsilon\}-\{\delta E\}^T[\varepsilon^s]\{E\}\right]dV\\-\int_{s_1}\{\delta q\}^T\{P_s\}ds_1+\int_{s_2}\delta\Phi\mu ds_2=0\end{array} \tag{3.17}$$

C. FINITE ELEMENT FORMULATION

To generate the electro-elastic matrix relations for a finite element, it was assumed that the surface of the piezoelectric layers which are in contact with the laminated substructures are suitably grounded. Also, since the thickness of the piezoelectric layers is very small, it is reasonable to assume that the electric potential functions, which yield zero potential at the interface between the actuator and/or the laminated substructure and provides a linear variation across the thickness of the sensor or actuator layer are as follows:

$$\Phi^L(x,y,z) = (z - h_{Lp})\Phi_0^L(x,y) \tag{3.18}$$

where Φ_0^L can be treated as the generalized electric coordinate similar to the generalized displacement coordinates at the mid-plane of the actuator and sensor layers. The generalized electric coordinates at any point within the element can then be expressed in terms of i nodal variables values via interpolation function N_Φ:

$$\Phi_0^L = \left[N_\Phi\right]\left\{\Phi_0^e\right\} \tag{3.19}$$

where $\left\{\Phi_0^e\right\}$ is the nodal generalized electric coordinate vector and is given by

$$\left\{\Phi_0^e\right\} = \left[\Phi_{01}^e \quad \Phi_{02}^e \quad \Phi_{03}^e \quad \Phi_{04}^e\right]^T \tag{3.20}$$

with Φ_{0i}^e (i = 1,..,4) is the generalized electric coordinate at the i^{th} node of the element and $\left[N_\Phi\right]$ is the shape function matrix, that is, the same linear shape function used for element coordinates x and y, which are given in equation (2.31).

$$N_i = 1/4(1 + \xi\xi_i)(1 + \eta\eta_i) \tag{3.21}$$

where ,

$$\left[N_\Phi\right] = \left[N_1 \quad N_2 \quad N_3 \quad N_4\right] \tag{3.22}$$

Thus;

$$\Phi^L(x,y,z) = (z - h_{Lp})\left[N_\phi\right]\left\{\Phi_0^e\right\} \tag{3.23}$$

The electric field vector $\{E\}$ is defined by the electrical potential energy Φ by using gradient operator ∇:

$$\{E\} = -\nabla\Phi^L \tag{3.24}$$

Substituting equation (3.23) in equation (3.24) , gives the electric field vector;

$$\{E\} = \left[Z_p\right]\left[B_\phi\right]\left\{\Phi_0^e\right\} \tag{3.25}$$

where ;

$$\left[B_\Phi\right] = \nabla\left[N_\Phi\right] \tag{3.26}$$

$$= \begin{bmatrix} N_{1,x} & N_{2,x} & N_{3,x} & N_{4,x} \\ N_{1,y} & N_{2,y} & N_{3,y} & N_{4,y} \\ N_1 & N_2 & N_3 & N_4 \end{bmatrix}$$

and

$$\left[Z_p\right] = \begin{bmatrix} -(z - h_{ip}) & 0 & 0 \\ 0 & -(z - h_{ip}) & 0 \\ 0 & 0 & -1 \end{bmatrix} \tag{3.27}$$

The strain vector $\left\{\varepsilon^0\right\}$ at the reference surface is defined by;

$$\left\{\varepsilon^0\right\} = [B]\left\{q_e\right\} \tag{3.28}$$

where ;

$\left\{q_e\right\}$ is the element displacement vector given in equation (2.37).

$[B]$ is the nodal strain-displacement matrix given in equation (2.38).

The generalized strain at a point is related to the reference surface strain as;

$$\{\varepsilon\} = [B_1]\{\varepsilon^0\} \tag{3.29}$$

Substitute equation (3.28) into equation (3.29) yields

$$\{\varepsilon\} = [B_1][B]\{q_e\} \tag{3.30}$$

where;

$$[B_1] = \begin{bmatrix} 1 & 0 & 0 & 0 & 0 & z & 0 & 0 & 0 & 0 & z^3 & 0 & 0 \\ 0 & 1 & 0 & 0 & 0 & 0 & z & 0 & 0 & 0 & 0 & z^3 & 0 \\ 0 & 0 & 1 & 0 & 0 & 0 & 0 & z & 0 & 0 & 0 & 0 & z^3 \\ 0 & 0 & 0 & 1 & 0 & 0 & 0 & 0 & z^2 & 0 & 0 & 0 & 0 \\ 0 & 0 & 0 & 0 & 1 & 0 & 0 & 0 & 0 & z^2 & 0 & 0 & 0 \end{bmatrix} \tag{3.31}$$

Substitution of equations (3.25) , (3.30) into equation (3.17) yields;

$$\int_V \rho\{\delta q_e\}^T\{N\}^T\{N\}\{\ddot{q}_e\}dV + \int_V \{\delta q_e\}^T[B]^T[B_1]^T[c][B1][B]\{q_e\}dV$$

$$- \int_V \{\delta q_e\}^T[B]^T[B_1]^T[e][Z_p][B_\Phi]\{\Phi_0^e\}dV - \int_V \{\delta\Phi_0^e\}^T[B_\Phi]^T[Z_p]^T[e]^T[B_1][B]\{q_e\}dV$$

$$- \int_V \{\delta\Phi_0^e\}^T[B_\Phi]^T[Z_p]^T[\varepsilon^s][Z_p][B_\Phi]\{\Phi_0^e\}dV$$

$$- \int_{s_1} \{\delta q\}^T[N]^T\{P_s\}ds_1 + \int_{s_2} \{\delta\Phi_0^e\}^T[N_\Phi]^T(z - h_{Lp})\mu ds_2 = 0 \tag{3.32}$$

D. EQUATIONS OF MOTION

1. Plate With Actuators Only

The variational equation (3.32) can be written in the form;

$$\begin{aligned}
&\int_V \rho[N]^T[N]dV\{\ddot{q}_e\}\{\delta q_e\}^T + \int_V [B]^T[B_1]^T[c][B_1][B]dV\{q_e\}\{\delta q_e\}^T \\
&- \int_V [B]^T[B_1]^T[e][Z_p][B_\Phi]dV\{\Phi_0^e\}\{\delta q_e\}^T - \int_V [B_\Phi]^T[Z_p]^T[e]^T[B_1][B]dV\{q_e\}\{\delta\Phi_0^e\}^T \\
&- \int_V [B_\Phi]^T[Z_p]^T[\varepsilon^s][Z_p][B_\Phi]dV\{\Phi_0^e\}\{\delta\Phi_0^e\}^T \\
&- \int_{S_1} [N]^T\{P_s\}ds_1\{\delta q_e\}^T + \int_{S_2} [N_\Phi]^T(z-h_{Lp})\mu ds_2\{\delta\Phi_0^e\}^T = 0
\end{aligned} \tag{3.33}$$

Thus the equation of motion in matrix form is

$$\begin{aligned}
[M_e]\{\ddot{q}_e\} + [k_{qq}]\{q_e\} - [k_{q\Phi}]\{\Phi_0^e\} &= \{P_M\} \\
[k_{\Phi q}]\{q_e\} + [k_{\Phi\Phi}]\{\Phi_0^e\} &= \{g\}
\end{aligned} \tag{3.34}$$

After adding artificial, linear, viscous damping to equation (3.34), the equations of motion will take the form;

$$\begin{aligned}
[M_e]\{\ddot{q}_e\} + [c_{qq}]\{\dot{q}_e\} + [k_{qq}]\{q_e\} - [k_{q\Phi}]\{\Phi_0^e\} &= \{P_M\} \\
[k_{\Phi q}]\{q_e\} + [k_{\Phi\Phi}]\{\Phi_0^e\} &= \{g\}
\end{aligned} \tag{3.35}$$

where;

$$[M_e] = \int_V \rho [N]^T [N] dV \qquad (3.36)$$

$$= \int_A [N]^T [\overline{m}][N] d(area)$$

The shape function matrix $[N]$ is given by

$$[N] = \sum_{i=1}^{4} \begin{bmatrix} N_i & 0 & 0 & 0 & 0 & 0 & 0 \\ 0 & N_I & 0 & 0 & 0 & 0 & 0 \\ 0 & 0 & N_I & 0 & 0 & 0 & 0 \\ 0 & 0 & 0 & N_I & 0 & 0 & 0 \\ 0 & 0 & 0 & 0 & f_i & g_i & h_i \\ 0 & 0 & 0 & 0 & f_{i,x} & g_{i,x} & h_{i,x} \\ 0 & 0 & 0 & 0 & f_{i,y} & g_{i,y} & h_{i,y} \end{bmatrix} \qquad (3.37)$$

and

$$[\overline{m}] = \begin{bmatrix} I_1 & 0 & 0 & 0 & 0 & 0 & 0 \\ 0 & I_1 & 0 & 0 & 0 & 0 & 0 \\ 0 & 0 & I_2 & 0 & 0 & 0 & 0 \\ 0 & 0 & 0 & I_2 & 0 & 0 & 0 \\ 0 & 0 & 0 & 0 & I_1 & 0 & 0 \\ 0 & 0 & 0 & 0 & 0 & I_2 & 0 \\ 0 & 0 & 0 & 0 & 0 & 0 & I_2 \end{bmatrix} \qquad (3.38)$$

in which I_1 and I_2 are the normal and rotational inertia, respectively;

$$(I_1, I_2) = \sum_{i=1}^{n} \int_{z_i}^{z_{i+1}} \rho^i [1, z^2] dz \qquad (3.39)$$

where ρ^i is the mass density of the i^{th} piezoelectric layer.

The damping matrix $[c_{qq}]$ is defined as a proportional damping, i.e.

$$[c_{qq}] = \alpha[m_{qq}] + \beta[k_{qq}], \tag{3.40}$$

and

$$[k_{qq}] = \int_v [B]^T [B_1]^T [c][B_1][B] dv \tag{3.41}$$
$$= \int_A [B]^T [\overline{D}][B] dA$$

where the rigidity matrix $[\overline{D}]$ for n number of layers is given by

$$[\overline{D}_{ij}] = \sum_{k=1}^{n} \int_{z_k}^{z_{k+1}} c_{ij}(1, z, z^2, z^3, z^4, z^6) dz \qquad \text{(for j, i =1,...6)} \tag{3.42}$$

and its elements are given explicitly in equation (2.20) and

$$[k_{q\Phi}] = \int_v [B]^T [B_1]^T [e][Z_p][B_\Phi] dV \tag{3.43}$$
$$= \int_A [B]^T [BeZ][B_\Phi] dA$$

where $[B_1 eZ]$ for m number of piezoelectric layers is given by;

$$[BeZ] = \sum_{k=1}^{m} \int_{z_k}^{z_{k+1}} [B_1]^T [e][Z_p] dz \tag{3.44}$$

and

$$[k_{\Phi q}] = \int_v [B_\Phi]^T [Z_p]^T [e]^T [B_1][B] dV = [k_{q\Phi}]^T \tag{3.45}$$

and

$$[k_{\Phi\Phi}] = \int_V [B_\Phi]^T [Z_p]^T [\varepsilon^s][Z_p][B_\Phi] dV \qquad (3.46)$$

$$= \int_A [B_\Phi]^T [Z\varepsilon^s Z][B_\Phi] dA$$

where $[Z\varepsilon^s Z]$ for m number of piezoelectric layers is given by;

$$[Z\varepsilon^s Z] = \sum_{k=1}^{m} \int_{z_k}^{z_{k+1}} [Z_p]^T [\varepsilon^s][Z_p] dz \qquad (3.47)$$

The mechanical excitation force is given by

$$[\mathrm{P}_M] = \int_{s_1} [N]^T \{P_s\} ds_1 \qquad (3.48)$$

Thus the consistent load vector at node i is

$$\{P_M\} = \int_{s_1} q_0 \begin{bmatrix} 0 \\ 0 \\ 0 \\ 0 \\ f_i \\ g_i \\ h_i \end{bmatrix} ds_1 \qquad (3.49)$$

in which q_0 is the intensity of load per unit area, and the element load vectors $\{P_M\}$ can be obtained as;

$$\{P_M\} = [P_{M1} \quad P_{M2} \quad P_{M3} \quad P_{M4}]^T \qquad (3.50)$$

The electrical excitation or the actuating term {g} is as follows:

$$\{g\} = \int_{s_2} [N_\Phi]^T (z - h_{lp}) \mu ds_2 \qquad (3.51)$$

To specify the voltage, the distributed applied charge density required to create a prescribed electric potential distribution on the surface of the actuator layer can be determined as;

$$\mu(x,y) = -\frac{\varepsilon_{33}^{s}}{(z-h_{lp})}\Phi^{L}(x,y,z)\Big|_{z=h_{Op}} \tag{3.52}$$

where h_{Op} and h_{lp} are the distances from structure middle surface to the outer and the inner surfaces of the piezoelectic actuator layer, respectively. Assembling all the equations gives the global dynamic system equations

$$\begin{aligned}[M]\{\ddot{q}\} + [C]\{\dot{q}\} + [K_{qq}]\{q\} - [K_{q\Phi}]\{\overline{\Phi}\} &= \{F\} \\ [K_{\Phi q}]\{q\} + [K_{\Phi\Phi}]\{\overline{\Phi}\} &= \{G\}\end{aligned} \tag{3.53}$$

Note that the mechanical equation is coupled with the electrical equation; in which $\{F\}$ is the global mechanical excitation and $\{G\}$ is the electrical excitation. In active vibration control application, $\{G\}$ is the feedback voltage determined by the control algorithm. In the static case, equation (3.53) becomes;

$$\begin{aligned}[K_{qq}]\{q\} - [K_{q\Phi}]\{\overline{\Phi}\} &= \{F\} \\ [K_{\Phi q}]\{q\} + [K_{\Phi\Phi}]\{\overline{\Phi}\} &= \{G\}\end{aligned} \tag{3.54}$$

By performing a condensation of the $\{\overline{\Phi}\}$ degrees of freedom from equation (3.54), the equation of motion will be as follows:

$$[K^{*}]\{q\} = \{F\} + [K_{q\Phi}][K_{\Phi\Phi}]^{-1}\{G\} \tag{3.55}$$

where;

$$[K^{*}] = [K_{qq}] + [K_{q\Phi}][K_{\Phi\Phi}]^{-1}[K_{\Phi q}] \tag{3.56}$$

and the electrical potential vector is;

$$\{\overline{\Phi}\} = [K_{\Phi\Phi}]^{-1}(\{G\} - [K_{\Phi q}]\{q\}) \tag{3.57}$$

which can be used to calculate the voltage distribution. In the free vibration analysis, $\{G\}$ is set to zero so that the voltage distribution associated with each mode can be estimated. Also from equation (3.55), the feedback force $\{F_f\}$ can be expressed as

$$\{F_f\} = [K_{q\Phi}][K_{\Phi\Phi}]^{-1}\{G\} \tag{3.58}$$

2. Plate With Actuators And Sensors

For actuator and sensor the variational equation (3.32) will takes the form:

$$\begin{aligned}
&\int_v \rho[N]^T[N]dV\{\ddot{q}_e\}\{\delta q_e\}^T \\
&+[\int_v [B]^T[B_1]^T[c][B_1][B]dV\{q_e\}\{\delta q_e\}^T - \int_v [B]^T[B_1]^T[e][Z_p][B_\Phi]dV\{\Phi_0^e\}\{\delta q_e\}^T \\
&- \int_v [B_\Phi]^T[Z_p]^T[e]^T[B_1][B]dV\{q_e\}\{\delta\Phi_0^e\}^T - \int_v [B_\Phi]^T[Z_p]^T[\varepsilon^s][Z_p][B_\Phi]dV\{\Phi_0^e\}\{\delta\Phi_0^e\}^T]_a \\
&+[\int_v [B]^T[B_1]^T[c][B_1][B]dV\{q_e\}\{\delta q_e\}^T - \int_v [B]^T[B_1]^T[e][Z_p][B_\Phi]dV\{\Phi_0^e\}\{\delta q_e\}^T \\
&- \int_v [B_\Phi]^T[Z_p]^T[e]^T[B_1][B]dV\{q_e\}\{\delta\Phi_0^e\}^T - \int_v [B_\Phi]^T[Z_p]^T[\varepsilon^s][Z_p][B_\Phi]dV\{\Phi_0^e\}\{\delta\Phi_0^e\}^T]_s \\
&- \int_{s_1} [N]^T\{P_s\}ds_1\{\delta q_e\}^T + \int_{s_2} [N_\Phi]^T(z-h_{Lp})\mu ds_2\{\delta\Phi_0^e\}^T = 0
\end{aligned} \tag{3.59}$$

Since δq_e and $\delta\Phi_0^e$ are arbitrary, equation (3.61) is satisfied only if

$$\left[M_e\right]\{\ddot{q}_e\}+\left[k_{qq}\right]\{q_e\}-\left[k_{q\Phi}\right]_a\{\Phi_0^e\}_a-\left[k_{q\Phi}\right]_s\{\Phi_0^e\}_s=\{P_M\} \tag{3.60}$$

$$\left[k_{\Phi q}\right]_a\{q_e\}+\left[k_{\Phi\Phi}\right]_a\{\Phi_0^e\}_a=\{g\} \qquad \text{'Actuator'}$$

$$\left[k_{\Phi q}\right]_s\{q_e\}+\left[k_{\Phi\Phi}\right]\{\Phi_0^e\}_s=0 \qquad \text{'Sensor'}$$

After adding artificial damping and assembling all the equations, the global dynamic system equations are;

$$[M]\{\ddot{q}\}+[C]\{\dot{q}\}+\left[K_{qq}\right]\{q\}-\left[K_{q\Phi}\right]_a\{\overline{\Phi}\}_a-\left[K_{q\Phi}\right]_s\{\overline{\Phi}\}_s=\{F\} \tag{3.61}$$

$$\left[K_{\Phi q}\right]_a\{q\}+\left[K_{\Phi\Phi}\right]_a\{\overline{\Phi}\}_a=\{G\} \qquad \text{'Actuator'}$$

$$\left[K_{\Phi q}\right]_s\{q\}+\left[K_{\Phi\Phi}\right]_s\{\overline{\Phi}\}_s=0 \qquad \text{'Sensor'}$$

where $\{q\}$, $\{\Phi\}_a$, and $\{\Phi\}_s$ are the global, nodal, generalized, displacement coordinates, and the global, nodal, generalized, electric coordinates for actuator and sensor, respectively.

The global, nodal, generalized, electric coordinates can be condensed using equation (3.61), yielding the system equations.

$$[M]\{\ddot{q}\}+[C]\{\dot{q}\}+\left[K^{*}\right]\{q\}=\{F^{*}\} \tag{3.62}$$

where;

$$\{F^{*}\}=\{F\}+\left[K_{q\Phi}\right]_{a}\left[K_{\Phi\Phi}\right]_{a}^{-1}\{G\} \tag{3.63}$$

$$\left[K^{*}\right]=\left[K_{qq}\right]+\left[K_{q\Phi}\right]_{a}\left[K_{\Phi\Phi}\right]_{a}^{-1}\left[K_{\Phi q}\right]_{a}+\left[K_{q\Phi}\right]_{s}\left[K_{\Phi\Phi}\right]_{s}^{-1}\left[K_{\Phi q}\right]_{s} \tag{3.64}$$

Since the charge applied to the sensor layer is zero (G=0), the voltage from the sensor layer can be written as;

$$\{\overline{\Phi}\}_{s}=-\left[K_{\Phi\Phi}\right]_{s}^{-1}\left[K_{\Phi q}\right]_{s}\{q\} \tag{3.65}$$

The values of the matrices in equation (3.60), m_{qq}, k_{qq}, $k_{q\Phi a}$, $k_{\Phi qa}$, and $k_{\Phi\Phi a}$ can be computed from equations (3.36), (3.41), (3.43), (3.45) and (3.46). The matrices $k_{q\Phi s}$, $k_{\Phi qs}$, and $k_{\Phi\Phi s}$ can be computed the equations (3.43), (3.45), and (3.46) for the sensor layers. The mechanical and electric loads are computed using equations (3.49) and (3.51).

E. NUMERICAL INTEGRATION

By using Gauss Legendre quadrature, a full integration technique of a 3×3 Gauss points (see Appendix A) are used to compute the integration of each element of the equations of motion of both cases, using actuators only or using actuators and sensors (3.34) and (3.60). Thus equations (3.36), (3.41), (3.43), (3.45), and (3.46), can be numerically integrated as follows:

$$\begin{aligned}\left[M_e\right] &= \int_{A_e} [N]^T[\overline{m}][N]dA_e \\ &= \int_{-1}^{+1}\int_{-1}^{+1}[N]^T[\overline{m}][N]|J|d\xi d\eta\end{aligned} \tag{3.66}$$

$$\begin{aligned}\left[k_{qq}\right] &= \int_{A_e} [B]^T[\overline{D}][B]dA_e \\ &= \int_{-1}^{+1}\int_{-1}^{+1}[B]^T[\overline{D}][B]|J|d\xi d\eta\end{aligned} \tag{3.67}$$

$$\begin{aligned}\left[k_{q\Phi}\right] &= \int_{A_e} [B]^T[BeZ]\left[B_\Phi\right]dA_e \\ &= \int_{-1}^{+1}\int_{-1}^{+1}[B]^T[BeZ]\left[B_\Phi\right]|J|d\xi d\eta\end{aligned} \tag{3.68}$$

$$\begin{aligned}\left[k_{\Phi\Phi}\right] &= \int_{A_e} \left[B_\Phi\right]^T[Z\varepsilon^s Z]\left[B_\Phi\right]dA_e \\ &= \int_{-1}^{+1}\int_{-1}^{+1}\left[B_\phi\right]^T[Z\varepsilon^s Z]\left[B_\phi\right]|J|d\xi d\eta\end{aligned} \tag{3.69}$$

$$\{P_M\} = \sum_{i=1}^{4} \int_{A_e} q_0 \begin{bmatrix} 0 \\ 0 \\ 0 \\ 0 \\ f_i \\ g_i \\ h_i \end{bmatrix} dA_e \tag{3.70}$$

$$\{P_M\} = \sum_{i=1}^{4} \int_{-1}^{+1}\int_{-1}^{+1} q_0 \begin{bmatrix} 0 \\ 0 \\ 0 \\ 0 \\ f_i \\ g_i \\ h_i \end{bmatrix} |J| d\xi d\eta \tag{3.71}$$

$$\{g\} = \int_{A_e} [N_\Phi]^T (z - h_{lp}) \mu dA_e \tag{3.72}$$

$$= \int_{-1}^{+1}\int_{-1}^{+1} [N_\Phi]^T (z - h_{lp}) \mu |J| d\xi d\eta$$

where A_e is the master element area.

F. VALIDATION

To demonstrate the performance of the finite element formulation developed in the present study, the numerical results were compared to the exact solution [Ref. 65], and existing finite element simulations [Ref. 78]. A square smart plate, consisting of a three-layered ($0^0/90^0/0^0$) cross-ply laminated plate with the thickness 3 mm was used. A two piezoelectric PVDF layers 40 μm each, served as actuator on the top surface, and

a second as sensor on the bottom surface. The elastic properties that simulate a high modulus graphite/epoxy composite are [Ref. 13].

E_{11}= 172.4 GPa (25×10^6 psi) E_{22}=6.9 GPa (10^6 psi);

$G_{12}=G_{13}$=3.45 GPa (0.5×10^6 psi); G_{23}=1.38 GPa (0.2×10^6);

$\nu_{12}=\nu_{13}$=0.25

The piezoelectric PVDF layers properties are [Ref. 73]:

Dielectric permittivity

e_{31} = 0.0460 C/m^2

e_{32} = 0.0460 C/m^2

e_{33} = 0.0000 C/m^2

Dielectricity

$\varepsilon_{11}^s = 0.1062 \times 10^{-9}$ F/m

$\varepsilon_{22}^s = 0.1062 \times 10^{-9}$ F/m

$\varepsilon_{33}^s = 0.1062 \times 10^{-9}$ F/m

Poisson ratio $\nu = 0.29$

Mass density $\rho = 0.1800 \times 10^4$ kg/m^3

Modulus of elasticity $E=2 \times 10^{\wedge 4}$ N/m^2

The mechanical loading and the electrical potential distribution is described by:

$$q = q_0 \sin(\pi x / a)\sin(\pi y / b)$$

and

$$\Phi(x,y,h_{Op}) = V \sin(\pi x / a)\sin(\pi y / b);$$

where q_0 is the intensity of load per unit area (N/m^2), and V is the amplitude of Φ in volts. The deflection is normalized as :

$$\overline{w} = \frac{100E_T}{q_0 \lambda h} w$$

where;

E_T is the transverse Young's modulus of the graphite/epoxy layers

λ is the span to the thickness ratio

h is the structure thickness

q_0 = 10 N/m^2 .

Figures (3.3), and (3.4) show the bending deflections verses length to thickness ratios for a smart plate subjected to a double sinusoidal distribution for both mechanical and electrical loads, respectively. Figure (3.5) shows a normalized central deflection for a simply supported smart plate subjected to a different applied voltage values A three dimensional plot of the finite element grid points deflections (81 nodes) under the same loads is shown in Figure (3.6).

From the results we can conclude that a new finite element model is developed using a simple higher order shear deformation theory to analyze a smart composite plate. The numerical results are compared with the exact solution [Ref. 65], and existing finite element simulations [Ref. 78]. This result validates the present finite element model. The error of the model comes in to the picture at small span to thickness ratios (3 and/or 4) but it decreases dramatically as the span to the thickness ratio increases and it attains nearly the exact when the ratio exceeds one hundred. The plate deflections can be increased by increasing the applied voltage to the actuators.

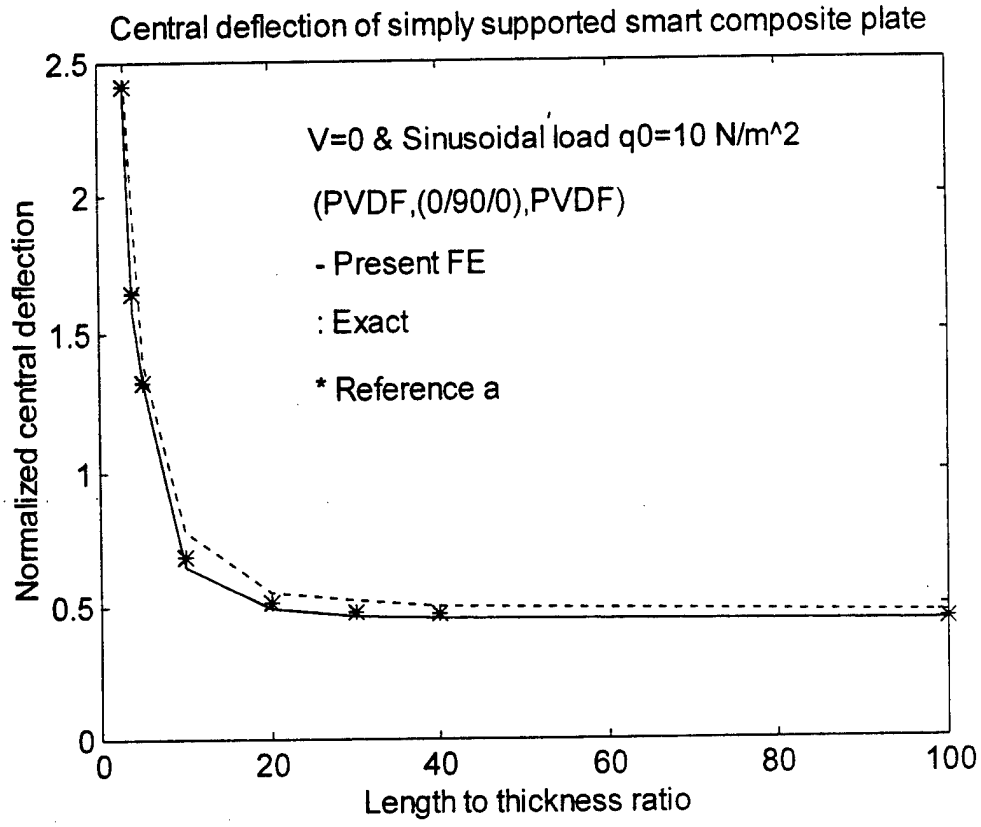

Exact/ [Ref. 65]; Reference a, FE/[Ref. 78]

Figure 3.3: Bending deflection vs. length to thickness ratio for a plate subjected to a double sinusoidal mechanical load.

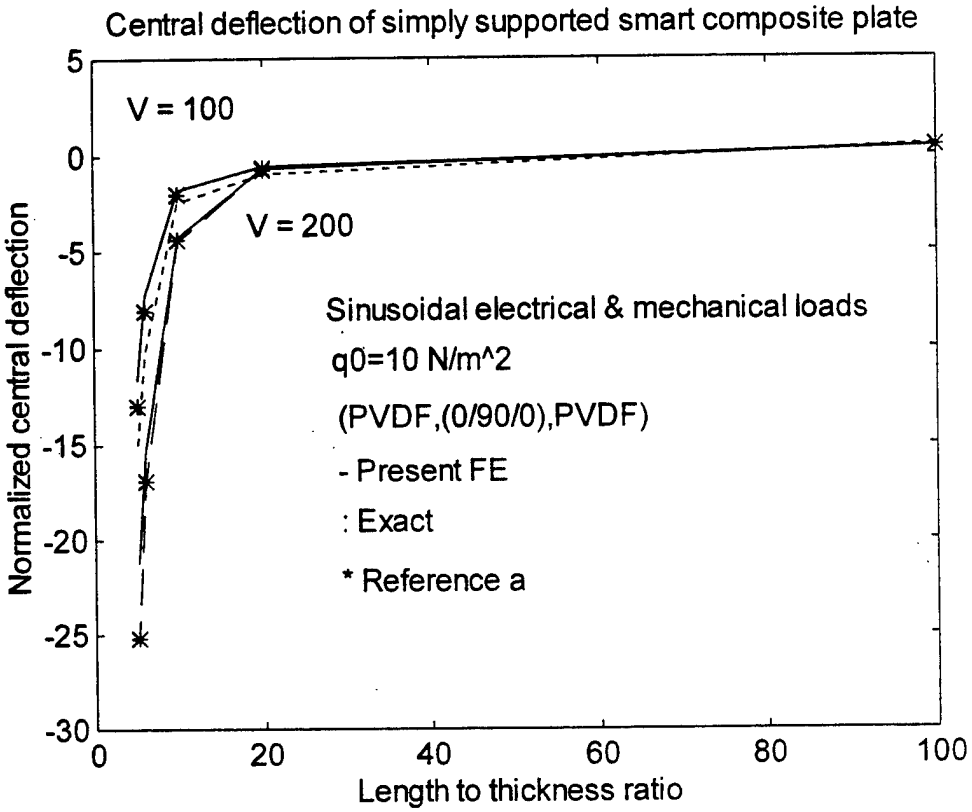

Exact/ [Ref. 65]; Reference a, FE/[Ref. 78]

Figure3.4: Bending deflection vs. length to thickness ratio for a plate subjected to double sinusoidal electrical and mechanical loads.

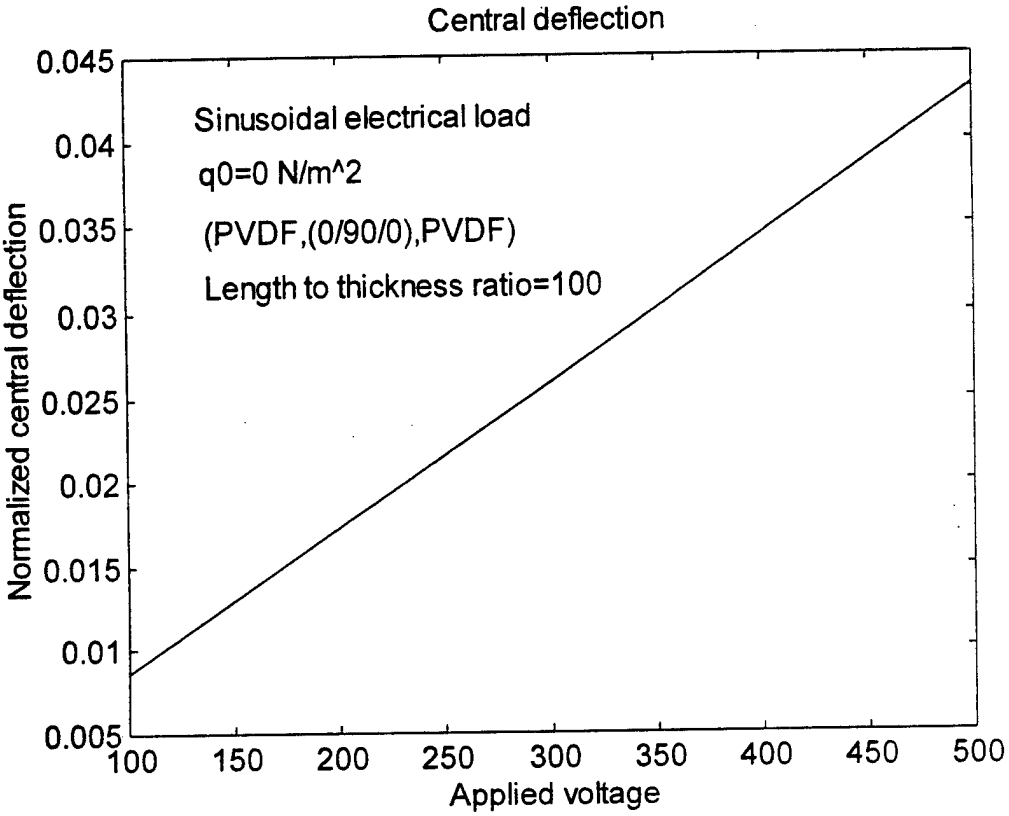

Figure 3.5: Normalized central deflection vs. applied voltage for a plate subjected to a uniformly distributed electrical load.

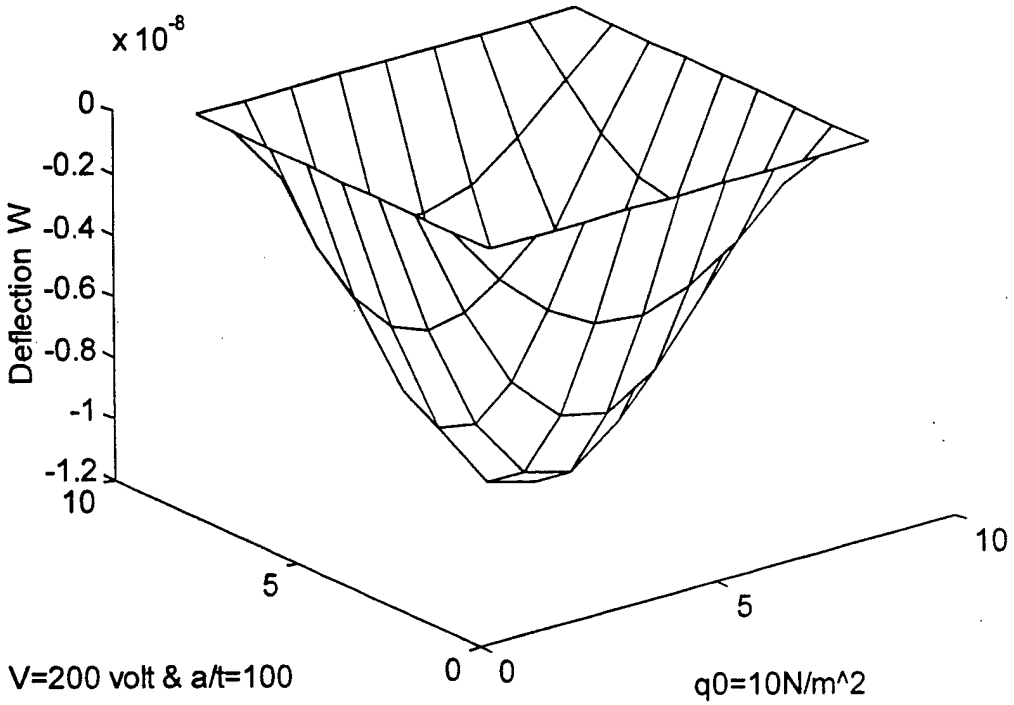

Figure 3.6: Grid point deflection for simply supported plate subjected to a double sinusoidal electrical and mechanical loads.

VI. SHAPE CONTROL AND OPTIMIZATION

A. INTRODUCTION

Future technologies in active changes in the structure shape such as airfoils spacecraft antenna, turbine blades, etc. justify and necessitate the study of using piezoelectric actuators to control the shape of structure deformed quasi-statically. In the previous chapter, a finite element model was used to calculate the change in the shape of a composite plate when the voltage is applied to the piezoelectric actuators.

In this part of the analysis, a new model is developed to determine voltage applied to the piezoelectric actuator to achieve minimum error between the desired shape and the actual shape with prescribed actuator(s) placements. The mathematical model is developed based on a kinematical relation between a point in the actual shape and a corresponding point in the desired shape for each element of the finite element grid. The system of equations for the error function is formulated based on a finite element technique. The optimization algorithm is applied to the error (objective) functions through a finite element analysis program called OPTSHP. The code performs the analysis using a finite element technique and determines the plate deformation due to the applied voltage to each actuator. It is also able to call a Matlab optimization function to compute the minimum voltages applied to each actuator.

B. PROBLEM STATMENT

Consider the problem of a plate with known original shape and actuator configuration where the desired shape is specified. Thus it is desired to find actuator voltages to achieve the prescribed shape, which minimizes the error between the desired shape and the actual shape, for a prescribed actuator(s) position, to achieve a minimum error (objective) function.

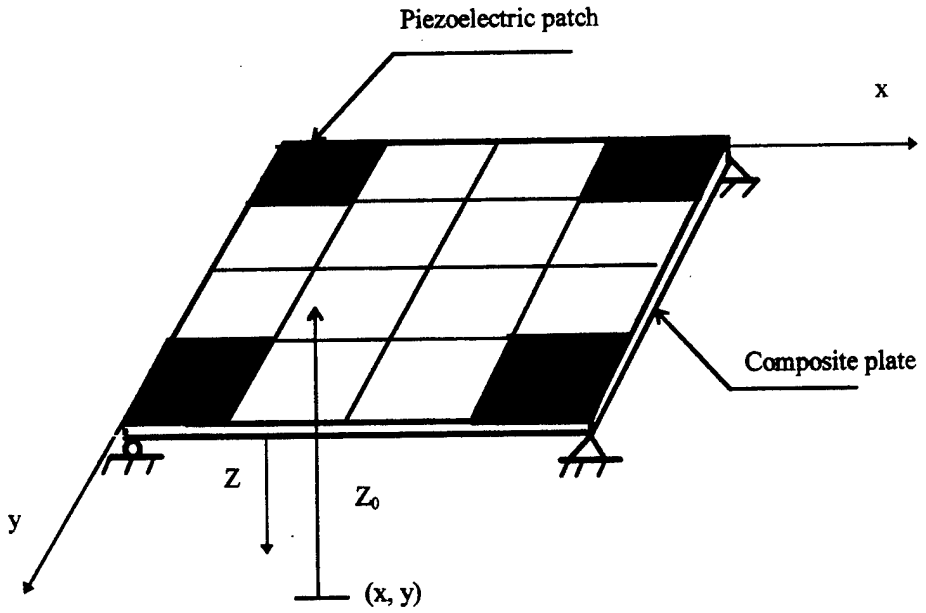

Figure 4.1 : z_0 coordinate shows a point location on element of the finite element grid

The analysis is based on small deformation theory. Therefore the specified desired shape must be within the region of ' small deformation' from the original shape. Also, the analysis uses the shape change of a reference surface. Thus within the approximations used , the shapes of either the 'top' or the 'bottom' surface of the element can be taken as the reference surface.

The shape of each element of the finite element grid is described via a suitably chosen reference surface. The shape of this reference surface is defined by a single z_0-coordinate of every point element surface. The z_0-coordinate is perpendicular to the x-y plane as

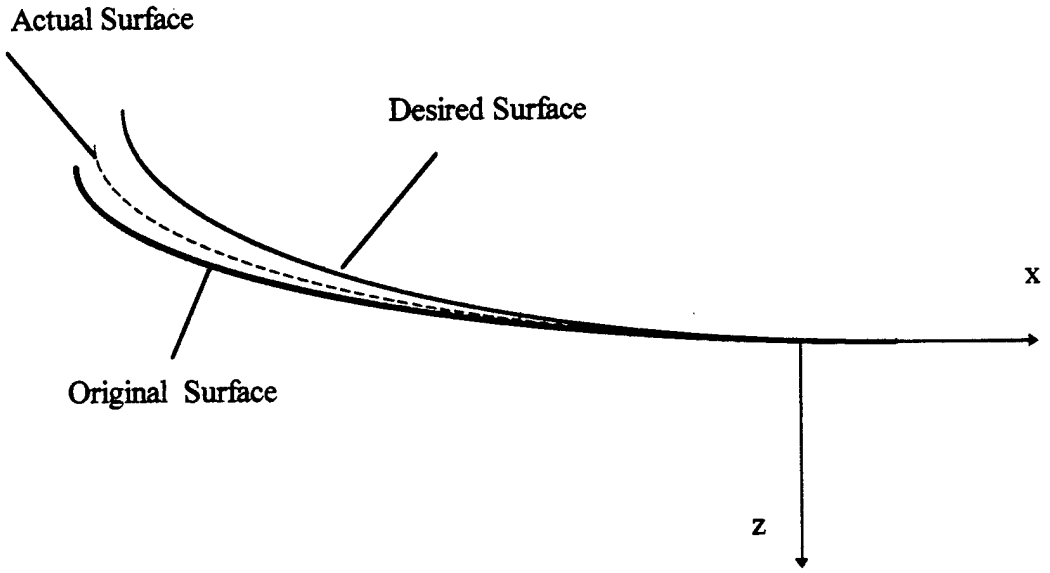

Figure 4.2: Original Surface, Actual surface, and Desired surface in the x-z plane

shown in Figure (4.1). The shape can be specified by a polynomial function in x and y such as:

$$z_O = a_o + a_1 x + a_2 y + a_3 xy + a_4 x^2 + a_5 y^2 \qquad \text{(length units)} \qquad (4.1)$$

Also the desired shape can be specified by the same way;

$$z_{des} = b_o + b_1 x + b_2 y + b_3 xy + b_4 x^2 + b_5 y^2 \qquad \text{(length units)} \qquad (4.2)$$

where a_i and b_i are constants.

C. ERROR FUNCTION Λ

Assume that a given set of voltages is applied to a specified number of actuators which result in a change in the shape of the plate and give a new configuration of the structure, (dashed line in Figure 4.2.) which represent the actual shape. An error function will be introduced which includes the difference between the actual shape and the desired

one [Ref. 90].

The error function will take the form:

$$\Lambda = \int_{\Omega_e} \overline{\Delta}^2 dxdy \qquad \text{(length}^4\text{)} \qquad (4.3)$$

where;

Λ is proportional to the distance between the reference surface of the desired shape and the actual reference surface

Ω_e is the element domain.

$\overline{\Delta}$ represents the difference between the z-coordinate on the reference surface of the desired shape and the z-coordinate of a corresponding point on the actual reference surface.

The error function can also be the sum of the error square at each element

$$\Lambda = \sum_{i=1}^{n} \Delta^2 \qquad (4.4)$$

where; Δ represents the difference between the z-coordinate of a point on the desired shape and the z-coordinate of a corresponding point on the actual surface for each element of the finite element grid.

Thus the objective is to make the error function Λ as small as possible such that the desired surface and the actual surface are nearly identical (i.e., $\Lambda \rightarrow 0$) for a prescribed actuator(s) position over the finite element grid, with optimal applied voltages for these prescribed optimal placements .

From Figure 4.3 the distance Δ is defined as;

$$\Delta = (z_0 + \delta z_0) - (z_{des} + \delta z_{des}) \qquad \text{(length units)} \qquad (4.5)$$

To evaluate each term in this equation, we consider a nodal point A on the original

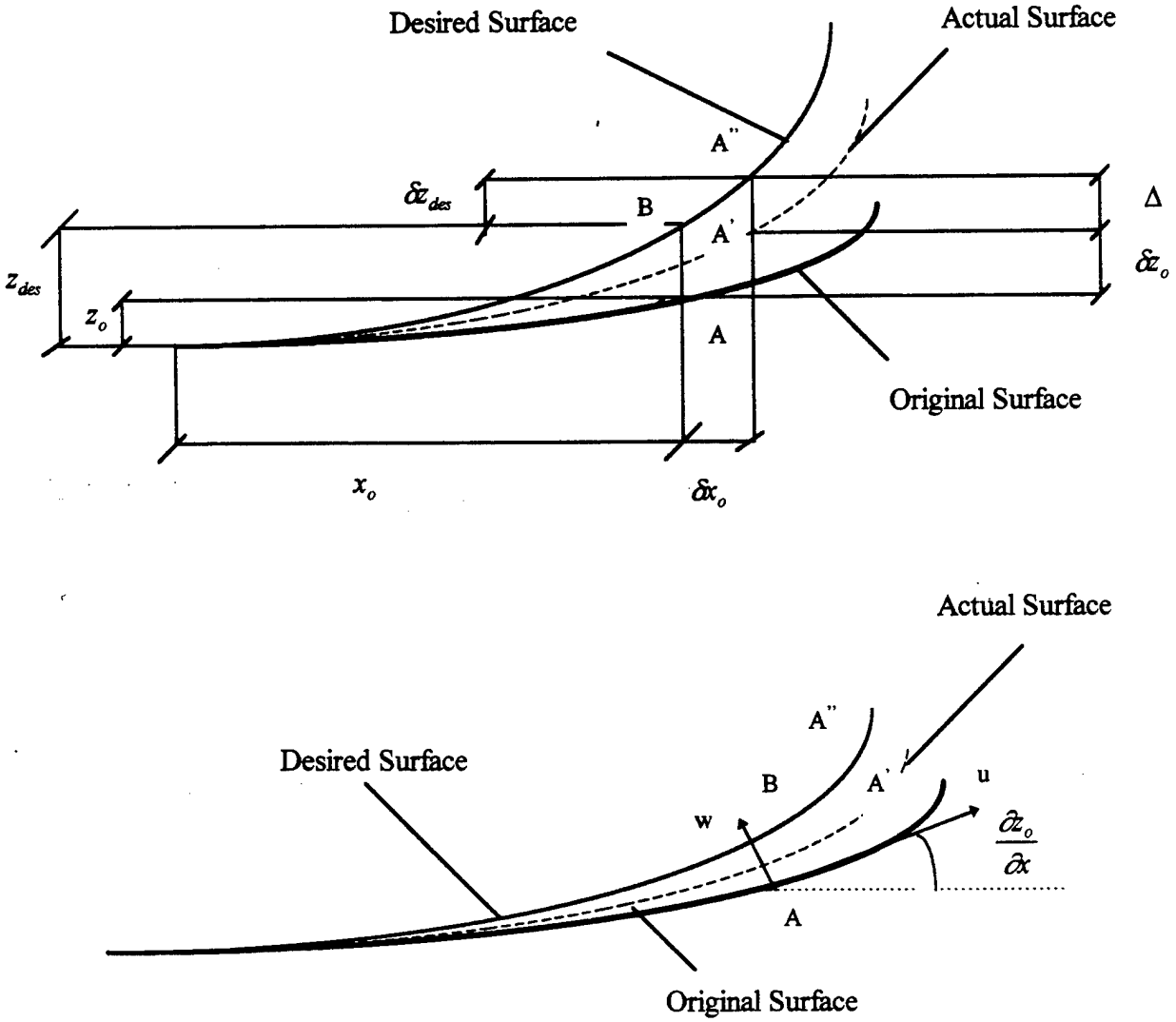

Figure 4.3: Difference between the actual surface and the desired surface in the x-z plane "From Ref. [91]."

reference surface at (x_0,y_0). Thus z_0 is the z-coordinate of the point A on the original reference surface, δz_0 is the difference between the z-coordinate of point A on the original reference surface and the z-coordinate of the corresponding point A' in the actual surface , which can be expressed as :

$$\delta z_0 = \left(\frac{\partial z_0}{\partial x} u + \frac{\partial z_0}{\partial y} v + w \right)_A \tag{4.6}$$

where ;

u, v and w are the displacements of the node A.

u is the displacement tangential to the reference surface in the axis x-z plane;

v is the displacement tangential to the reference surface in the off-axis y-z plane;

w is the deflection normal to the reference surface;

z_{des} is the z-coordinate of point B on the desired reference surface at (x_0,y_0).

The point on the desired reference surface corresponding to point A' on the actual reference surface is point A'' located at $(x_0 + \delta x_0, y_0 + \delta y_0)$. δz_{des} is the difference between the z-coordinates of points A'' and B.

It can be approximated by the first two terms of a Taylor series expansion.

$$\delta z_{des} = \left(\frac{\partial z_{des}}{\partial x} \right)_B \delta x_0 + \left(\frac{\partial z_{des}}{\partial y} \right)_B \delta y_0 \tag{4.7}$$

The distances δx_0 and δy_0 are the changes in the x- and y-coordinates between points A'' and B.

$$\delta x_0 = \left(u - w \frac{\partial z_0}{\partial x} \right)_A \tag{4.8}$$

$$\delta y_0 = \left(v - w \frac{\partial z_0}{\partial y} \right)_A$$

The following parameters are introduced which depend on the geometry of the original and desired surface,

$$\eta_1 = 1 + \left(\frac{\partial z_{des}}{\partial x} \right)_B \left(\frac{\partial z_0}{\partial x} \right)_A + \left(\frac{\partial z_{des}}{\partial y} \right)_B \left(\frac{\partial z_0}{\partial y} \right)_A \tag{4.9}$$

$$\eta_2 = \left(\frac{\partial z_0}{\partial x} \right)_A - \left(\frac{\partial z_{des}}{\partial x} \right)_B$$

$$\eta_3 = \left(\frac{\partial z_0}{\partial y} \right)_A - \left(\frac{\partial z_{des}}{\partial y} \right)_B$$

By using this parameter the objective function will take the form:

$$\Lambda = \int_{\Omega_e} \left[(z_0 - z_{des}) + \eta_1 w + \eta_2 u + \eta_3 v \right]^2 dx dy \tag{4.10}$$

D. FINITE ELEMENT FORMULATION

A bilinear isoparametric rectangular element is used to describe the shape of the element. The element coordinates, x and y are interpolated using a linear shape function N_i, which has the form:

$$N_i = 1/4(1 + \xi\xi)(1 + \eta\eta_i) \tag{4.11}$$

where;

N_i is the linear interpolation function.

ξ, η are the master element coordinates.

x, y are the actual element coordinates.

The actual element coordinates x and y can be transformed to the master element by the same way as in the finite element analysis. The mathematical relations for the element transformation will have the form:

$$x = x_c + \xi a / 2; \tag{4.12}$$

$$y = y_c + \eta b / 2;$$

and

$$\xi = 2/a\,(x - x_c);$$

$$\eta = 2/b\,(y - y_c)$$

By substituting equation (4.12) in equations (4.1) and (4.2), the actual and the desired shape equations will have the form;

$$z_o = a_o + a_1(x_c + \xi a/2) + a_2(y_c + \eta b/2) + a_3(x_c + \xi a/2)(y_c + \eta b/2) \tag{4.13}$$
$$+ a_4(x_c + \xi a/2)^2 + a_5(y_c + \eta b/2)^2$$

and

$$z_{des} = b_o + b_1(x_c + \xi a/2) + b_2(y_c + \eta b/2) + b_3(x_c + \xi a/2)(y_c + \eta b/2) \tag{4.14}$$
$$+ b_4(x_c + \xi a/2)^2 + b_5(y_c + \eta b/2)^2$$

(z_0 could be zero, for a flat plate, or a first order polynomial)

By the chain rule of partial differentiation,

$$\frac{\partial z_o}{\partial x} = \frac{\partial z_0}{\partial \xi}\frac{\partial \xi}{\partial x} + \frac{\partial z_o}{\partial \eta}\frac{\partial \eta}{\partial x} \tag{4.15}$$

$$\frac{\partial z_0}{\partial y} = \frac{\partial z_0}{\partial \xi}\frac{\partial \xi}{\partial y} + \frac{\partial z_0}{\partial \eta}\frac{\partial \eta}{\partial y}$$

and

$$\frac{\partial z_{des}}{\partial x} = \frac{\partial z_{des}}{\partial \xi}\frac{\partial \xi}{\partial x} + \frac{\partial z_{des}}{\partial \eta}\frac{\partial \eta}{\partial x} \qquad (4.16)$$

$$\frac{\partial z_{des}}{\partial y} = \frac{\partial z_{des}}{\partial \xi}\frac{\partial \xi}{\partial y} + \frac{\partial z_{des}}{\partial \eta}\frac{\partial \eta}{\partial y}$$

By using equations (4.16) and (4.17), the three geometric parameters η_1, η_2, and η_3, which are expressed in equation (4.9), can be computed. The objective function equation (4.10) takes the form:

$$\Lambda = \int_{\Omega_e} \left[(z_0(\xi,\eta) - z_{des}(\xi,\eta)) + \eta_1(\xi,\eta)w + \eta_2(\xi,\eta)u + \eta_3(\xi,\eta)v \right]^2 dxdy \qquad (4.17)$$

The electric excitation may be factored out of displacements u,v, and w in equation (4.17) by introducing the vectors $\tilde{u}$, $\tilde{v}$ and $\tilde{w}$, which can be defined as follows. The degrees of freedom of the system can be determined from the equations of motions (3.57) and (3.64) for both cases of actuator and actuator and sensor that are given in chapter three in short form as:

$$\{q\} = [K^*]^{-1}\{F^*\} \qquad (4.18)$$

where;

$\{q\}$ is the array of the degrees of freedom $\{U_0, V_0, \phi_{0x}, \phi_{0y}, W_0, w_x, \text{and } w_y\}$

$[K^*]^{-1}$ is the inverse of the structure stiffness matrix (given in equations (3.58) and equation (3.66)).

$\{F^*\}$ is the applied electric and mechanical loads vector, in the case of the actuator only which is described in chapter three as;

$$\{F^*\} = \{F\} + [K_{q\Phi a}][K_{\Phi\Phi a}]^{-1}\{G\} \qquad (4.19)$$

in case of applied electric load only.

$$\{F^*\} = \left[K_{q\Phi a}\right]\left[K_{\Phi\Phi a}\right]^{-1}\{G\} \tag{4.20}$$

where $\{G\}$ is the global electric actuating force in which for one element g is defined as;

$$\{g\} = \int_{S_2}\left[N_\Phi\right]^T (z - h_{lp})\mu ds_2 \tag{4.21}$$

and the distributed applied charge density is described as;

$$\mu(x,y) = -\frac{\varepsilon_{33}^s}{(z-h_{lp})}\Phi(x,y,z)\Big|_{z=h_{Op}} \tag{4.22}$$

which is function of the amplitude of the electric potential distribution (V in volt).

The displacement $u, v,$ and w are defined via the interpolation shape function as:

$$u = \sum_{i=1}^{4} N_i u_i \tag{4.23}$$

$$v = \sum_{i=1}^{4} N_i v_i$$

$$w = \sum_{i=1}^{4} f_i w_i$$

$u_i, v_i,$ and w_i are the displacements at the nodal point in the x, y, and z direction respectively, which can be picked out from the deformation array $\{q\}$ expressed in equation (4.18) such as:

$$u_i = \tilde{K}_u\{F^*\} \tag{4.24}$$

$$v_i = \tilde{K}_v\{F^*\}$$

$$w_i = \tilde{K}_w\{F^*\}$$

where;

$\tilde{K}_u, \tilde{K}_v$, and $\tilde{K}_w$ is the flexibility influence coefficient rows corresponding to the displacements u_i, v_i, and w_i in the global matrix inverse $\left[K^*\right]^{-1}$.

By substituting u_i, v_i and w_i equation (4.23) takes the form:

$$\tilde{u} = \sum_{i=1}^{4} N_i u_i = \sum_{i=1}^{4} N_i \tilde{K}_u \{F^*\} \tag{4.25}$$

$$\tilde{v} = \sum_{i=1}^{4} N_i u_i = \sum_{i=1}^{4} N_i \tilde{K}_v \{F^*\}$$

$$\tilde{w} = \sum_{i=1}^{4} f_i w_i = \sum f_i \tilde{K}_w \{F^*\}$$

where;

f_j is the shape function used for the deflection w at node j,

N_i is the shape function used for the displacement u, and v at node j, and $\tilde{u}, \tilde{v}$, and $\tilde{w}$ are the displacements in the three directions, which are computed from the finite element analysis of the plate.

These displacements are a function of the voltage applied to each actuator. To factor out the voltage in the objective function, $\tilde{u}, \tilde{v}$ and $\tilde{w}$, values are used instead of u, v, and w in equation (4.17) and one can obtains;

$$\Lambda = \int_{\Omega_e} \left[(z_0(\xi,\eta) - z_{des}(\xi,\eta)) + \eta_1(\xi,\eta)\tilde{w}(V) + \eta_2(\xi,\eta)\tilde{u}(V) + \eta_3(\xi,\eta)\tilde{v}(V) \right]^2 dxdy \tag{4.26}$$

which is a function of the amplitude of the electric potential distribution (V in volt).

E. NUMERICAL INTEGRATION

Equation (4.26) can be integrated numerically using Gauss-Legendre quadrature (see Appendix A). A full integration technique of a 3 × 3 Gauss point is used for each element. Thus, the error function for the one element can be written as;

$$\Lambda = \int_{-1}^{1}\int_{-1}^{1}\left[\left(z_0(\xi,\eta) - z_{des}(\xi,\eta)\right) + \eta_1(\xi,\eta)\tilde{w}(V) + \eta_2(\xi,\eta)\tilde{u}(V) + \eta_3(\xi,\eta)\tilde{v}(V)\right]^2 |J| d\xi d\eta \tag{4.27}$$

where $|J|$ is the determinant of the Jacobian matrix.

The structure objective function is defined as the summation of the error for each element such as:

$$\overline{\Lambda} = \sum_{i=1}^{m} \Lambda \tag{4.28}$$

subjected to

$$\text{Lower limit} \leq V \leq \text{Upper limit}$$

where m is the number of elements of the finite element grid, and V is the amplitude of the electric potential distribution applied at each actuator (in voltage).

F. OPTIMIZATION ALGORITHM

A Matlab function $f\min$ and $f\min s$ are used to find the minimum of a scalar function. The $f\min$ function is used to minimize a function of one variable on a fixed interval. The problem is mathematically stated as :

$$\begin{aligned} &\underset{x}{\text{minimize}} \quad f(x) \\ &\text{subjected to:} \\ &\qquad x_1 \le x \le x_2 \end{aligned} \tag{4.29}$$

where $f(x)$ and x are scalars.

The $f\min$ function is used to optimize the objective function in the a case of constant applied voltage to each actuator (V is scalar).

The function $f\min s$ is used to find the minimum of a scalar function of several variables starting from an initial estimate, which is generally referred to as unconstrained nonlinear optimization, and is mathematically stated as:

$$\underset{x}{\text{minimize}} \quad f(x) \tag{4.30}$$

where x is a matrix or vector and f is a scalar function.

The function $f\min s$ is used when different values of the voltage are applied to the piezoelectric actuators (V is a vector) . $f\min s$ uses the simplex search algorithm of Nelder and Mead[102], for minimization of a function of n variables, which depend on the comparison of function values at the (n+1) vertices of a general simplex, followed by the replacement of the vertex with the highest value by another point. The simplex adapts itself to local landscape and contracts to the final minimum. The method is shown to be effective and computationally compact. A procedure is given for the estimation of the Hessian matrix in the neighbourhood of the minimum needed in statistical estimation problems.

G. SOLUTION PROCEDURE

The flow chart of the solution procedure to compute the optimal voltages applied to the actuators and to minimize the objective (error) function is shown in Figure 4.4. The procedure is as follows:

1. Input the structural data, such as material properties for both graphite epoxy and piezoelectric materials, plate dimensions, actuators dimensions, boundary conditions and the applied voltages to the actuator.
2. Assume an initial guess for the applied voltages to each actuator at prescribed selected positions.
3. Call the optimization algorithm using a Matlab function $f\min s$ (in case of different voltages applied to different actuators) or $f\min$ (in case of same voltage applied to all actuators).
4. Compute the plate deformation due to the current applied voltage, using the finite element analysis.
5. Evaluate the objective function and applied voltages.
6. Check the convergence of the objective function and voltages. If they converge, the program will terminate.
7. Otherwise, update the current applied voltages to the actuator(s) and then go to step three and repeat the procedure.

H. VALIDATION

As illustrated in the flow chart, Figure 4.4, the optimal location of the actuator(s) position to get a minimum error function at a specified applied voltage is determined. The OPTSHP code for the optimization algorithm has been tested.

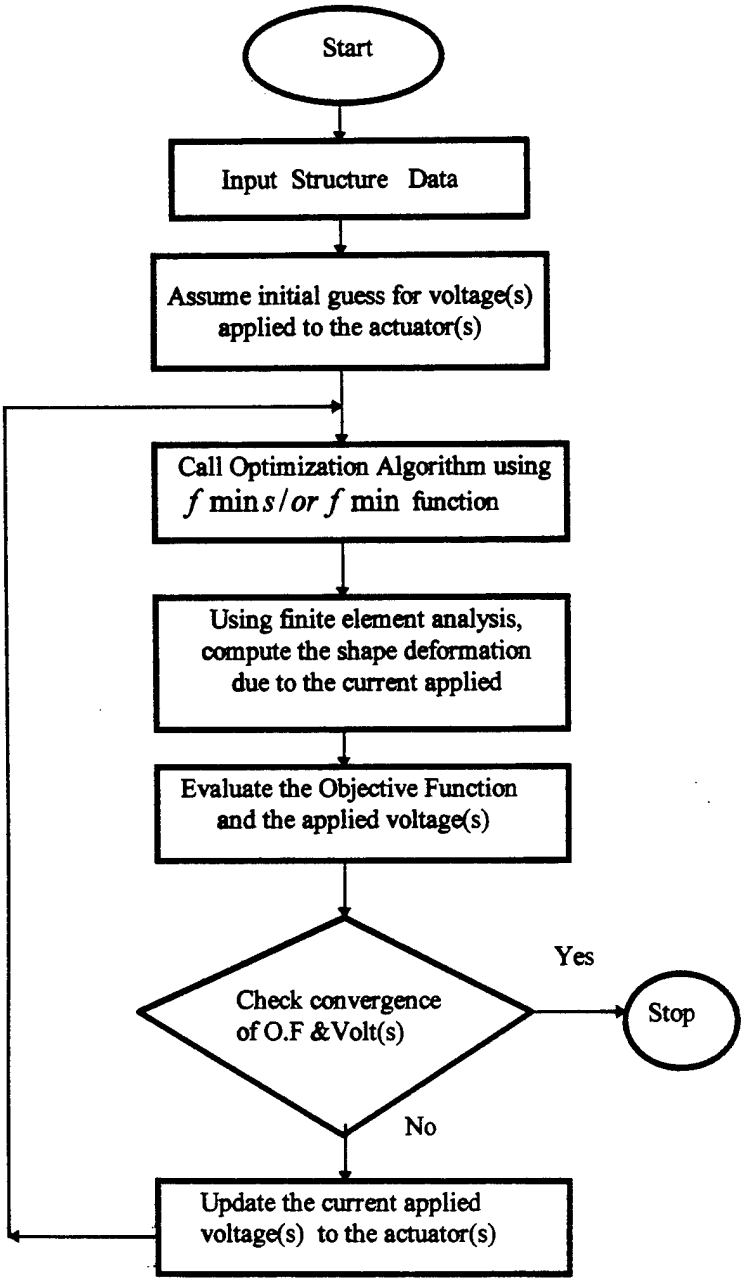

Figure 4.4: Flow chart of solution procedure

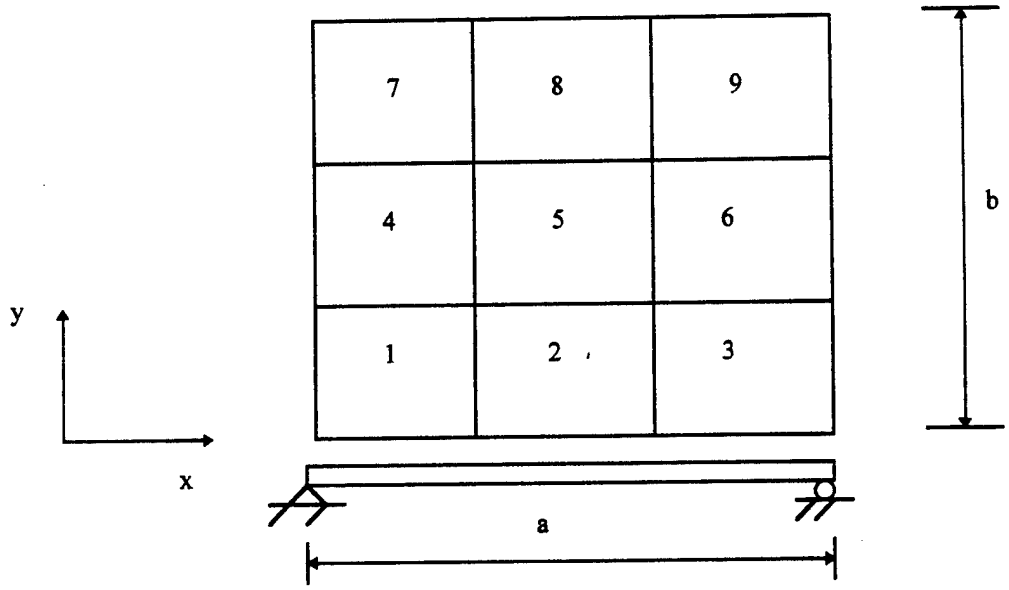

Figure 4.5 Element numbers for different actuator positions for a simply supported square composite plate (a= b).

A square fiber-reinforced composite plate with three layers ($0^0/90^0/0^0$) and one piezoelectric layer patch on the top surface and another one on the bottom surface was used. The length to thickness ratio equal fifty, and the materials properties for graphite/epoxy are as follows [Ref. 13].

E_{11}= 172.4 GPa (25×10^6 psi) E_{22}=6.9 GPa (10^6 psi);

$G_{12}=G_{13}$=3.45 GPa (0.5×10^6 psi); G_{23}=1.38 GPa (0.2×10^6);

$\nu_{12}=\nu_{13}$=0.25

The piezoelectric PVDF layers properties are [Ref. 73]:

Dielectric permittivity

e_{31} = 0.0460 $C/m^{\wedge 2}$

$e_{32} = 0.0460$ C/m^2

$e_{33} = 0.0000$ C/m^2

Dielectricity

$\varepsilon_{11}^s = 0.1062 \times 10^{-9}$ F/m

$\varepsilon_{22}^s = 0.1062 \times 10^{-9}$ F/m

$\varepsilon_{33}^s = 0.1062 \times 10^{-9}$ F/m

Poisson ratio $\nu = 0.29$

Mass density $\rho = 0.1800 \times 10^4$ kg/m^3

Modulus of elasticity $E=2 \times 10^{\wedge 4}$ N/m^2

The mechanical loading is taken to be zero, and the electrical potential distribution is assumed to be uniformly distributed with amplitude V. The deflection is normalized as :

$$\overline{w} = \frac{100E_T}{q_0 \lambda h} w$$

where;

E_T is the transverse Young's modulus of the graphite/epoxy layers

λ is the span to the thickness ratio (equal fifty)

h is the structure thickness

A nine element model was used for different positions of the actuators as shown in Figure 4.5. The original shape is chosen as a flat plate ($z_0 = 0$) and the desired shape is selected as: $z_{des} = 1 \times 10^{-9} x^2 - 4.2 \times 10^{-10} xy + 6 \times 10^{-8} y^2$.

Example 1.

In this case the error between the actual shape and the desired shape due to a specified amount of the applied voltage to the actuator is computed by placing the actuator(s) at different positions on the finite element grid (Figure 4.5). The error function values are given in Table 4.1 for an applied voltage equal to 100 volts for each actuator position.

Example 2.

The predicted voltages and the grid points transverse deflections, for both the actual and the desired transverse deflections, (in-plane deformations are not included) are computed for two cases. Figure (4.6) shows the first case, when the actuator is placed at element number five. The second case, when two actuators are used at elements two and eight, is shown in Figure 4.7.

Example 3.

The optimal value of voltage applied at the actuator(s) to obtain minimum error between the actual shape and the desired shape (minimum error function) can be computed as shown in the flow chart, Figure 4.4, using the Matlab *f* min function with certain upper and lower limits of the applied voltage, such as $-100 < V < 100$. The optimal voltage applied to the actuator for different positions on the grid and the corresponding minimum value of the error function are given in Table 4.2.

The reported values were the global minimums. This was accomplished by applying different initial values of voltages (i.e. -500 to 500 Volt.) to the actuator and determining the numerical value of the objective function at these different voltages. The minimum value of the error function found was identical to the value computed by the optimization algorithm.

Table 4.1: Error function values at different actuator positions for applied voltage equal 100 volt.

Actuator Position	*Error Function Value*
Element # 1	f= 5.87619804 e-18
Element # 2	f= 5.05453907 e-18
Element # 3	f= 4.44646994 e-18
Element # 4	f= 7.68074043 e-18
Element # 5	f= 9.30776749 e-18
Element # 6	f= 4.28947367 e-18
Element # 7	f= 5.86952426 e-18
Element # 8	f= 5.04220635 e-18
Element # 9	f= 4.44063580 e-18

- The applied voltage at each actuator is 100 Volts.

Example 4.

In the case of four actuators used at a time, the voltages and error function values are given in Table 4.3. Table 4.4 shows the results for two actuators used at a time. The results in both cases were obtained by using the Matlab function $f\min s$ with unconstrained value on the applied voltage.

An optimization algorithm is applied to get minimum applied voltages to the actuators to minimize the error function. Tables 4.3 and 4.4 show that location of the actuators play an important role in minimizing the error.

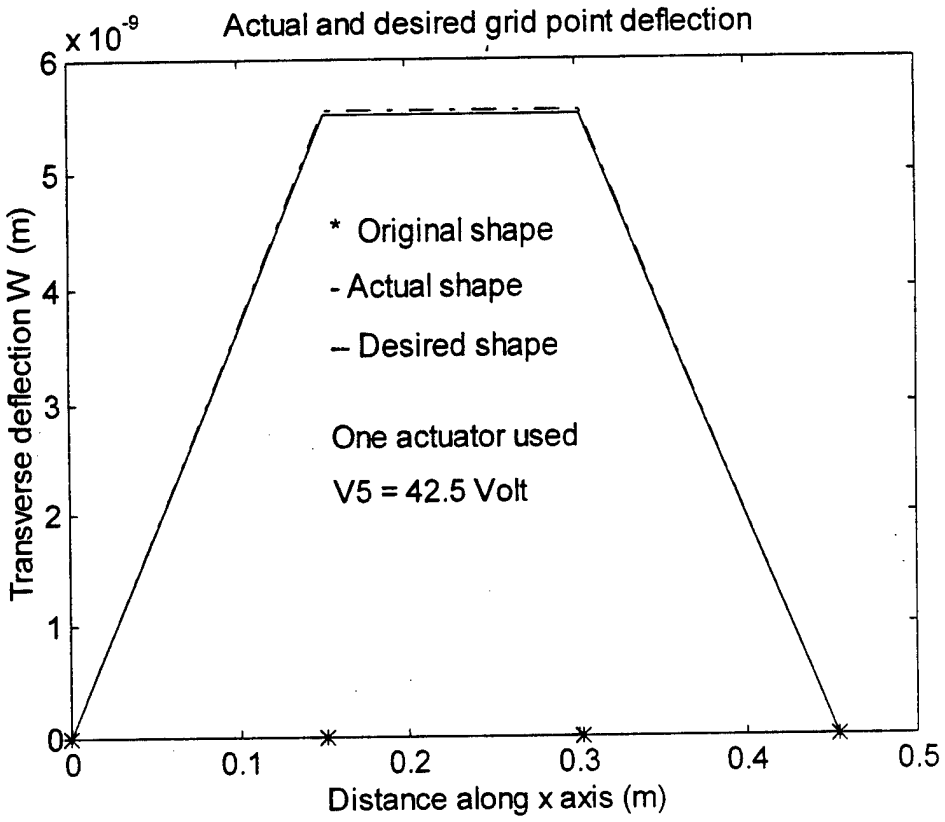

Figure 4.6: Actual and desired transverse deflection at the grid point for actuator at fifth element.

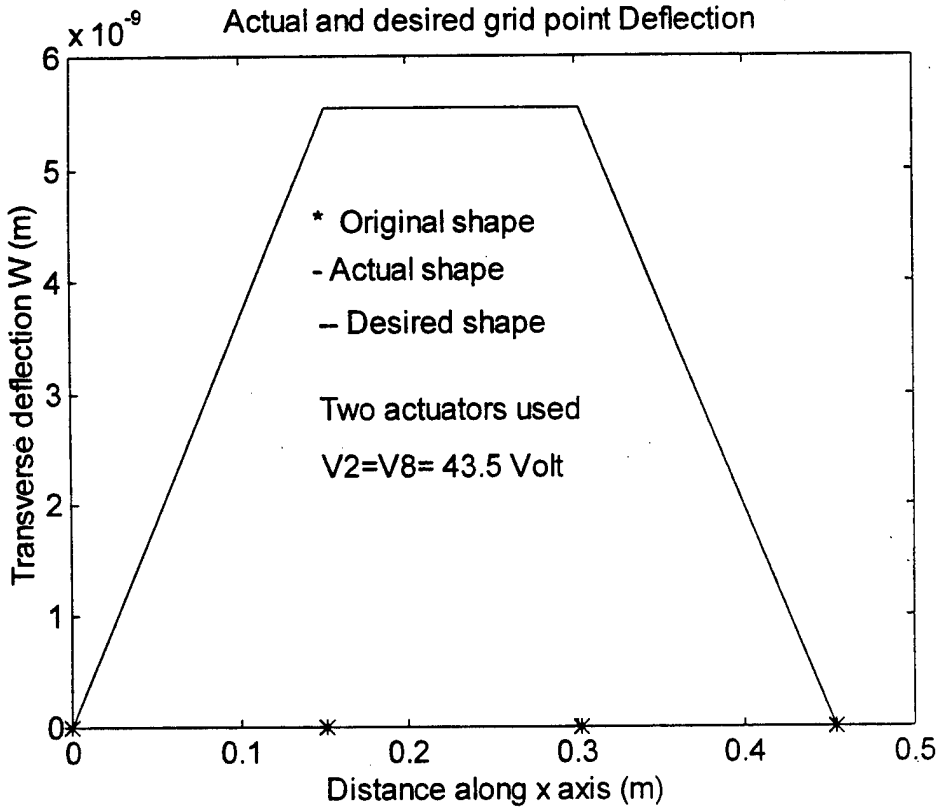

Figure 4.7: Actual and desired transverse deflection at the grid point for actuators at elements two and eight.

Table 4.2: Optimal applied voltage and error function at different actuator positions.

Actuator Position	Minimum Applied Voltage (Volt.)	*Minimum Error Function*
Element # 1	V = 78.226	f = 5.83495108e-18
Element # 2	V = 70.944	f = 4.78995246e-18
Element # 3	V = 99.999	f = 4.44647064e-18
Element # 4	V = 34.161	f = 5.88349351e-18
Element # 5	V = 37.346	f = 4.74690856e-18
Element # 6	V = 75.062	f = 4.03165923e-18
Element # 7	V = 78.611	f = 5.82972138e-18
Element # 8	V = 71.141	f = 4.78117803e-18
Element # 9	V = 99.999	f = 4.44063651e-18

Table 4.3: Optimal applied voltages and error functions for the case of four actuators used at a time.

Actuators Positions	Minimum Applied Voltages (Volt.)	*Minimum Error Function*
Elements #s 1, 3, 7 & 9	V_1 = -21.060 V_3 = 98.104 V_7 = -16.473 V_9 = 101.482	f = 4.0531138e-18
Elements #s 2, 4, 8 & 6	V_2 = 18.404 V_4 = -29.429 V_6 = 65.262 V_8 = 22.349	f = 4.01531283e-18

Table 4.4: Optimal applied voltages and error functions for the case of pair of actuator used at a time.

Actuators Positions	Minimum Applied Voltages (Volt.)	*Minimum Error Function*
Elements #s 1 & 7	$V_1 = 41.612$ $V_7 = 47.265$	f= 5.78007896e-18
Elements #s 2 & 8	$V_2 = 35.943$ $V_8 = 39.934$	f= 4.74678213e-18
Elements #s 3 & 9	$V_3 = 85.710$ $V_9 = 90.547$	f= 4.0583368e-18
Elements #s 1 & 3	$V_1 = -26.368$ $V_3 = 175.055$	f= 4.10114654e-18
Elements #s 4 & 6	$V_4 = -8.231$ $V_6 = 79.660$	f= 4.01544062e-18
Elements #s 7 & 9	$V_7 = 26.0895$ $V_9 = 175.193$	f= 4.09288468e-18
Elements #s 1 & 9	$V_1 = -17.007$ $V_9 = 170.053$	f= 4.10970645e-18
Elements #s 3 & 7	$V_3 = 169.712$ $V_7 = -16.138$	f= 4.12087738e-18

V. CONCLUSIONS

A finite element model was developed to analyze the behavior of a smart composite plate. This intelligent plate was composed of distributed sensor and actuator layers made of PVDF or PZT and a laminate of graphite/epoxy layers. In the analysis, the piezoelectric layer was treated as a normal lamina. A simple higher order shear deformation theory with Hamilton's principle was used to formulate the equations of motion. A four node, bilinear, isoparametric, rectangular element, with seven degrees of freedom at each node was developed. The electric potential was treated as a generalized electric coordinate like the generalized displacement coordinates at the mid-plane of the actuator and sensor layers. A Matlab code 'CMPZ' was developed to analyze the structure.

Several conclusions can be made from the results. The present finite element method can be used for static and dynamic analyses for both thick and thin composite structures with distributed piezoelectric sensors and actuators. The numerical results generated by the developed code agree very well with the exact solution and other published finite element solutions. This validates the finite element model. The method developed is much simpler to formulate and more efficient than models based on hexahedral or tetrahedral solid elements and/or three dimensional brick elements. The error of the method increased for small span to thickness ratios and decreased dramatically for higher span to thickness ratios. A Hermite cubic interpolation function was used to approximate the transverse deflections, however, the method does not suffer from the shear correction, which is problematic in the first order shear deformation theory. The developed displacement model includes the parabolic distribution of the transverse shear stresses and the non-linearity of in-plane displacements across the thickness. This is an advantage over the classical laminated plate theory, which neglects the effects of transverse shear stresses. The number of degrees of freedom of the element used in the present method is one third the number of degrees of freedom of the element used in the model developed by the higher order shear deformation theory, which of course saves computational time.

For shape control and optimization, an optimization algorithm based on a finite element method was developed. Kinematical relations were used to formulate the objective (error) function as the summation of the mean square error between a point in the actual surface and a corresponding point in the desired surface integrated for each element of the finite element grid. This approach is an improvement over the method where surface error is determined only at the nodal points.

The optimal voltage applied at each actuator to achieve a specified shape with minimum error between the actual shape and the desired shape was computed using an optimization code. The Matlab code 'OPTSHP' is developed in conjunction with Matlab functions which gave very satisfactory results. The code is able to determine the value of the error function for different actuator(s) positions for a specified amount of the applied voltage to the actuator(s). The model is applied for both cases, either constant voltage applied to the actuator(s) or different voltages applied to several actuators. The procedure proposed in this work was implemented for a composite plate with any demonstrated number of piezoelectric actuators. It was demonstrated from the examples that the desired shape was made to chosen match the actual shape, which satisfies small deformation theory. The procedure was tested for more general layouts of actuators and the optimization algorithm was applied to get optimal applied voltages to the actuators to minimize the error function.

Future work is proposed in the following areas;

1. Generalization of the finite element model to non-rectangular elements and shell elements.
2. Optimization of the actuator placements.
3. Closed loop shape control to compensate for varying external mechanical and thermal loads.

APPENDEX A. NUMERICAL INTEGRATION

For the isoparametric element considered in this work, an exact evaluation of the integration for mass, stiffness and the equivalent nodal loads was not always possible because of the algebraic complexity of the differential equations representing the element used. Since the interpolation functions are easily derivable for a rectangular element, and it is easier to evaluate integrals over rectangular geometry, we transform the finite element integral statements, defined over quadrilaterals, to a rectangle. In such a case, it is necessary to use some numerical integration technique. One of the most accurate and convenient methods is Gaussian quadrature, which involves approximation of the integrand by a polynomial of sufficient degree, because the integral of a polynomial can be evaluated exactly [Ref. 93]. If an integral;

$$P = \int_{x_1}^{x_2} F(x)dx \tag{A.1}$$

with function $F(x)$ is approximated by a polynomial;

$$F(x) \approx \sum_{I=1}^{N} F_I \Psi_I(x) \tag{A.2}$$

where F_I denotes the value of $F(x)$ at the I[th] point of the interval (x_1,x_2) and $\Psi_I(x)$ are polynomials of degree $N-1$. The representation can be viewed as the finite element interpolation of $F(x)$, where F_I is the value of the function at the I[th] node. For our rectangular element the integral will take the form;

$$\int_{\Omega_e} F(x,y)dxdy = \int_{\hat{\Omega}_e} F(\xi,\eta)|J|d\xi d\eta = \int_{-1}^{1}\int_{-1}^{1} F(\xi,\eta)|J|d\xi d\eta \approx \sum_{I=1}^{M}\sum_{J=1}^{N} F(\xi_I,\eta_J)|J(\xi,\eta)|R_I R_J \tag{A.3}$$

where;

Ω_e is the actual element domain with its x, and y coordinates (Fig. 2.3)

$\hat{\Omega}_e$ is a linear master element with its r and s coordinates (Fig.2.3)

(ξ, η) denote the Gauss points in the ξ and η directions. (Fig 2.3)

R_I and R_J denote the corresponding Gauss weights (see Table. A.1)

M and N denote the number of quadrature points. (in most, cases, the interpolation functions are of the same degree in both ξ and η direction, i.e. $M = N$.

$|J|$ is the determinant of the Jacobian matrix J, in which , $|J| > 0$ everywhere in the element Ω_e.

Geometrically, the Jacobian represents the ratio of an area element in the actual element to the corresponding area element in the master element:

$$dA = dxdy = |J| d\xi d\eta \tag{A.4}$$

The number of Gauss points is based on the formula;

$$N = \text{int}eger(1/2(p+1)) \tag{A.5}$$

which means that the smallest integer greater than $1/2(p+1)$; where p is the degree of the polynomial which may be integrated exactly employing equation (A.5).

Table A.1 gives the integration order, weighting factor and the location of the Gauss points for linear, quadratic, and cubic elements [Ref. 94]. The maximum degree of the polynomial refers to the degree of the highest polynomial in ξ and η that is present in the integral $F(\xi, \eta)$ of equation (A.3).

Table A.1:

Weights and Gauss points for the Gauss- Legendre Quadrature.

N	$\pm\xi_i$	R_i
1	0.0	2.0
2	0.5773502692	1.0
3	0.7745966692	0.5555555556
	0.0	0.8888888889
4	0.8611363116	0.3478548451
	0.3399810436	0.6521451549
5	0.9061798459	0.2369268851
	0.5384693101	0.4786286705
	0.0	0.5688888889
6	0.9324695142	0.1713244924
	0.6612093865	0.3607615730
	0.2386191861	0.4679139346
7	0.9491079123	0.1294849662
	0.7415311856	0.2797053915
	0.4058451514	0.3818300505
	0.0	0.4179591837
8	0.9602898565	0.1012285363
	0.7966664774	0.2223810345
	0.5255324099	0.3137066459
	0.1834346425	0.3626837834

N=2, Linear; N=3, Quadratic; N=4 Cubic, etc.

N × N =the order of integration.

ξ = Location of integration points in master element.

R = Weighting factor.

APPENDEX B. COMPUTER PROGRAMS

Two Matlab codes were developed, 'COMPZ' and 'OPTSHP'. The 'COMPZ' code is a finite element analysis program for a smart composite plate. The program is able to compute the static and the dynamic response of the structure, bending deformation, free vibration, and stress analysis subjected to both mechanical and electric load for various boundary conditions. The program is able to solve a composite plate with and without piezoelectric layers. The composite laminates could be graphite epoxy with reinforced fiber or aluminum layers. The piezoelectric elements can be segmented or continuous elements and can be either surface bonded or embedded in the laminated plate. The procedure to run the program is as follows:

1. Mesh generation :

   Input the number of point in x direction N_x

   Input the number of point in y direction N_y

   Input the plate length in x direction L_x

   Input the plate length in y direction L_y

   Input the plate thickness in z direction Lthk

   Input the number of patches their lengths in x direction (if any)

   Input the number of patches their lengths in y direction (if any)

The program will generate the mesh automatically and compute the elements numbers, nodes coordinates, and the elements conductivity.

2. Structures Data:

   Input type of the structures, simply supported or cantilever plate.

   Input materials constants for the structures core (graphite epoxy or aluminum) and for the piezoelectric material. E_1, E_2, etc.

3. Applied Loads:

Input the intensity of the load per unite area q_0.

Input the amplitude of the applied voltage V.

4. Method of analysis:

Input quarter plate analysis.

Input full plate analysis.

Composite plate analysis.

Smart composite plate analysis, with piezoelectric materials,

Complete cover the surface, or

Uniform patches cover the surface

5. Result

Plate deflection

Natural frequency and mode shape

Stress value for each layer

The "OPTSHP" code is an optimization program using the finite element technique in which the optimization algorithm is applied to the objective function by using a Matlab function $f\min s$ through finite element analysis subroutines. The code is able to compute the plate deformation due to the applied voltage and/or mechanical load and determine the optimal placement of actuator. Also the code is able to compute the minimum amount of the applied voltages to each actuator by using a Matlab function $f\min s$ and $f\min$. The steps to run the code are:

1. Mesh generation :

Input the number of point in x direction N_x

Input the number of point in y direction N_y

Input the plate length in x direction L_x

Input the plate length in y direction L_y

Input the plate thickness in z direction Lthk

Input the number of patches

Input the patches element numbers

2. Structures Data:

Input type of the structures, simply supported or cantilever plate.

Input materials constants for the structures core (graphite epoxy or aluminum) and for the piezoelectric material. E_1, E_2, etc.

3. Applied Loads:

Input the intensity of the load per unite area q_0 (if any)

Input the initial value of the applied voltage V.

4. Method of analysis:

Input full plate analysis.

Smart composite plate analysis, with piezoelectric materials,

Uniform patches cover the surface

5. Determine the patch location:

Input initial guess for patch position and compute the objective function

The program will do finite element analysis and compute the plate deflection due to the applied voltage at this place.

Input the second guess at other location of the finite element grid.

Repeat this check and compare the values of the objective function for each case and pick the minimum value which represent the optimal place to get minimum error between the actual and the desired shape.

6. Determine the optimal amount voltages applied to each actuator:

   Input initial value of the applied voltages for the each actuator at the selected position.

   Call the optimization algorithm using the Matlab function $f\min s$ and

   $f\min$, they will perform a finite element analysis for this value of the voltages.

   The code will update the voltage values and repeat the analysis again.

   The code will check the global minimum of the objective function and will stopped at the global minimum with minimum amount of voltages applied to each actuators.

LIST OF REFERENCES

[1] Edward F. Crawley, ' Intelligent structures for aerospace: A technology overview and assessment', AIAA J., Vol. 32, No. 8, 1994.

[2] B. Jaffe, R.S. Roth, and S. Marzullo, ' Piezoelectric properties of lead zirconate-lead titanate soild solution ceramics', J. Appl. Phys. Vol.25, pp809-810, 1954.

[3] H. kawai, ' The piezoelectricity of polyvinylidene fluoride', Japan Journal of Applied Physic, Vol.8,p975,1969.

[4] J. N. Reddy, 'A simple higher order theory for laminated composite plates', J. Appl. Mech.,Vol.51, pp745-752,1984.

[5] E. Reissner and Y. Stavsky,' Bending and stretching of certain types of heterogeneous Aerolotropic elastic plate', J. Appl. Mech., Vol.28, pp402-408, 1961.

[6] Y. Stavsky, ' Bending and stretching of laminated aerolotropic plate ', Proc. Am. Soc. Civil Engrs., J. Engr. Mech. Div., Vol.87, p31, 1961.

[7] S. B. Dong, K. S. Pister and R. L. Taylor, ' On the theory of laminated anisotropic shell and plates', J. Aerospace Sc., Vol.29,pp969-975, 1962.

[8] C. W. Bert and B. L. Mayberry, ' Free vibration of unsymmetriclly laminated anisotropic plate with clamped edges', J. comp. Mater., Vol3,pp282-293, 1969.

[9] R. D. Mindlin,' Influence of rotary Inertia and shear on flexural motions of isotropic elastic plate',Vol.18,pp31-38, 1951.

[10] Y. Stavsky, 'On the theory of symmetrically heterogeneous plates having the same thickness variation of the elastic moduli', in topics in Appl. Mech. (Eds. D. Abir, F.ollendorff and M. Reiner), American Elsevier, N.Y, p105, 1965.

[11] P.C. Yang, C.H. Norris and Y. Stavsky,' Elastic wave propagation in heterogeneous plates', AIAA J.,Vol.11,pp178-183,1973.

[12] J.M. Whitney, ' The effect of transverse shear deformation on the bending of laminated plates', J. Composite Materials, Vol.3, p534, 1969.

[13] N. J. Pagano, ' Exact solutions for composite laminates in cylindrical bending', J. Comp. Mater.,Vol.3(3),pp398-411,1969.

[14] N. J. Pagano, 'Exact solutions for rectangular bi-directional composites and sandwich plates', J. Comp. Mater.,Vol.4,pp20-34,1970.

[15] N. J. Pagano and S. D. Wang, ' Further study of composite laminates under cylindrical bending', J. Comp. Mater., Vol.5, pp521-528, 1971.

[16] N. J. Pagano and S. J. Hatfield, ' Elastic behavior of multilayers bidirectional composites', AIAA J., Vol.10,pp931-933, 1972.

[17] Green, A. E., and Naghdi, P. M., 'A theory of laminated composite plates', IMA J. Appl. Mathematics, Vol.29,p1, 1982.

[18] Rehfield, L. W., and Valisetty, R. R., ' A comprehensive theory for planar bending of composite laminates', Computer&structures,Vol.16, pp441,1983.

[19] Pagano, N. J. and Soni, S. R.,'Global-local laminated variational model', Int. J. Solids & Struct.,Vol.19,p207,1983.

[20] J. M. Whitney & N. J. Pagano, 'Shear Deformation in Heterogeneous Anisotropic plates', J. Appl. Mechs., Vol.37,pp1031-1036, Dec.1970.

[21] J. M. Whitney, 'Stress analysis of thick laminated composite and sandwich plates', J. Comp. Mats., Vol.6, pp426-440, 1972.

[22] J. M. Whitney and C. T. Sun, 'A Higher-Order theory for extensional motion of laminated composites', J. Sound and Vibration, Vol.30., pp85-97,1973.

[23] K. H. Lo, R. M. Christensen, and E. M. Wu, 'A Higher-Order Theory of plate deformation, part2: Laminated plates', J. Appl. Mechs.,Vol.44, pp667-676,1977.

[24] R.B. Nelson and D. R. Lorch, 'A refined theory of laminated orthotropic plates', J. Appl. Mechs., Vol.41,TRANS. ASME, Vol.96, series E, pp177-183, 1974.

[25] J. N. Reddy, 'A simple higher-order theory for laminated compositeplates', J. Appl. Mech., Vol.51,pp745-752, 1984.

[26] J. N. Reddy, 'Simple finite elements with relaxed continuity for nonlinear analysis of plates', Proce. Of 3rd Inter. Conf. In Australia,pp265-281,1979.

[27] J. N. Reddy, ' A penalty plate bending element for the analysis of laminated anisotropic composite plates', Int. J. numer. Methods engn.,Vol.15, pp1187-1206,1980.

[28] J. N. Reddy and W.C. Chao, 'Large-deflection and large-amplitude free vibrations of laminated composite material plates', Computer & Structures, Vol.13,pp341-347,1981.

[29] J. N. Reddy, 'On the solutions to forced motions of rectangular composite plates', J. Appl. Mechs., Vol.49,pp403-408,June 1982.

[30] J. N. Reddy, 'Short communications: A note on symmetry considerations in the transient response of unsymmetrically laminated anisotropic plates', Int. J. numer. Methods engn., Vol.20,pp175-194,1984.

[31] N. S. Putcha and J. N. Reddy, ' Arefined mixed shear flexible finite element for the nonlinear analysis of laminated plates', Computer &Structures, Vol.22, No.4, pp529-538,1986.

[32] J. N. Reddy, ' Ageneralization of two dimensional theories of laminated composite plates', Commun. Appl. Numer. Method, Vol.3, pp173-180,1987.

[33] N. D. Phan and J. N. Reddy,' Analysis of laminated composite plates using a Higher order shear deformation theory', Int. J. numer. Methods engn.,Vol.21,pp2201-2219,1985.

[34] J. N. Reddy and E. J. Barbero, 'A plate bending element based on a generalize laminated plate theory', Int. J. numer. Methods engn., Vol.28, pp2275-2292, 1989.

[35] J. N. Reddy and A. A. Khdeir, 'Buckling vibration of laminated composite plates', AIAA J.,Vol.27, No.12,1989.

[36] J. M. Reddy,' Free vibration of anti-symmetric angle-ply laminated plate including transverse shear deformation by finite element method', J. Sound & Vibration,Vol.66, pp565-576, 1979.

[37] Ahmed K. Noor and Michael D. Mathers, 'Finite element analysis of anisotropic plates', Int. J. numer. Methods engn.,Voll1, pp289-307,1977.

[38] Ahmed K. Noor and Michael D. Mathers, ' Anisotropy and shear deformation in laminated composite plates', AIAA J., Vol.14, No.2, pp282-285,1976.

[39] Ahmed K. Noor, 'Free vibrations of multi-layered composite plates', AIAA J., Vol.11, pp1038-1039, 1973.

[40] A. S. Mawenya and J. D. Davies,' Finite element bending analysis of multilayer plates', Int. J. numer. Methods engn.,Vol.8,pp215-225,1974.

[41] S. C. Panda and R. Natarajan,' Finite element analysis of laminated composite plate', Int. J. numer. Methods engn.,Vol.14, pp69-79,1979.

[42] R. C. Fortier and J. N. Rossettos, 'The vibration of shear deformable curved anisotropic composite plates', J. Appl. Mechs.,Vol.40,p299,1973.

[43] P. K. Sinha and A. K. Rath, 'Vibration and buckling of cross-ply laminated circular cylindrical panels', Aeronaut. Quart.,Vol.29,p211, 1975.

[44] S. B. Dong, 'Studies relating to the structural dynamic behavior of laminated plates and shells. Ucla-eng-7236, University of California, LA,1972.

[45] A. K. Ghosh and S. S. Dey, ' Simple finite element for the analysis of laminated plates', comput. & Struct.,Vol.44,No.3,pp585-596,1992.

[46] A. K. Gosh and S. S. Dey, ' Free vibration of laminated composite plates : A simple finite element based on higher order theroy', Comput. & Struct.,Vol.52, No.3,pp397-404, 1994.

[47] Walter Guyton Cady, 'Piezoelectricity', Vol.1, Dover,N.Y, 1964, (1ST ed. McGraw-Hill comp. Int.,1946, Int. series in physics)

[48] Takuro Ikeda, 'Fundamentals of piezoelectricity', Oxford unive. Press, N.Y, 1990.

[49] J.F. Nye, 'Physical properties of crystals', Oxford unive. press, N.Y, 1957.

[50] H. F. Tiersten, ' Linear piezoelectric plate vibrations', plenum press, N.Y, 1969.

[51] N. N. Rogacheva, 'The theory of piezoelectric shells and plates', CRC Press, Boca Raton, etc., 1994.

[52] E. F. Crawley and J. de Luis, ' Use of piezoelectric actuators as elements of Intelligent structures', AIAA J.,Vol.25, pp1373-1385,1987.

[53] E. F. Crawley and K. B. Lazarus, 'Induced strain actuation of isotropic and anisotropic plates', AIAA J., Vol.29, No.6, pp944-951, 1990.

[54] E. F. Crawley and Eric H. Anderson, 'Detailed models of piezoelectric actuation of beams', J. Intl. Mater. Syst. & struct.,Vol.1,1990.

[55] E. F. Crawley, J. de Luis, N. W. Hagood, & E. H. Anderson, 'Development of piezoelectric technology for applications in control of intelligent structures', presented at Amer. Control Conference,Vol.1,1990.

[56] C. K. Lee, 'Theory of laminated piezoelectric plates for design of distributed sensors/actuators.PartI:Governing equations and reciprocal relationships', J. Acoust. Soc. America, Vol.87(3),pp1144-1158,1990.

[57] C. K. Lee and F. C. Moon,'Modal sensors and actuators', J. Appl. Mech., Vol.57, pp434-441,1990.

[58]C. K. Lee and F. C. Moon, 'Laminated piezopolymer plates for torsion and bending sensors and actuators', J. Acoust. Soc. America, Vol.85(6),1989.

[59] Bor-Tsuen Wang and Craig A. Rogers, 'Laminated plate theory for spatially distributed induced strain actuators', J. Composite Materials, Vol.25,April 1991.

[60] H. S. Tzouand J. P. Zhong, 'Electromechanics and vibrations of piezoelectric shell distributed systems', J. Dynamic syst., Measurement, and control, Vol.115, pp506-517, 1993.

[61] J. A. Mitchell and J. N. Reddy, 'A refined hybrid plate theory for composite laminates with piezoelectric laminae', Int. J. Soilds struct., Vol.32, No.16,pp2345-2367,1995.

[62] N. W. Hagood, W. H. Chung and Von Flotow, ' Modeling of piezoelectric actuators dynamics for active structural control', J. Intel. Mater. Syst. And struct., Vol.1,1990.

[63] M. C. Ray, K. M. Tao and B. Samanta,' Exact analysis of coupled electroelastic behaviour of piezoelectric plate under cylindrical bending', Comput. & Struct., Vol.45, No.4,pp667-677, 1992.

[64] M.C. Ray, K. M. Rao and B. Samanta,' Exact Solution for static analysis of intelligent structure under cylindrical bending', Comput. & Structures,Vol.47,No.6,pp1031-1042, 1993.

[65] M. C. Ray, R. Bhattacharya, and B. Samanta, 'Exact solution for static analysis of intelligent structures', AIAA J., Vol.31, No.9,Sep.1993.

[66] Stephen Brooks and Paul Heyliger,' Static behavior of piezoelectric laminates with distributed and patched actuators', J. Intel. Mater. Syst. & struct.,Vol.5,Sep 1994.

[67] Jong S. Lee and Long Z. Jiang, ' Exact electoelastic analysis of piezoelectric laminae via state space approach', Int. J. Solids Struct., Vol.33,No.7,pp977-990,1996

[68] Paul Heyliger and Stephen Brooks,' Free vibration of piezoelectric laminates in cylindrical bending', Int. J. Solids Struct.,Vol.32, No.20, pp2945-2960, 1995.

[69] Henno Allik and Thomas J. R. Huges,' Finite element method for piezoelectric vibration', Int. J. numer. Meths. Engng., Vol.2, pp151-157, 1970.

[70] H. S. Tzou and C.I. Tseng, 'Distributed piezoelectic sensor/actuator design for dynamic measurement/control of distributed parameter systems : A piezoelectric finite element approach', J. Sound & Vibration,Vol.138(1),pp17-34,1990.

[71] Yukio Kagawa and Graham M. L. Gladwell, ' Finite element analysis flexure-type vibrator with electrostrictive transducers', IEEE Trans. Sonic & Ultrasonic, Vol.17, No.1,1970.

[72] Graham F. McDearman,' The addition of piezoelectric properties to structures finite element programs by matrix manipulations', J. Acoust., Soc. Am., Vol.76(3),1984.

[73] H. S. Tzou, C. I. Tseng and G. C. Wan,' Distributed structural dynamics control of flexible manipulators-II. Distributed sensor and active electromechanical actuator', Comput. & Struct., Vol.35, No.6, pp679-687,1990.

[74] Sung Kyu Ha, Charles Keilers, and Fu-kuo Chang,' Finite element analysis of composite structures containing distributed piezoceramic densors and actuators', AIAA J. ,Vol.30, No.3,March 1992.

[75] Woo-seok Hwang and Hyun Chul Park,'Finite element modeling of piezoelectric sensors and actuators', AIAA J., Vol.31, No.5, May 1993.

[76] Woo-Seok Hwang, Hyun Chul Park and Woon bong Hwang, ' Vibration control of laminated with piezoelectric sensor/actuator : Finite element formulation and modal analysis', J. Int. Mater. Syst. & Struct., Vol.4,1993.

[77] K. Chandrashekhara and A. N. Agarwal,' Active vibration control of laminated composite plates using piezoelectric devices: A finite element Approach', J. Int. Mater. Syst. & Struct., Vol.4, Oct. 1993.

[78] M. C. Ray, R. Bhattacharyya and B. Samanta, ' Static analysis of an intelligent structure by the finite element method', computer & structures, Vol.52,No. 4,pp617-631,1994.

[79] A. Baz, and S. Poh, 'Performance of an active control system with piezoelectric actuators', J. sound & Vibration, Vol.126, No.2, pp327-343, 1988.

[80] Aditi Chatto Padhyay and Charles E. Seeley, 'A multi-objective design optimization procedure for control of structures using piezoelectric materials', J. Intl. Mater. Syst. & Struct., Vol.5, May 1994.

[81] H. S. Tzou, 'Distributed modal identification and vibration control of continua: Theory and applications', Transn. ASME, J. Dynamic Syst., Measurements & control, Vol.13, pp494-499, Sep 1991.

[82] H. S. Tzou and C. I. Tseng, 'Distributed modal identification and vibration control of continua: Piezoelectric finite element formulation and analysis',Transt. ASME, J. Dynm. Syst., Measurements, & control, Vol.113, pp508-505, Sep 1991.

[83] E. H. Anderson and N. W. Hagood, 'Simultaneous piezoelectric sensing/actuation: Analysis and application to controlled structures', J. Sound & Vibration, Vol.174(5), pp617-639, 1994.

[84] N. W. Hagood, W. H. Chung and A. Von Flotow,' Modelling of piezoelectric actuator dynamics for structural control', J. Intl. Mater., Syst. & Struct., Vol.1,pp327-354, 1990.

[85] C.R. Fuller, ' Active control of sound transmission/Radiation from elastic plates by vibration input: I. Analysis', J. Sound & Vibration, Vol. 136(1), pp1-15,1990.

[86] Boe-Tsuen Wang, Chris R. Fuller, and Emilies K. Dimitriadis, 'Active control of structurally radiated noise multiple piezoelectric actuators', AIAA J., Vol.29,No.11, pp1802-189,1990.

[87] Bor-Tsuen Wang, Ricardo A. Burdisso and Chris R. Fuller, 'Optimal placement of piezoelectric actuators for active structural acoustic control', J. Int. Mater. Syst. & Struct., Vol.5, pp67-77,1994.

[88] Bor-Tsuen Wang and Chris R. Fuller,' Near field pressure intensity, and wave-number distributions for active structural acoustic control of plate radiation: Theoretical analysis', J. Acoust. Soc. Am.,Vol.92(3), pp1489-1498,1992.

[89] K. Ghosh and R. C. Batra, 'Shape conrtol of plates using piezoceramic elements', AIAA J.,1995.

[90] Sunil Kumar Agrawal and Daqun Tong, 'Modeling and shape controlof piezoelectric actuator embedded elastic plates', J. Int. Mater syst. & struct., Vol.5,July 1994.

[91] David B. Koconis, Laszlo P. Kollar and George S. Springer, 'Shape control of composite plates and shells with embedded actuators: I. Voltage specified, II. Desired shape specified ', J. Composite Materials, Vol.28,No.5,pp415-483,1994.

[92] S.Varadarajan and K. Chandrashekhara,' Adaptive shape control of laminated composite plates using piezoelectric materials', Proc. AIAA J., 1996.

[93] J. N. Reddy, 'An introduction to the finite element method second ed.', McGraw-Hill, Inc.

[94] William Weaver, Jr. and Paul R. Johnston, 'Finite elements for structural analysis', Prentice -Hill, Inc.

[95] O.O. Ochoa and J. N. Reddy,' Finite element analysis of composite laminates', Kluwer Academic Publishers.

[96] Robert M. Jones, 'Mechanics of composite materials', Hemisphere Pub.Corp., NY.

[97] Ronald F. Gibson,'Principles of composite material mechanics', McGraw-Hill, Inc., N.Y

[98] O. C. Ziewnkiewicz and Y. K. Cheung, 'The finite element method for the analysis of ealstic, isotropic and orthotropic slabs', Proc. Inst. Civil Engrs., Vol.28, pp471-488, 1964.

[99] E. Hinton and J. S. Campbell, 'Local and global smothing of discontinuous finite element functions using a least square method', Int. J. Numer. Meths. Engng., Vol.8, pp461-480, 1974.

[100] H. S. Tzou, 'Piezoelectric shells: Distributed sensing and control of continua ',Kluwer Academic Publishers.

[101] S. S. Rao, 'Optimization theory and applications', Wiley Estern Limited, 1978

[102] J. A. Nelder and R. Mead, 'A Simplex Method for Function Minimization,' Computer Journal Vol. 7,pp.308-313.

[103] Spendley, W., Hext, G. R., and Himsworth, F. R.,'Sequential Application of Simplex Designs in Optimisation and Evolutionary Operation,' Technometrics,Vol. 4,p441,1962.

[104]K. Moser, H. Lehar and A. Schmid, 'About the analysis of laminated composite structures, finite element in engineering applications', pp.395-416, INTES Gmg H, Stuttgart (1987).

INITIAL DISTRIBUTION LIST

	No. Copies
1. Defense Technical Information Center 8725 John J. Kingman Road., Ste 0944 Ft. Belvoir, VA 22060-6218	2
2. Dudley Knox Library Naval Postgraduate School 411 Dyer Rd. Monterey, California 93943-5101	2
3. Chairman, Code AA Department of Aeronautics and Astronautics Naval Postgraduate School Monterey, California 93943-5002	1
4. Professor Brij N. Agrawal, Code AA/Ag Department of Aeronautics and Astronautics Naval Postgraduate School Monterey, California 93943-5002	1
5. Professor Garald H. Lindsey, Code AA/GL Department of Aeronautics and Astronautics Naval Postgraduate School Monterey, California 93943-5002	1
6. Professor Sandra L. Scrivener, Code AA/SS Department of Aeronautics and Astronautics Naval Postgraduate School Monterey, California 93943-5002	1
7. Professor Joshua H. Gordis, Code ME/JG Department of Mechanical Engineering Naval Postgraduate School Monterey, California 93943-5002	1
8. Professor Sherif Michael, Code ECE/SM Department of Electrical Engineering. Naval Postgraduate School Monterey, California 93943-5002	1

9. Professor Donald A. Danielson, Code AA/ DD 1
Department of Mathematics
Naval Postgraduate School
Monterey, California 93943-5002

10. Professor Fariba Fakhroo , Code/Ff 1
Department of Mathematics
Naval Postgraduate School
Monterey, California 93943-5002

11. Professor Terry R. McNelly , Chairman Code ME 1
Department of Mechanical Engineering
Naval Postgraduate School
Monterey, California 93943-5002

12. Professor H. S. Tzou 1
Department of Mechanical Engineering
University of Kentucky, Lexington,
Kentucky 40506-0046, U.S.A.

13. Professor E. H. Anderson 1
Department of Aeronautics and Astronautics,
Massachusetts Institute of Technology,
Cambridge, Massachusetts 02139, U.S.A.